An Advanced-Louver Cooling Scheme for Gas Turbines – Adiabatic Effectiveness and Heat Transfer Performance

Zhang Xuezhi

A Thesis

in

The Department

of

Mechanical and Industrial Engineering

Presented in Partial Fulfillment of the Requirements
for the Degree of Master of Applied Science at
Concordia University
Montreal, Quebec, Canada

December 2004

Your file Votre référence
ISBN: 0-494-04437-3
Our file Notre référence
ISBN: 0-494-04437-3

ABSTRACT

An Advanced-Louver Cooling Scheme for Gas Turbines –

Adiabatic Effectiveness and Heat Transfer Performance

Zhang Xuezhi

The thermal performance of a novel film-cooling scheme for a high temperature gas turbine application is introduced. The new jet, with both forward and laterally diffused exit, enables the coolant to spread wider and more uniform over the downstream surface, when compared with the traditional circular hole. As a result, the coolant momentum is reduced in the normal direction, and thus the occurrence of jet lift-off is avoided. This novel film-cooling scheme is superior to traditional cooling scheme since less amount of coolant can provide the same protection under the same conditions, making more efficient use of the coolant air.

Systematic simulations have been carried out on two benchmark cases. The performances of different turbulence models as well as different wall treatments have been isolated and evaluated. Turbulence was modeled using four classes of turbulence models, namely k-ϵ (including its 3 variants), k-ω, Reynolds-Stress, and Spalart-Allmaras. Three-dimensional simulations were carried out by numerically solving the Reynolds-averaged Navier-Stokes equations. For the first time, to the best of author's knowledge, the jet lift-off effect is clearly captured in the simulations at high blowing ratios, and the results are in

excellent agreement with experimental data. The new methodology established in the two benchmark cases has been applied to the new scheme.

It was found that the conduction error on the test surface in experimental work intended for the measurement of the heat transfer coefficient is considerably larger than believed by the technical community. Modeling conjugate heat transfer by considering the effect of heat conduction in the testing plate can yield more realistic results, especially in the spanwise direction. The proposed cooling scheme can completely eliminate the possibility of jet liftoff and provide more uniform protection over the surface. It can efficiently reduce the presence of hot spots in the blade and significantly reduce thermal stress. The proposed cooling scheme gave considerably lower heat transfer coefficient at the centerline in the near hole region when compared to the traditional cylindrical hole, especially at high blowing ratio where traditional cylindrical hole undergoes liftoff. The heat transfer coefficient is much lower in the spanwise direction as well, thus providing more efficient protection over the surface.

This work is dedicated

to

my parents, my wife and my son.

Table of Contents

List of Figures

List of Tables

Nomenclature

C_p Specific heat at constant pressure, (kJ/kg·K)

d Hydraulic diameter of hole at exit plane, (m)

D.R. Density ratio, D.R. $= \frac{\rho_j}{\rho_\infty}$

E Total energy, (J)

G_b Generation of turbulence kinetic energy due to buoyancy

G_k Generation of turbulence kinetic energy

h Heat transfer coefficient, (W/m^2K), $h = \frac{q''}{T_w - T_{aw}}$

h_o Heat transfer coefficient without film cooling, (W/m^2K), $h_o = \frac{q''}{T_w - T_\infty}$

I Momentum flux ratio, $I = \frac{\rho_j U_j^2}{\rho_\infty U_\infty^2}$

k Turbulent kinetic energy, (m^2/s^2)

L Length of injection hole (for cylindrical holes), (m)

m Blowing ratio (or rate), $m = \frac{\rho_j U_j}{\rho_\infty U_\infty}$

P Pressure, (Pa)

P_r Molecular Prandtl number

q Surface heat flux per unit area, (W/m^2)

Re_D Reynolds number based on freestream velocity and injection diameter, $Re_D = \frac{\rho_\infty U_\infty d}{\mu_\infty}$

T	Temperature, (K)
U	Velocity, (m/s)
u_i	Averaged velocity component, (m/s)
u_i'	Fluctuating velocity component, (m/s)
$u_i'u_j'$	Reynolds-Stress tensor
$\vec{v}$	Overall velocity vector, (m/s)
V.R.	Velocity ratio, $V.R. = \frac{U_j}{U_\infty}$
x	Streamwise coordinate, (m)
y	Vertical coordinate, (m)
z	Spanwise coordinate, (m)
y^+	Non-dimensional wall distance, ($y^+ = \frac{\rho u_\tau y_p}{\mu}$)
y_p	Coordinate normal to the wall surface, (m)

GREEK SYMBOLS

ϵ	Dissipation rate of turbulent kinetic energy, (m^2/s^3)
η	Local adiabatic film cooling effectiveness, ($\eta = \frac{T_{aw} - T_\infty}{T_j - T_\infty}$)
μ	Dynamic (laminar) viscosity, (kg/m·s)
ρ	Density, (kg/m^3)
τ	Shear stress, (Pa)
$\bar{\bar{\tau}}$	Stress tensor, (Pa)
ω	Specific dissipation rate, (s^{-1})

SUBSCRIPTS AND SUPERSCRIPTS

aw	Adiabatic wall
eff	Effective values
f	Conditions with film cooling
j	Refers to the jet
l	Length scales for turbulent eddy
lam	Laminar quantities
o	Conditions in the absence of film cooling
r	Reference conditions
t	Turbulence quantities
turb	Turbulence quantities
w	Wall conditions
∞	Mainstream conditions at inlet plane and in freestream

ABREVIATIONS

CFD	Computational fluid dynamics
DES	Detached eddy simulation
LES	Large Eddy Simulations
RANS	Reynolds-averaged Navier-Stokes
RNG	Renormalization Group
RSM	Reynolds Stress Model
RST	Reynolds Stress Transport

Chapter 1

Introduction

1.1 Background and motivation

Gas turbines find many applications in aircraft propulsion, land-based power generation and many other industries. From thermodynamics analysis, it is very clear that thermal efficiency and power output of gas turbines increase with increasing turbine inlet temperature. Thus, gas turbine engine designers are constantly trying to raise the turbine inlet temperature as high as possible. However, the turbine engine inlet temperature is limited by current available materials, and until major improvements are made to the materials, engine designers have to seek other ways to raise turbine inlet temperature. Turbine cooling turns out to be one solution in that it allows engine designers to increase the turbine inlet temperature while maintaining a constant blade temperature. With new thermal resistant materials and new cooling technologies, the inlet temperatures of the gas turbine have been raised significantly over the last three decades. Modern gas turbine engines typically operate at inlet temperatures of 1800-2000 K, which is far beyond the allowable metal temperature. Film cooling, one of the most widely used turbine cooling technologies, is extensively employed to provide protection of the metal against the severe thermal environment.

A secondary fluid, called the coolant, is injected into a hot mainstream through some discrete holes, and afterwards forms a thin layer of film covering the downstream area,

thus protecting the surface against a severe harsh thermal environment. As air is readily available and can be extracted from the compressor easily, it has become the most commonly used coolant in modern gas turbines.

A typical film-cooled turbine blade is shown in figure 1.1. Usually the blade is hollow with some multiple serpentine passages inside. As cooler air, diverted from the compressor, passes through these passages it cools the blade by convection heat transfer. The coolant is then ejected into the hot main stream through some discrete holes. Ideally, the cooling air remains close to the surface after injection and forms an insulating layer between the hot gas steam and the wall of the blade, thus reducing the blade temperature by reducing the amount of energy transferred from the hot gas to the surface.

A considerable effort has been made to understand the coolant film behavior and its interaction with the mainstream flow. Cooling performance is influenced by a variety of parameters, such as the blowing ratio, the density ratio, wall curvature, free-stream turbulence intensity, compressibility, flow unsteadiness, the hole size, shape and location, and the angle of injection. From the viewpoint of protection of blades, more coolant results in better coverage of the surface downstream of the jets, while on the other hand, too much coolant can incur a severe efficiency penalty. The designer's goal is to ultimately minimize the coolant consumption while maximizing the cooling efficiency. At the same time, acceptable temperature and thermal stress levels on the turbine blade surface must be produced.

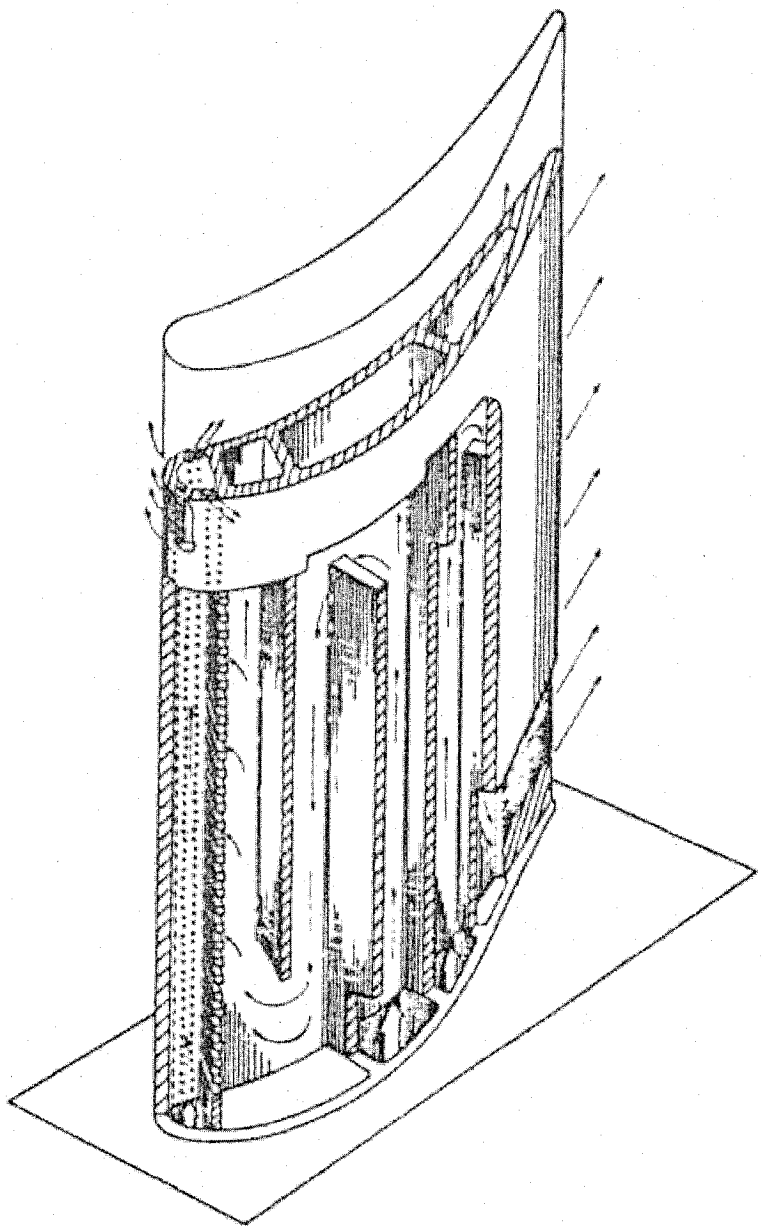

Figure 1.1 Film and convection-cooled blade (Boyce, 2002).

The traditional cylindrical hole undergoes jet liftoff at high blowing ratio, which means the coolant penetrates into the mainstream and so hot mainstream tucks in below the jet, causing the deterioration of protection. In order to make the use of the coolant more efficiently, the jet liftoff effect should be avoided. Meanwhile, a good spread of coolant in the spanwise direction is desirable, since uniform coolant coverage can significantly reduce the presence of hot or cold spots on the protected surface, and also significantly reduce the thermal stress level on the turbine blade. Traditional cylindrical holes poorly spread the coolant in the spanwise direction. Thus, a new cooling scheme is proposed with the intention of avoiding jet liftoff at high blowing ratio while spreading the coolant more evenly in the spanwise direction.

Compared with the traditional circular hole, the new scheme proposed by PWC (Pratt & Whitney Canada) and investigated by our group at Concordia University, as shown in figure 1.2, combines both the advantages of traditional film cooling with those of impingement cooling. The hole that transports coolant fluid from the inside to the outside of the blade is designed in such a way that the coolant must go through a bend before exiting the blade, thus impinging on the blade material. The flared hole exit was also designed to reduce the coolant momentum and ensure wide lateral spreading of the coolant on the downstream surface. This scheme is expected to produce the greatest coverage of the blade with the least amount of mixing, and using the least possible amount of coolant.

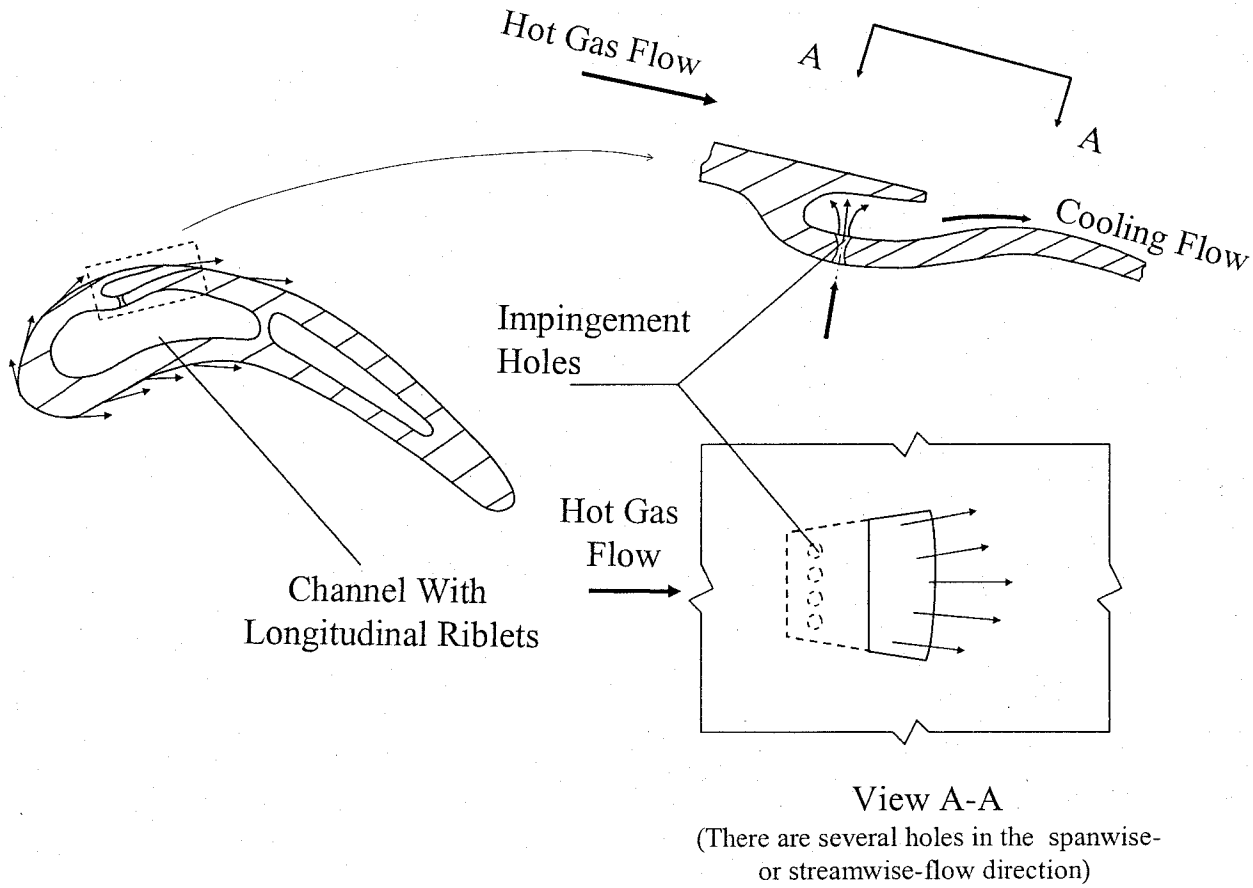

Figure 1.2 Proposed cooling scheme.

Since the compound hole has more advantage over traditional cylindrical hole in spreading the coolant more evenly, thus making the use of coolant more efficient, much attention has been paid to the development of new film-hole geometries, such as compound-angle holes and shaped holes. Any new cooling scheme must undergo extensive test and study before it can be successfully used in real engine applications. There are virtually an infinite number of different new geometries, which could have better performance than the schemes used today. However, any kind of experimental study on these new geometries would be expensive and time consuming, and so reliable numerical predictions of the performance of new scheme is in great demand. The mystery of turbulence has yet to be satisfactorily solved, and so empirical turbulence models proposed by scientists and engineers are the only available tool in CFD analysis of turbulence flow.

This study will systematically explore the predictive capacity of the turbulence models in capturing the correct trend in terms of adiabatic effectiveness and the heat transfer coefficient in film cooling applications. There are many such publications in the open literature, but most of the conclusions are hardly convincing since the contradiction among authors is common. In order to justify the new methodology, systematic simulations have been performed on different schemes at different blowing ratios and density ratios. For the first time, to the best of author's knowledge, the jet lift-off effect is clearly captured in the simulations at high blowing ratios, and the results are in excellent agreement with experimental data. The new methodology established in the two benchmark cases has been applied to the new scheme.

1.2 Film cooling fundamentals

Film cooling is quite different from traditional convective heat transfer problems, which involves only two temperatures. Consider a simple case of convective heat transfer as shown in figure 1.3, which was first studied by Isaac Newton who proposed the equation:

$$q = h(T_w - T_\infty) \tag{1.1}$$

where q heat flux

h surface heat transfer coefficient

T_w wall surface temperature

T_∞ far field temperature

This equation is nothing but the definition of convective heat transfer coefficient and it is based on a flat plate. However, in the film cooling application, there are three temperatures, upstream temperature, coolant temperature and wall temperature, see figure 1.4. In order to accommodate this problem as well as other multiple temperature problems, some researchers have proposed the following equation:

$$q = h(T_r - T_w) \tag{1.2}$$

where T_r refers to the appropriate reference or driving temperature which may vary with position, and T_w is the local wall temperature. The definition of the reference temperature has a significant effect on the magnitude of heat transfer coefficient. If T_r is defined as the far field or upstream temperature, then the reference temperature is a constant. If T_r is defined as the adiabatic local wall temperature (T_{aw}), then the reference or driving temperature will vary accordingly. In the open literature, the adiabatic local wall temperature is universally used as the reference temperature:

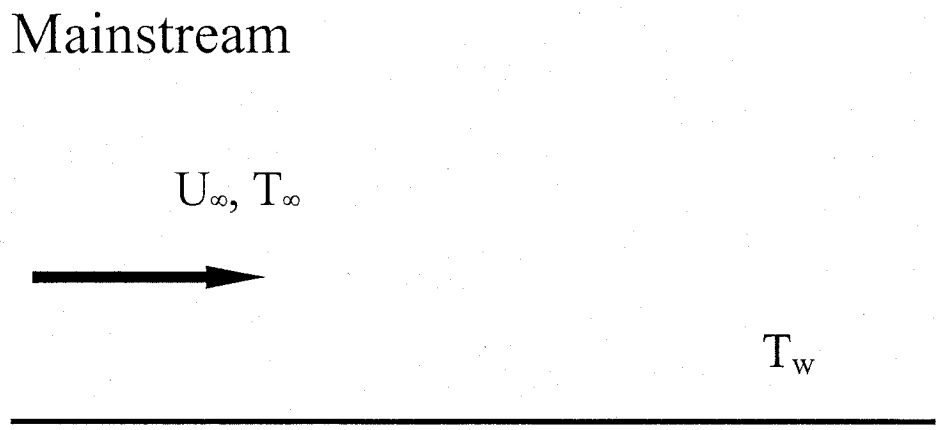

Figure 1.3 Schematic of a two-temperature convection problem.

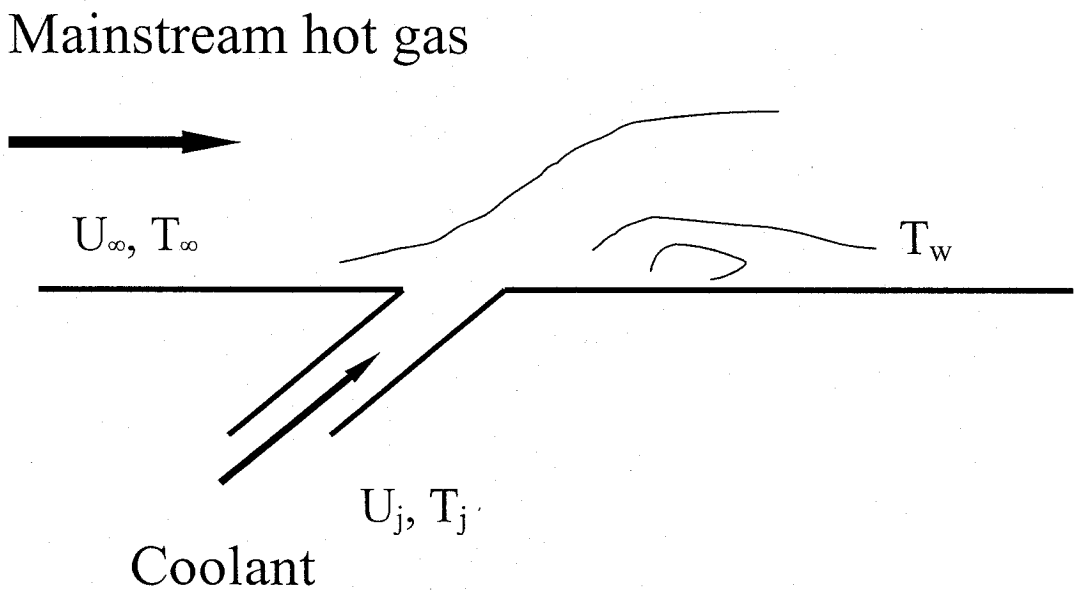

Figure 1.4 Schematic of a film cooling - 3 temperature problem.

$$q = h_f (T_{aw} - T_w) \tag{1.3}$$

or

$$h_f = \frac{q}{T_{aw} - T_w} \tag{1.4}$$

In an adiabatic wall with heated jets circumstance, q goes to zero, and the wall temperature (T_w) equals to adiabatic wall temperature (T_{aw}). Therefore, ($T_{aw} - T_w$) goes to zero, and so h will not be zero since h is supposed to be independent of temperature difference. The adiabatic wall temperature is usually presented in dimensionless form as the film cooling effectiveness, defined as:

$$\eta = \frac{T_{aw} - T_\infty}{T_j - T_\infty} \tag{1.5}$$

The value of η ranges from 0 to 1.0. Considering an adiabatic situation, if at one location the wall is well cooled, especially in the near hole area downstream of the jet, and the local wall temperature is close to the temperature of the jet, which means the wall is well protected, then the effectiveness will approach 1. On the other hand, if at another location, the coolant hardly reaches there and the local wall temperature is close to that of the mainstream, the wall is then totally exposed to the mainstream, and so the effectiveness will approach 0. In other words, the film cooling effectiveness indicates the degree of protection from film cooling.

The film cooling heat transfer coefficient h is a function of both the local wall temperature (T_w) and the local adiabatic wall temperature (T_{aw}). The adiabatic effectiveness η, on the other hand, is a function of only the local adiabatic temperature (T_{aw}). Hence, effectiveness is much easier to measure or calculate, which is why most

experimental and computational studies have focused on adiabatic film cooling effectiveness.

Chapter 2

Literature Review

2.1 Experimental Investigations

2.1.1 Adiabatic effectiveness

Goldstein et al. (1968) were among the first to study film cooling with injection through holes on a flat plate. A row of long jets with the length of 1 meter was used to guarantee the establishment of a well-defined velocity profile at the point of injection. The adiabatic effectiveness was found to be considerably different from that of two-dimensional continuous slots. Pedersen et al. (1977), utilizing the heat-mass transfer analogy, measured the adiabatic effectiveness with large density differences between the mainstream and the secondary fluid. Air was mixed with either helium, carbon dioxide, or refrigerant F-12, and was subsequently injected into the mainstream. The resulting local gas concentrations were measured on the wall instead of directly measuring the local temperature. It was shown that the film effectiveness was strongly dependent on the density ratio.

Bergeles et al. (1977) studied the injection of a single jet at 30° through a flat plate focusing mainly on the region immediately surrounding the injection hole, since the vicinity of the jet exit had, to that time, received little attention. Maximum effectiveness occurred when blowing ratio was about 0.5, and this was consistent with the results from other studies. For values of blowing ratio below 0.3, it was observed that the injected jet

remained attached to the surface, and so the effectiveness increased as blowing ratio increased. For values of blowing ratio above 0.5, the jet lifted off from the surface and penetrated into the mainstream thus decreasing the effectiveness as blowing ratio is augmented.

Dibelius, Pitt, and Wen (1990) examined the effects of injection angle (30, 45, and 90 degrees), film-hole spacing (2, 3, and 5 diameters), and blowing ratio (0.5, 1, and 2) on the film cooling effectiveness and aerodynamic losses for a row of slots and a row of film-holes. It was found that the area averaged film cooling effectiveness increased as the relative spacing and the injection angle decreased. As the blowing rate increased, the area averaged film cooling effectiveness increased continuously for slots, while for injection holes, it varied very differently from case to case. Also, the cooling effectiveness was always higher for injection slots than for injection holes under equivalent conditions.

Sinha et al. (1991) investigated the effect of density ratio on the film-cooling effectiveness with a geometry consisting of short holes and plenum. In order to eliminate the conduction error within the testing plate, styrofoam was used as an insulating material in order to construct the plate. Depending on the blowing ratio, the jets either remained attached to the testing surface, detached then reattached, or fully detached.

Schmidt et al. (1996) studied the effects of surface roughness on film cooling performance, and showed that rough surfaces degraded the film cooling effectiveness with increasing degradation farther downstream. Yuen et al. (2003) studied the film

cooling characteristics of a single round hole using the liquid crystal thermographic technique which is considered to be more accurate than the traditional thermocouple method. Unfortunately, the results were erroneous since the test surface was no longer adiabatic, and this was due to the presence of a very thin stainless steel foil on the surface, which was used in order to provide a constant heat flux. Therefore, the results for adiabatic effectiveness differ from those of Sinha et al. (1991).

Rhee et al. (2002) measured the local film-cooling effectiveness for a single row of rectangular-shaped holes with a 35° inclination angle and 3 hole diameter spacing. Four different hole shapes, including a straight rectangular hole, a rectangular hole with laterally expanded exit, a circular hole and a two-dimensional slot, are tested. A thermochromic liquid crystal technique is employed to determine adiabatic film cooling effectiveness. It is shown that the rectangular holes provide better performance than the cylindrical holes and the penetration of jet is reduced significantly for the rectangular holes with lateral expanded exit, thus higher cooling performance is obtained.

Sargison et al. (2002) documented the performance of a new geometry – a converging slot-hole or console. The cooling performance of a single row of consoles was compared with that of typical 35° cylindrical hole, fan-shaped holes and a slot on a flat plate. A good lateral uniformity of adiabatic effectiveness is attained with the new console geometry and the laterally averaged adiabatic effectiveness results are quite similar to those of slot. However, the aerodynamic loss due to a console is significantly less than for a cylindrical hole.

Nasir et al. (2003) investigated the effects of triangular tabs at the exit of a film-cooling hole on the performance of cylindrical angled holes. The 3 tab orientations investigated are: tabs parallel to the film cooled surface, tabs oriented downward at -45° and tabs oriented upwards at 45°. Transient liquid crystal technique was used to measure the temperatures on the test surface. Results show that tabs oriented downwards provide the highest effectiveness at low blowing ratio while the tabs oriented horizontally provides the highest film effectiveness at higher blowing ratio more than 1. The improvements are attributed to the generation of secondary vortices by the tabs with the vorticity counter to the kidney vortex pair. This results in a reduction of jet penetration and improvement in film-cooling effectiveness.

2.1.2 Heat transfer coefficient

Eriksen et al. (1971) studied the film cooling on a flat plate by using two methods to measure the heat transfer coefficient. The first method consisted of operating a wind tunnel using heated injection and a heated wall, and afterwards measuring the wall temperature T_w. Another test run was performed in order to obtain the adiabatic wall temperature T_{aw} by using the same test conditions with an unheated wall. As a result, the heat transfer coefficient could be calculated from the heated wall temperature and the adiabatic wall temperature. The second method used unheated injection and a heated wall. Since the temperature of injection is equal to the upstream temperature, the adiabatic wall temperature is the same as the upstream temperature, and so the heat transfer coefficient is defined using the difference between the heated wall temperature

and the free stream temperature. Thermocouples were used to obtain measurements for temperature. In this experiment, both methods yielded nearly identical results for most cases. However, in certain cases, the heat transfer coefficient results given by these two methods was not very close, with an error of 5%, sometimes even 12%, in the near hole region. Since the first method is more complicated and difficult to implement, the second method, with unheated injection and heated wall, is widely used by most researchers.

Goldstein et al. (1982) showed that conduction in the spanwise or z- direction would tend to smooth out the measurements of effectiveness and heat transfer from their true distribution when stainless steel heater foils are employed in construction of constant heat flux plate. Thus, the lateral distribution can only be used for qualitative discussion. In another paper by the same author (1999), a special naphthalene sublimation technique and heat/mass transfer analogy was implemented to determine the film cooling performance. While the film cooling effectiveness results agreed with previous results, the heat transfer coefficient results did not due to conduction effects in the region of large temperature gradients.

Sen et al. (1996) presented the heat transfer coefficient for film cooling with compound angle holes. The constant heat flux plate in this case consisted of a 0.08-mm-thick serpentine model heating element embedded in a 0.18-mm-thick insulating Kapton film. As a result, the heat transfer coefficient distributions were slightly different than those of Eriksen (1971). Yuen et al. (2003) measured both the heat transfer coefficient and adiabatic effectiveness for a single jet with streamwise angles of 30, 60, and 90 degrees.

The same method as Eriksen et al. (1971) was applied in the experiment except for some differences. To generate a constant heat flux wall condition, a very thin stainless steel foil (0.2 mm) was placed on top of the convective heat transfer test surface, which was heated beneath by Inconel strips. On the other hand, Eriksen et al. (1971) used the stainless steel sheet directly as the heater by passing electrical current through it. Also, instead of using thermocouples, the liquid crystal thermography technique was employed in order to capture the wall temperatures. Generally speaking, the liquid crystal technique is thought to be more accurate than thermocouples, however, the results obtained were not close to those of other researchers with differences up to 20 to 60 percent, especially in the near hole region.

Di Ai et al. (2001), Vogel et al. (2003), Yu et al. (2002), Nasir et al. (2003) used the transient measurement technique to study film cooling by using a CCD camera to capture the wall temperatures. Doing so, avoids any use of instrumentation for constant heat flux, which may lead to more accurate results. In addition, it has been demonstrated that the transient liquid crystal technique is an effective means of experimentally examining film cooling performance.

Rhee et al. (2002) investigated film-cooling geometry with focus on rectangular-shaped film holes. Thermochromic liquid crystals were applied to determine heat transfer coefficients on the test surface. Their results indicate that, after a certain distance from the hole, the heat transfer coefficient was not significantly affected by the hole geometry. At low blowing ratio, the heat transfer coefficients for the circular hole were highest

among the geometry tested, while at high blowing ratio (m > 1.5), the rectangular holes have higher heat transfer coefficient due to the fact that near wall region is affected more significantly by the kidney-vortices. For the downstream region (x/d > 12), the spanwise averaged heat transfer coefficients increased slightly with the increasing blowing ratio.

2.2 Computational Investigations

2.2.1 Mesh

Patankar et al. (1977) implemented a fully elliptic finite-difference procedure to analyze situations of large blowing ratio (from 2 to 10) for a single, normally injected round film-hole. A high-Reynolds number version of the k-ε turbulence model described by Launder and Spalding (1974) was used, and their results were in fairly good agreement with experimental data. However, due to the costly nature of computing a fully elliptic scheme, it was necessary to use a low-resolution grid. The mesh consisted of 10 x 15 x 15 grid points, for a total of 2250 grid points, with more grid points being concentrated around the film hole. Only six cells were used to represent the film-hole.

Bergeles et al. (1978) modified the numerical procedure used by Patankar et al. (1977) and adapted it to suit low injection velocities only. This partially parabolic scheme, which the authors called semi-elliptic, required only a small fraction of computer resources for the complete three-dimensional discretization of the equations of motion. Due to the nature of this procedure, only relatively low blowing rates (0.1 for normal injection and 0.5 for 30° streamwise injection) could be used, since at low injection rates, the recirculation zone following the film-hole was so weak that neglecting it from the

numerical treatment would still produce reasonable results. Results were compared for grid sizes of 10 x 10, 15 x 15, and 19 x 19, and it was found that although the 10 x 10 array produced a nearly grid-independent distribution of streamwise velocity, a 19 x 19 array was needed to resolve the velocity normal to the plate. For the case of 30 degree injection, predicted results of velocity fields and film cooling effectiveness were in good agreement with experiments for blowing rates up to 0.5. However, in the normal injection case (90 degrees), results agreed with experimental data only up to a blowing rate of 0.1. They also found that the standard k-ε model, which assumes an isotropic eddy viscosity, was inadequate for the geometry tested.

Demuren and Rodi (1983) performed a computational study of the effect of varying the mainstream turbulence intensity for a row of round jets inclined at 35 degrees. They used a mesh consisting of 66, 41, and 14 grid points in the streamwise, heightwise, and spanwise directions, respectively. There was good agreement between the predicted and measured velocity contours. The temperature predictions agreed fairly well with experimental data at a turbulence intensity of 8.2%. The trends correctly predicted at the lower turbulence intensity, although the observed bifurcation of the jet was not reproduced as strongly. The results of film cooling effectiveness near the film-hole were good for the case of 8.2% turbulence intensity, while for the 4.8% turbulence intensity case, the results differed from experimental data. On the other hand, the results of film cooling effectiveness were in better agreement farther downstream.

Walters and Leylek (1996) applied a systematic computational methodology to the study of a row of three-dimensional round jets with 35° streamwise injection. Solutions were obtained using a multi-block, unstructured/adaptive grid with a fully explicit, time marching, Reynolds-averaged Navier-Stokes code. Grid independence was achieved with approximately 200 000 grid points. However, the method could not capture the jet lift-off and reattachment due to the coarseness of the grid in this region, since a minimum cell size is imposed by the use of wall functions used to obtain near-wall turbulence quantities.

2.2.2 Geometries and parameters

Andreopoulos et al. (1982) showed that the jet and mainstream interact strongly together, and that this interaction cannot be ignored when the computational domain is chosen. It is therefore necessary for the domain to include part of the region upstream of the film-hole exit.

Schönung and Rodi (1987) studied film cooling from a row of holes over flat plates as well as for gas turbine blades for different injection angles, relative film-hole spacings, blowing rates, and injection temperatures using a special two-dimensional boundary layer code. The influence of the different parameters on the film cooling effectiveness was predicted correctly and the quantitative agreement was satisfactory, except for configurations with low blowing rate. For these cases, curvature effects were observed to be important, but were not accounted for in their model. In general, the predicted heat transfer coefficients were in good agreement with experimental data, except for certain

configurations with large relative spacing and high blowing rates. In these cases, the model highly overpredicted the heat transfer coefficient in the near hole region.

Sathyamurthy and Patankar (1990) numerically investigated the effects of lateral injection angle (0, 45, and 90 degrees), film-hole spacing (3 and 5 diameters), and blowing rate (0.1, 0.2, 0.5, and 1) on the film cooling effectiveness for an infinite row of elliptic holes possessing a streamwise injection angle of 30 degrees. It was found that increasing lateral injection angles, increasing blowing rates, and reducing film-hole spacing all increased the laterally averaged film cooling effectiveness. Also, for laterally injected coolant, the laterally averaged film cooling effectiveness did not begin to decrease as blowing rates increased above 0.5, contrary to the case for streamwise injection. This means that lateral injection can operate at much higher blowing rates to achieve a better film cooling coverage than simple streamwise injection at comparable blowing rates.

Kim and Benson (1992) used a multiple-time-scale turbulence model in order to account for the non-equilibrium turbulence in a round hole discharging normally into the crossflow. They discretized the flow domain with 148, 61, and 94 grid points in the streamwise, spanwise and heightwise directions, respectively. The multiple-time-scale model correctly resolved the non-equilibrium turbulence created by the strong interaction of the jet and mainstream, and it was found that the turbulent transport of mass, momentum, and concentration depended strongly on this type of turbulence. The strong interaction between the jet and crossflow at the film-hole exit was also shown to

influence the flow and turbulence fields in the upstream region. In fact, it was found that the state of non-equilibrium turbulence is stronger in the upstream region than in the downstream region. This suggested that the upstream region must be included in the computational domain in order to obtain accurate numerical results and to properly evaluate the predictive capabilities of a turbulence model. Also, it was observed that the jet velocity, static pressure, and total pressure varied widely over the cross-section of the jet. This indicated that the use of a fixed boundary condition at the jet exit could possibly produce incorrect results.

Leylek and Zerkle (1993) analyzed a row of film-holes inclined at 35 degrees to the mainstream on a flat plate. They included the plenum and film-hole regions, as well as the crossflow region, in their computational domain. They used a total of 200 090 grid nodes, with 22 nodes in the lateral, 85 nodes in the vertical, and 107 nodes in the streamwise directions. Their study showed that the flow within the film-hole is extremely complex, containing counter-rotating vortices and local jetting effects. As Kim and Benson (1992) suggested, it is therefore incorrect to specify boundary conditions for the film-hole exit, or even the film-hole entrance. The best method is to simulate the plenum and film-hole regions along with the crossflow region. Turbulence closure was attained with the use of the standard k-ε turbulence model with generalized wall functions.

Ajersch et al. (1995) studied a row of six square jets injected at 90° to the crossflow using a multigrid, segmented, k-ϵ code with special near-wall treatment. The results indicated that the vertical velocity at the jet exit plane is non-uniform, especially at low velocity

ratios, which supports the conclusions of Leylek and Zerkle (1993) about including the injection pipe and plenum in the computational domain.

Garg et al. (1999, 2001, 2002) demonstrated that higher resolution of the grid normal to the hole-rim did not necessarily result in better prediction of the film cooling effect on the blade surface. It was concluded that different velocity and temperature distributions of coolant at the hole exit can lead to as much as a 60% change in the heat transfer coefficient at the blade surface. Therefore, accurate predictions of the heat transfer coefficient require that the region inside the cooling hole-pipes and the plenum within the airfoil be included.

Berhe and Patankar (1996) conducted three computational tests, each case with varying streamwise injection angle, blowing ratio, density ratio, film-hole length, and plenum flow. Results show generally good agreement with experiments. The laterally averaged effectiveness values were generally underpredicted due to the poor lateral spreading of the turbulence model. The authors found higher centerline effectiveness in the near-field with a length-to-diameter ratio of 4.9, and higher centerline effectiveness in the far-field for a ratio of 2.8. It was found that when the plenum height is greater than twice the film-hole diameter, the flow direction within the plenum has no influence on the film cooling effectiveness. They also found that the turbulence levels at the inlet to both the plenum and the mainstream have no effect on film cooling effectiveness.

Hyams et al. (1996) studied the physics of the film cooling process for shaped, inclined slot-jet. They varied the blowing ratio (from 1.0 to 2.0), the density ratio (from 1.5 to 2.0), and the slot length-to-width ratio (3.0 and 4.5). The non-dimensional distance y+ along the upstream and downstream wall, as well as inside of the slot, was maintained between 20 and 30, and the standard k-ϵ model with generalized wall functions was used for all the computational simulations. In turn, excellent agreement between predicted and measured data for all of the benchmark cases was obtained. This is great feat considering the fact that even with today's far more powerful computers, the technical community still struggle to capture the right trends as far as film-cooling effectiveness or heat transfer is concerned. It can be concluded that shaping both the slot exit and inlet can consistently increase effectiveness and decrease the heat transfer coefficient, and therefore improve film cooling performance. However, the conclusion that CFD can be successfully and practically applied as a design tool seems premature.

McGovern et al. (1997) investigated the dominant flow mechanisms responsible for film cooling performance with compound angle injection. The CFD solver by Fluent Inc. was used to perform actual CFD analysis with three strict convergence criterions: global mass and energy imbalances below 0.01%, residuals below 0.1% and dependent variables monitored in important areas not changing with further iterations. The vortex structure created by the interaction of the jet and the crossflow was found to dominate the film cooling performance by enhancing the mixing of the coolant and crossflow as well as by enhancing the lateral spreading of the coolant. Compound-angle injection significantly

altered the heat transfer coefficient such that it was augmented in all the cases due to the compounding effects.

Rhee (2002) investigated film-cooling geometry with focus on rectangular-shaped film holes. A thermochromic liquid crystals technique was applied to determine the heat transfer coefficients on the test surface. Numerical simulations were conducted using the commercial software package Fluent with the computational domain matching exactly the geometry used in experimental study. Their results indicate that the heat transfer coefficient is affected little by the hole geometry after a certain distance from the hole. At low blowing ratio, the heat transfer coefficients for the circular hole show the highest level among the geometry tested, however, at high blowing ratio (m >1.5) the rectangular holes have higher heat transfer coefficient than the cylindrical holes due to the fact that near wall region is affected more significantly by the kidney-vortices.

The present study is an extension of the work performed by Immarigeon (2004) in which the novel cooling scheme was introduced. Like most others in the literature, unstructured meshes were used in the simulations and the tetrahedron elements were adapted to change the y^+ value near the wall so that the near wall mesh requirements were strictly met. However, since it is very difficult to control the distribution of the elements, a large percentage of the elements were put in the far field region, and as a result, the benchmark case failed to capture the jet liftoff effect despite the fact the y^+ value issue was handled appropriately.

2.2.3 Turbulence models

Amer et al. (1992) compared four different turbulence models in a study of film cooling from two rows of elliptic holes inclined 30° in the streamwise direction. The film cooling effectiveness and velocity fields for both the standard and modified forms of the k-ε and k-ω turbulence models were compared. It was found that the ability of a turbulence model to predict experimental results depended on the blowing rate and on the distance away from the hole in the downstream direction. They concluded that each model performed well for certain situations, but that no model is suitable for all situations. The standard k-ω model tends to predict film-cooling effectiveness better at higher blowing rates than the other three models. The modified k-ε predicted effectiveness better than the standard k-ε for low blowing rates. The two k-ε models predicted similar values of average film cooling effectiveness, while the two k-ω models give identical values. Both versions of the k-ω model tended to poorly predict the velocity profiles for almost all blowing rates and locations downstream.

Zhou et al. (1993) examined a single row and two staggered rows of 30° streamwise injected round film-holes with a relative spacing of 4 diameters and lateral injection angles of 0 and 90 degrees. Since the k-ϵ model with standard wall functions limits the accuracy of the solution near the wall, they only used this model in regions away from the wall. The low-Re number k model given by Rodi et al. (1991) was used in the viscosity-affected regions near the wall. Results were compared with experimental work, and good agreement was shown at low mass flow ratios (0.2 and 0.4), yet differed significantly at the higher mass flow ratio (0.8). This disagreement was attributed to

deficiencies in the turbulence model. Their results show that lateral injection performed better, mainly near the film-hole, when compared to non-lateral injection.

Fukuyama et al. (1995) studied the mid-span film cooling effectiveness for single and double row injection. For the case of single row injection, the film cooling effectiveness for low blowing ratios (less than 0.5) agreed well with experiments. However, with increasing blowing ratio, this agreement diminished. For high blowing ratio, there was a tendency to underpredict the film cooling effectiveness in the near hole region and to overpredict it in the far downstream region. The influence of film-hole locations on the distribution pattern of film cooling effectiveness was well predicted. In the double row injection case, the film cooling effectiveness downstream of the second row was strongly enhanced by the presence of the upstream row, which was not observed in the experiments.

Walters et al. (1995) applied a novel methodology to a 2-D slot jet issuing normally into a crossflow, since simulations documented in the open literature suffered from deficiencies in four main areas: computational modeling, mesh system, discretization methods, and turbulence models. It was shown that errors introduced by an improper computational model could be significantly greater than those of turbulence model. Therefore, the turbulence model performance cannot be evaluated easily until its effects are isolated from those of the computational model, grid, or discretization scheme. It was found that heat transfer characteristics were insensitive to the turbulence model. Ironically, a simulation with a highly skewed coarse grid, low order discretization and

improper turbulence model may accidentally predict a certain value, for example h, very close to the experimental ones. However, that coincidence would unlikely occur if applied to another geometry.

Ferguson et al. (1998) studied jet-in-crossflow with attempts to isolate and analyze the true performance of several turbulence models and three near wall treatments. The three different near-wall treatments tested were the generalized wall functions, non-equilibrium wall functions, and the two-layer zonal model. The two-layer zonal model produced solutions more consistent with experimental results than the other wall treatment functions. The standard k-ϵ model performed better than the RNG and RSM models. In another investigation by Walters et al. (2000), particular attention was paid to the coolant structure as well as to the source and influence of counter-rotating vortices in the crossflow area with the goal of documenting the essential flow physics associated with jet-in-crossflow. In general, the wall function approach is good, except that it does not capture small-scale flow features. A selective application of the different turbulence models to different locations of the domain was recommended.

Hale (1999) studied short-hole film cooling performance with counter-flow and co-flow plenum both experimentally and numerically. By analyzing the experimental results and the numerical predictions, he concluded that the computational model was still inadequate for making detailed predictions of heat transfer coefficients downstream of the jet. However, the model does a good job of predicting the centerline effectiveness. In many instances, the effects of one parameter were not easily isolated from those of

another. Therefore, the relative performance of a film cooling configuration is dependent on the combination of the parameters. It is important to note that higher effectiveness values do not necessarily mean a better film cooling performance if heat transfer coefficients are not taken into account. It was demonstrated that the two-layer zonal model was capable of capturing the complex three-dimensional separation and recirculation region downstream of the jet, while the wall functions can not. The incapacity of the computational model to predict the surface heat transfer coefficient, with an over-predicted error between 40 and 100% for the spanwise-averaged heat transfer coefficient and associated local errors up to 300% for heat transfer coefficient, was attributed to deficiencies in the near-wall treatment.

Tyagi and Acharya (1999) performed large eddy simulations of rectangular jets in crossflow. They concluded that the anisotropy in the flow turbulence is not the major contributor to the lack of agreement. Instead, the discrepancy arises from the inability of these models to capture the effects of large scale unsteadiness in the near hole field. It was shown that the turbulence models did not accurately predict the near hole field statistics.

Hoda et al. (2000) compare a number of turbulence models in their predictions of film cooling effectiveness for a row of square holes injected normal to the mainstream. A non-uniform staggered grid of 59 x 60 x 140 points was used since it yielded grid independent results. They compare two Reynolds Stress Transport models (RST) with predictions using the k-ϵ model of Lam and Bremhorst (1981) and with Large Eddy Simulations

(LES) predictions. In general, the predictions of mean flow velocity and turbulent kinetic energy made by the RST models did not show any significant improvements when compared with the standard k-ϵ model.

Gartshore et al. (2001) performed a comparative computational analysis of the film-cooling effectiveness for 45° compound-oriented square and round holes placed, alternatively, in a plane wall with an inclination of 30°. Numerical simulations were conducted using the standard k-ϵ turbulence model, along with blowing ratios of 0.5, 1.0, and 1.5. The authors found that near the film-hole, and only at low blowing ratios, the square holes performed slightly better. However, for the higher blowing ratios and farther downstream, the round holes were superior. The results for the lowest blowing ratio were in fair agreement with experimental data, while those for higher blowing ratios differed significantly.

As a viable alternative, Kapadia et al. (2003) presented a Spalart-Allamaras based detached eddy simulation (DES), which was applied to a film cooled flat plate. DES combines LES and RaNS (Reynolds average Navier-Stokes) in such a way that RaNS technique can be used for the flow in thin shear layers and LES can be used for large separated zones. They reported that the DES simulation, which makes no assumption of isotropy downstream of the hole, captured the description of the dynamic flow structures best. The results for the centerline adiabatic effectiveness distribution are the only curves in the open literature that do not monotonically decrease in the streamwise direction.

Since the native k-ϵ or k-ω models can give extremely unreasonable predictions of heat transfer in turbine passages, Medic and Durbin (2002) attempted a new approach by simply modifying the native models in the following manner. The turbulence model, two layer k-ϵ, standard and modified k-ω and v^2-f, were implemented into an implicit finite volume solver based on a variant of the well-known SIMPLE method. In comparison with the native k-ϵ model, which grossly overpredicts heat transfer in the downstream region, the modified models yielded satisfactory predictions of the overall heat transfer coefficient level, except for at high blowing ratios, which lead to the jet lift off from the wall. They believed that excessive levels of turbulent kinetic energy are predicted by standard two-equation models in regions of large rate of strain. Anomalous turbulent energy was fixed by the modification of production and time-scale bound. A limiter was applied to the turbulent time scale only in the high Reynolds region. Despite the fact that their modification lacked any physical meaning, this simple modification did improve predictions substantially. Their explanation was that by implementing this limiter, spurious turbulence energy production by the turbulence model could be prevented.

Lakehal (2002) computed the jets in crossflow by solving the governing equations using a three-dimensional finite volume method. Direct Numerical Simulation (DNS) method was employed with a novel development in the modeling practice such that the anisotropy of turbulent transport coefficients for all transport equations are included in the turbulence model since isotropic turbulence models are not adequate for this class of flow with the lateral spreading of the heat flux being systematically underpredicted. The anisotropy correction method improved the accuracy of the computational study.

However, agreement with the measurements deteriorated with increasing mass flux ratio, and the laterally averaged film cooling effectiveness was generally too low due to the underpredicted lateral spreading of the temperature field by the two-layer k-ϵ model.

2.3 Summary

In order to increase their efficiency, the inlet temperatures of gas turbines have been raised significantly in the last three decades. Modern gas turbine engines typically operate at inlet temperatures of 1800-2000 K, which is far beyond the allowable metal temperature. Film cooling becomes increasingly important in the aerospace industry in cooling of the turbine blades. Many experimental and computational studies have been conducted in order to study the cooling process of gas turbine blades, understand this complex flow and heat process, and devise the best possible cooling schemes.

Methods that have been mainly investigated include heat transfer and film cooling (Hyams and Leylek, 2000, Cho et al. 2001, Gartshore et al., 2001, Goldstein et al., 2001, Cutbirth and Bogard, 2002, and Yuen 2003), impingement cooling (Son et al., 2001, Taslim et al., 2001, and Li et al., 2001), and advanced internal or external cooling (Azad et al., 2000, and Taslim et al., 2001). These methods are commonly studied with the following parameters: injection orientations (Brittingham, et al., 2000, Jung et al., 2000, Gritsch et al., 2001 and Dittmar et al., 2003), hole length (Burd et al., 1998, and Harrington et al., 2001), free stream turbulence (Ekkad et al., 1998, Al-Hamadi et al., 1998, Maiteh and Jubran, 1999, Mayhew et al., 2003, and Saumweber et al., 2003), hole entrance effects (Hale et al., 2000, Wilfert and Wolff, 2000, Brittingham and Leylek,

2000, Gritsch et al., 2003), hole exit tapering (Kohli and Bogard, 1999, and Sargison et al., 2002, Nasir et al., 2003), hole exit expanding (Yu et al., 2002, Rhee et al., 2002, Sargison et al., 2002, Gritsch et al., 2003, York and Leylek, 2003, and Kim and Kim, 2004), surface roughness (Schmidt et al., 1996) and density ratio effects (Ammari et al., 1990, Ekkad et al., 1998,), measurement techniques (Sen et al., 1996, Goldstein et al., 1999, Di Ai et al., 2001, Baldauf, et al., 2002, Vogel et al., 2003, Cho et al., 2001, Yuen and Martinez-Botas, 2003). Only key references have been given here, and earlier reports may be traced through the reference lists of the papers cited. From these reports and their references, some broad generalizations can be made about the methods, geometries, and conditions affecting the performance of internal or external cooling schemes of gas turbine blades:

2.3.1 Adiabatic effectiveness

- Hole geometry is an important parameter for film cooling performance. Laterally-and-forward-expanded holes provide higher values of spanwise averaged effectiveness than laterally-expanded holes. Flared holes have the best overall performance, especially at high blowing rates. Compound angle injection, whether for shaped or circular holes, leads to an increase in spanwise averaged effectiveness compared to that obtained with standard circular holes.
- For standard circular holes on a flat surface with low mainstream turbulence intensities, the downstream effectiveness is optimum for blowing ratios of approximately 0.5. For blowing rates above this value, the coolant jet undergoes lift-off. This allows the hot gases to come in contact with the surface, which

causes the effectiveness to decrease. The jet lift-off effect is not captured at all in the predictions. This is attributed to many factors such as the deficiency of turbulence models, the use of isotropic eddy viscosity models, the presence of recirculation region, as well as the use of wall functions. The effectiveness in the spanwise direction is systematically underpredicted.

- Compound angle injection, whether for shaped or circular holes, leads to an increase in spanwise averaged effectiveness compared to that obtained with standard circular holes. Hole spacing affects the ability of adjacent jets to coalesce. Small hole spacing results in better coverage of the wall, and thus higher effectiveness values than larger ones. A pitch-to-diameter ratio of 3 was commonly used in film cooling studies. An increase in mainstream turbulence intensity decreases the spanwise averaged adiabatic film cooling effectiveness due to the enhanced mixing of the mainstream and coolant flow. Rough surfaces degraded the film cooling effectiveness with increasing degradation farther downstream.
- Due to the speed of computer early computational study of film cooling was confined to 2 dimensional or 3 dimensional with small meshes in the order of thousand nodes. Only in the last 2 decades did the powerful computer make it possible to use a mesh with the size in the order of millions of cells. It is necessary to include the plenum and film hole in the computational domain in order to ensure a realistic profile at the exit of the jet, and to account for the interaction between the mainstream, the jet, and the plenum.

- Different turbulence models have been applied to a variety of experimentally measured cases and the predictions vary significantly with different turbulence models. Of the several near wall treatments, two-layer wall treatment produced more consistent solution than the standard wall or non-equilibrium wall functions. The higher order discretization scheme results in less numerical diffusion and yields more accurate results than the lower order scheme.

2.3.2 Heat transfer coefficient

- At both high and low blowing ratio, for traditional cylindrical hole, the heat transfer asymptotically approaches $h_f/h_o = 1$ for $x/d > 10$. The magnitude of h_f/h_o increases with increasing blowing ratio. Higher blowing ratio causes high penetration and mixing with the mainstream, resulting in an enhanced heat transfer coefficient and reduced lateral jet spread. The heat transfer coefficient decreases rapidly for the first 10 diameters downstream of the hole, then gradually decreases farther downstream.
- Holes with expanded exits have lower heat transfer coefficients at elevated blowing ratios when compared to cylindrical holes. Variation of the relative spacing or the free-stream turbulence level resulted only in slight changes of the heat transfer coefficient. Increasing the mainstream turbulence intensity results in an increase in the local heat transfer level, especially at low blowing ratio.
- The magnitude of the heat transfer coefficient along the centerline is the lowest for any given hole geometry and the greatest around the side-edge of an injection hole due mainly to the interaction between the injection and the mainstream.

Normal jets penetrate deeper and interact more with the mainstream, resulting in higher heat transfer coefficients. With inclined jets, the interaction with the mainstream is lower, and shows less of an increase in heat transfer.

- In contrast to the fact that all the results of adiabatic effectiveness from different researchers are similar to one another, the results of the heat transfer coefficient by different researchers vary widely depending on how the constant heat flux is instrumented. Conduction error in the spanwise direction on the test surface is much larger than believed and would tend to smooth out the heat transfer from their true distribution when stainless steel heater foils are employed in construction of constant heat flux plate.
- Geometry and mesh system exert considerable influence on the numerical solutions. The effect of the geometry and the mesh on the solution could be so large that the performance of the turbulence models and wall treatments can be completely masked and their performance cannot be accurately evaluated.
- The numerical simulation is not very reliable and predictions vary significantly with the different turbulence models. The incapacity of the computational model to predict the surface heat transfer coefficient, with an over-predicted error between 40 and 100% for the spanwise-averaged heat transfer coefficient and associated local errors up to 200% for local heat transfer coefficient, was attributed to deficiencies in the near-wall treatment and turbulence modeling.

2.4 Objectives and Contributions of this study

The literature survey shows that the jet-in-cross flow is quite complicated, consequently, the simulations usually do not agree very well with the experimental data. In many efforts to evaluate the performance of different turbulence models or wall treatments in film cooling application, numerical errors usually were too large to allow clear conclusions to be drawn. The quality of the mesh plays such an important big role in determining the solution, that the performance of turbulence models could be completely masked. As a result, a poor quality mesh could accidentally produce excellent results. Lack of consistency is prevalent and the reliability of many methods in CFD analysis for film cooling is seriously in doubt. Before numerical simulation of jet-crossflow becomes reliable, designers will still have to rely heavily on the basis of empirical correlation, as well as industry proprietary test data.

The objectives of this study are as followings:

1. Develop a reliable methodology and procedure of simulating the jet-in-crossflow using the current turbulence models which can be successfully utilized in the real design process.
2. Evaluate the performance of different turbulence models as well as different wall treatments in film cooling applications.
3. Numerically investigate the cooling performance of a new scheme for the engines of next generation.

This study will systematically explore the predictive capacity of the current turbulence models in film cooling applications in terms of both adiabatic effectiveness and heat transfer coefficient. In order to establish a new methodology, extensive numerical simulations will be carried out on two benchmark cases of simple geometry, long jets without plenum and short jets with plenum. The new methodology established in the two benchmark cases will then be applied to a new scheme. Compared with the traditional circular hole, the new scheme combines both the advantages of traditional film cooling and with those of impingement cooling. The hole that transports coolant fluid from the inside to the outside of the blade is designed in such a way that the coolant must go through a bend before exiting the blade, thus impinging on the blade material. The flared hole exit was also designed to reduce the coolant momentum and ensure wide lateral spreading of the coolant on the downstream surface. This scheme is expected to produce the greatest coverage of the blade with the least amount of mixing, and using the least possible amount of coolant.

For the first time in the literature (to the best knowledge of author) of film cooling simulations, the jet liftoff effect in the traditional cylindrical hole is undoubtedly captured and the possible reasons are given. The present study, through modeling conjugate heat transfer cases, has also showed that conduction errors on the test surface are much larger than believed in previous experimental investigations. The proposed cooling scheme gives considerable higher adiabatic effectiveness and lower heat transfer coefficient at the centerline in the near hole region than the traditional cylindrical hole, especially at high

blowing ratio when traditional cylindrical hole undergoes liftoff and in the spanwise direction as well, thus provides more efficient protection over the surface.

Chapter 3

Mathematical Modeling

3.1 Conservation equations

The assumptions made for the flow are identical to those used in experiments, and are as follows: (1). three-dimensional steady state; (2). incompressible; (3). viscous; (4). Newtonian flow; (5). turbulent; (6). single phase (air); (7). no source of fluid or heat generation in the domain; (8). gravitational force negligible.

The flow is governed by the Navier-Stokes, or conservation equations, and under the above assumptions, the conservation equations of continuity, momentum and energy become:

Continuity:

$$\nabla \cdot (\rho \vec{v}) = 0, \tag{3.1}$$

Momentum:

$$\nabla \cdot (\rho \vec{v} \vec{v}) = -\nabla p + \nabla \cdot (\bar{\bar{\tau}}), \tag{3.2}$$

where

$$\bar{\bar{\tau}} = \mu \left[(\nabla \vec{v} + \nabla \vec{v}^{T}) - \frac{2}{3} \nabla \cdot \vec{v} I \right], \tag{3.3}$$

Energy:

$$\nabla \cdot \left[\vec{v}(\rho E + P)\right] = \nabla \cdot \left[k_{eff} \nabla T + \left(\bar{\bar{\tau}}_{eff} \cdot \vec{v}\right)\right]. \tag{3.4}$$

3.2 Turbulence modeling

Turbulent flows are characterized by fluctuating fields of small scale and high frequency, which are very computationally expensive in engineering calculations. To make the equations easier to solve, the instantaneous governing equations have been time-averaged to remove the small scales, and as a result, new unknown variables have been created. These unknown variables have been defined differently in terms of known quantities, and have given rise to various turbulence models. When considering all types of problems, no single turbulence model is deemed superior over the others.

In Reynolds averaging, the variables in the instantaneous Navier-Stokes equations are decomposed into mean and fluctuating components. For example, the velocity components can be expressed as:

$$u_i = \bar{u}_i + u_i', \tag{3.5}$$

where $\bar{u}_i$ and u_i' are the mean and fluctuating velocity components respectively.

Substituting all new flow variables into the instantaneous continuity and momentum equations and dropping the overbar yields the so-called Reynolds-Averaged Navier-Stokes (RANS) equations:

$$\frac{\partial}{\partial x_i}(\rho u_i) = 0, \tag{3.6}$$

$$\frac{\partial}{\partial x_i}\left(\rho u_i u_j\right) = -\frac{\partial p}{\partial x_i} + \frac{\partial}{\partial x_j}\left[\mu\left(\frac{\partial u_i}{\partial x_j} + \frac{\partial u_j}{\partial x_i} - \frac{2}{3}\delta_{ij}\frac{\partial u_l}{\partial x_l}\right)\right] + \frac{\partial}{\partial x_j}\left(-\rho\overline{u_i' u_j'}\right). \tag{3.7}$$

These equations have the same general form as the instantaneous Navier-Stokes equations, with the variables now representing time-averaged values. Additional terms now appear, such as $\overline{\rho u_i' u_j'}$, which represent the effect of turbulence and must be modeled in order to close the equations. The most common method employs the Boussinesq hypothesis, which relates the Reynolds stress to the mean velocity:

$$-\overline{\rho u_i' u_j'} = \mu_t \left(\frac{\partial u_i}{\partial x_j} + \frac{\partial u_j}{\partial x_i} \right) - \frac{2}{3} \left(\rho k + \mu_t \frac{\partial u_i}{\partial x_i} \right) \delta_{ij} \tag{3.8}$$

This equation is used in the k-ϵ models, the k-ω models, and the Spalart-Allmaras model. In the present work, four classes of turbulence models have been selected in order to perform the simulations by solving the Reynolds-averaged Navier-Stokes equations, and they are the Spalart-Allmaras model, the k-ϵ models (including its 3 variants), the k-ω models, and the Reynolds Stress models.

3.2.1 Spalart-Allmaras Model

The Spalart-Allmaras Model proposed by Spalart and Allmaras (1992) is a one-equation model which solves a transport equation for the kinetic turbulent viscosity. The transport equation for kinematic viscosity $\tilde{\nu}$ is

$$\frac{\partial}{\partial x_i}(\rho \tilde{\nu} u_i) = G_\nu + \frac{1}{\sigma_{\tilde{\nu}}} \left\{ \frac{\partial}{\partial x_j} \left[(\mu + \rho \tilde{\nu}) \frac{\partial \tilde{\nu}}{\partial x_j} \right] + C_{b2} \rho \left(\frac{\partial \tilde{\nu}}{\partial x_j} \right)^2 \right\} - Y_\nu \tag{3.9}$$

where G_ν and Y_ν are the production of turbulent viscosity and the destruction of turbulent viscosity, respectively. $\sigma_{\tilde{\nu}}$ and C_{b2} are constants. ν is the molecular kinematic viscosity. The turbulent viscosity is computed as

$$\mu_t = \rho\tilde{\nu} f_{v1} \qquad f_{v1} = \frac{\chi^3}{\chi^3 + C_{v1}^3} \qquad \chi \equiv \frac{\tilde{\nu}}{\nu}$$

G_ν is computed as

$$G_\upsilon = C_{b1}\rho\tilde{S}\tilde{\nu} \qquad \tilde{S} \equiv S + \frac{\tilde{\nu}}{\kappa^2 d^2} f_{v2} \qquad f_{v2} = 1 - \frac{\chi}{1 + \chi f_{v1}}$$

C_{b1} and κ are constants and d is the distance from the wall. S is found from

$$S \equiv \left|\Omega_{ij}\right| + C_{prod} \min\left(0, \left|S_{ij}\right| - \left|\Omega_{ij}\right|\right) \qquad C_{prod} = 2.0 \qquad \left|\Omega_{ij}\right| \equiv \sqrt{2\Omega_{ij}\Omega_{ij}}$$

$$\left|S_{ij}\right| \equiv \sqrt{2S_{ij}S_{ij}} \qquad \Omega_{ij} = \frac{1}{2}\left(\frac{\partial u_i}{\partial x_j} - \frac{\partial u_j}{\partial x_i}\right) \qquad S_{ij} = \frac{1}{2}\left(\frac{\partial u_j}{\partial x_i} + \frac{\partial u_i}{\partial x_j}\right)$$

Y_ν is computed as $\quad Y_\nu = C_{\omega 1}\rho f_\omega \left(\frac{\tilde{\nu}}{d}\right) \qquad f_\omega = g\left(\frac{1 + C_{\omega 3}^6}{g^6 + C_{\omega 3}^6}\right)^{1/6}$

$$g = r + C_{\omega 2}\left(r^6 - r\right) \qquad r \equiv \frac{\tilde{\nu}}{\tilde{S}\kappa^2 d^2}$$

$C_{\omega 1}$, $C_{\omega 2}$, and $C_{\omega 3}$ are constants. The model constants have the following values:

$$C_{b1} = 0.1355,\ C_{b2} = 0.622,\ \sigma_{\tilde{\nu}} = \frac{2}{3},\ C_{v1} = 7.1$$

$$C_{\omega 1} = \frac{C_{b1}}{\kappa^2} + \frac{1 + C_{b2}}{\sigma_{\tilde{\nu}}},\ C_{\omega 2} = 0.3,\ C_{\omega 3} = 2.0,\ \kappa = 0.4187$$

At walls the modified viscosity $\tilde{\nu}$ is set to be zero.

Turbulent heat transfer is given by

$$\frac{\partial}{\partial x_i}\left[u_i\left(\rho E + p\right)\right] = \frac{\partial}{\partial x_j}\left[\left(k + \frac{c_p \mu_t}{\mathrm{Pr}_t}\right)\frac{\partial T}{\partial x_j} + u_i\left(\tau_{ij}\right)_{eff}\right] \tag{3.10}$$

where k and E are the thermal conductivity and total energy respectively. $\left(\tau_{ij}\right)_{eff}$ is defined as

$$\left(\tau_{ij}\right)_{eff} = \mu_{eff}\left(\frac{\partial u_j}{\partial x_i} + \frac{\partial u_i}{\partial x_j}\right) - \frac{2}{3}\mu_{eff}\frac{\partial u_i}{\partial x_i}\delta_{ij} \tag{3.11}$$

3.2.2 The k-ϵ model

3.2.2.1. Standard k-ϵ model

The standard k-ϵ model (Launder and Spalding, 1972) is a semi-empirical two-equation model based on the Boussinesq approximation of Reynolds stresses. Two additional scalar variables, the turbulent kinetic energy k and the turbulence dissipation rate ϵ, are solved in order to model the turbulence effects. The k and ϵ transport equations are

$$\frac{\partial}{\partial x_i}(\rho k u_i) = \frac{\partial}{\partial x_j}\left[\left(\mu + \frac{\mu_t}{\sigma_k}\right)\frac{\partial k}{\partial x_j}\right] + G_k + G_b - \rho\varepsilon - Y_M, \tag{3.12}$$

$$\frac{\partial}{\partial x_i}(\rho \varepsilon u_i) = \frac{\partial}{\partial x_j}\left[\left(\mu + \frac{\mu_t}{\sigma_\varepsilon}\right)\frac{\partial \varepsilon}{\partial x_j}\right] + C_{1\varepsilon}\frac{\varepsilon}{k}(G_k + C_{3\varepsilon}G_b) - C_{2\varepsilon}\rho\frac{\varepsilon^2}{k}, \tag{3.13}$$

where G_k represents the generation of turbulence kinetic energy due to the mean velocity gradients, and G_b is the generation of turbulence kinetic energy due to buoyancy. Y_M represents the contribution of fluctuating dilatation in compressible turbulence to the dissipation rate. σ_k and σ_ϵ are the turbulent Prandtl numbers for k and ϵ respectively. Model constants $C_{1\epsilon}$, $C_{2\epsilon}$, C_μ, σ_k and σ_ϵ have been determined from experiments, and they are

$C_{1\epsilon} = 1.44$, $C_{2\epsilon} = 1.92$, $C_\mu = 0.09$, $\sigma_k = 1.0$, and $\sigma_\epsilon = 1.3$.

The turbulent viscosity μ_t is found using k and ϵ in the following formula:

$$\mu_t = \rho C_\mu \frac{k^2}{\varepsilon}. \tag{3.14}$$

3.2.2.2. The RNG k-ϵ model

The RNG (renormalization group) k-ϵ model (Yakhot and Orszag, 1986) is similar to the standard k-ϵ model. Its transport equations for k and ϵ are

$$\frac{\partial}{\partial x_i}(\rho k u_i) = \frac{\partial}{\partial x_j}\left(\alpha_k \mu_{eff} \frac{\partial k}{\partial x_j}\right) + G_k + G_b - \rho\varepsilon - Y_M , \tag{3.15}$$

$$\frac{\partial}{\partial x_i}(\rho \varepsilon u_i) = \frac{\partial}{\partial x_j}\left(\alpha_\varepsilon \mu_{eff} \frac{\partial \varepsilon}{\partial x_j}\right) + C_{1\varepsilon}\frac{\varepsilon}{k}(G_k + C_{3\varepsilon}G_b) - C_{2\varepsilon}\rho\frac{\varepsilon^2}{k} - R_\varepsilon . \tag{3.16}$$

The turbulent viscosity is defined as

$$d\left(\frac{\rho^2 k}{\sqrt{\varepsilon\mu}}\right) = 1.72\frac{\hat{\nu}}{\sqrt{\hat{\nu}^3 - 1 + C_\nu}}d\hat{\nu} , \tag{3.17}$$

where $\hat{\nu} = \mu_{eff}/\mu$ and $C_\nu \approx 100$

The R_ε term in the ϵ equation is given by

$$R_\varepsilon = \frac{C_\mu \rho \eta^3 (1 - \eta/\eta_0)}{1 + \beta\eta^3}\frac{\varepsilon^2}{k}, \tag{3.18}$$

where $\eta = Sk/\varepsilon$, $\eta_0 = 4.38$, and $\beta = 0.012$. The model constants are

$$C_{1\varepsilon} = 1.42 \text{ and } C_{2\varepsilon} = 1.68 .$$

3.2.2.3. Realizable k-ϵ model

The main differences between the standard k-ϵ model and the realizable k-ϵ model (Shih, Liou, Shabbir, Yang, and Zhu, 1995) are that: (a) a new variable C_μ is used instead of a constant in the definition of turbulent viscosity and (b) a new equation for dissipation rate ϵ is implemented.

The transport equations for k and ϵ in the realizable k-ϵ model are

$$\frac{\partial}{\partial x_i}(\rho k u_i) = \frac{\partial}{\partial x_j}\left[\left(\mu + \frac{\mu_t}{\sigma_k}\right)\frac{\partial k}{\partial x_j}\right] + G_k + G_b - \rho\varepsilon - Y_M, \tag{3.19}$$

$$\frac{\partial}{\partial x_i}(\rho \varepsilon u_i) = \frac{\partial}{\partial x_j}\left[\left(\mu + \frac{\mu_t}{\sigma_\varepsilon}\right)\frac{\partial \varepsilon}{\partial x_j}\right] + \rho C_1 S_\varepsilon - \rho C_2 \frac{\varepsilon^2}{k + \sqrt{\nu\varepsilon}} + C_{1\varepsilon}\frac{\varepsilon}{k} C_{3\varepsilon} G_b, \tag{3.20}$$

where C_2 and $C_{1\epsilon}$ are constants, and C_1 is given by

$$C_1 = \max\left[0.43, \frac{\eta}{\eta + 5}\right] \text{ and } \eta = S\frac{k}{\varepsilon}.$$

The k equation is the same as that of the standard k-ϵ model, while the ϵ equation is quite different.

The turbulent viscosity is computed from

$$\mu_t = \rho C_\mu \frac{k^2}{\varepsilon}, \tag{3.21}$$

where C_μ, this time, is not a constant and is given by

$$C_u = \frac{1}{A_0 + A_s \dfrac{kU^*}{\varepsilon}}. \tag{3.22}$$

where

$$U^* \equiv \sqrt{S_{ij}S_{ij} + \tilde{\Omega}_{ij}\tilde{\Omega}_{ij}}, \quad \tilde{\Omega}_{ij} = \Omega_{ij} - 2\varepsilon_{ijk}\omega_k, \text{ and } \quad \Omega_{ij} = \overline{\Omega_{ij}} - \varepsilon_{ijk}\omega_k$$

$\overline{\Omega_{ij}}$ is the mean rate-of-rotation tensor viewed in a rotating reference frame with the angular velocity ω_k. Also, A_0 and A_s are constants given by

$$A_0 = 4.04, \; A_s = \sqrt{6}\cos\phi,$$

where

$$\phi = \frac{1}{3}\cos^{-1}\left(\sqrt{6}W\right), \qquad W = \frac{S_{ij}S_{jk}S_{ki}}{\sqrt{S_{ij}S_{ij}}}, \text{ and } S_{ij} = \frac{1}{2}\left(\frac{\partial u_j}{\partial x_i} + \frac{\partial u_i}{\partial x_j}\right).$$

From these equations, it can be seen that C_μ is a function of the mean strain and rotation rates, the angular velocity of the system rotation, and the turbulence field k and ϵ. The constants are set at

$$C_{1\epsilon} = 1.44,\ C_2 = 1.9,\ \sigma_k = 1.0, \text{ and } \sigma_\epsilon = 1.2.$$

The production of turbulence kinetic energy G_k is found from

$$G_k = \mu_t S^2,$$

where S is the modulus of the mean rate-of-strain tensor, and defined by

$$S \equiv \sqrt{2S_{ij}S_{ij}}\ .$$

The generation of turbulence due to buoyancy is calculated as

$$G_b = \beta g_i \frac{\mu_t}{\mathrm{Pr}_t}\frac{\partial T}{\partial x_i},$$

where

$$\beta = -\frac{1}{\rho}\left(\frac{\partial \rho}{\partial T}\right)_P.$$

3.2.2.4. Turbulent heat transfer in k-ϵ model

According to the concept of Reynolds's analogy to turbulent momentum transfer, the energy equation or turbulent heat transfer is given by:

$$\frac{\partial}{\partial x_i}\left[u_i(\rho E + p)\right] = \frac{\partial}{\partial x_j}\left(k_{eff}\frac{\partial T}{\partial x_j} + u_i\left(\tau_{ij}\right)_{eff}\right), \tag{3.23}$$

where E is the total energy, k_{eff} is the effective thermal conductivity. $\left(\tau_{ij}\right)_{eff}$ is defined as

$$\left(\tau_{ij}\right)_{eff} = \mu_{eff}\left(\frac{\partial u_j}{\partial x_i} + \frac{\partial u_i}{\partial x_j}\right) - \frac{2}{3}\mu_{eff}\frac{\partial \mu_i}{\partial x_i}\delta_{ij}. \tag{3.24}$$

The effective thermal conductivity is given by

$$k_{eff} = k + \frac{c_p \mu_t}{\mathrm{Pr}_t}. \tag{3.25}$$

3.2.3 The k-ω model

The standard k-ω model (Wilcox, 1998) is an empirical model, and its transport equations of the turbulence kinetic energy k and specific dissipation rate ω are:

$$\frac{\partial}{\partial x_i}(\rho k u_i) = \frac{\partial}{\partial x_j}\left(\Gamma_k \frac{\partial k}{\partial x_j}\right) + G_k - Y_k, \tag{3.26}$$

$$\frac{\partial}{\partial x_i}(\rho \omega u_i) = \frac{\partial}{\partial x_j}\left(\Gamma_\omega \frac{\partial \omega}{\partial x_j}\right) + G_\omega - Y_\omega. \tag{3.27}$$

The effective diffusivities Γ_k and Γ_ω are given by

$$\Gamma_k = \mu + \frac{\mu_t}{\sigma_k} \quad \text{and} \quad \Gamma_\omega = \mu + \frac{\mu_t}{\sigma_\omega},$$

where σ_k and σ_ω are turbulent Prandtl numbers for k and ω, respectively.

The turbulent viscosity μ_t is computed as

$$\mu_t = \alpha^* \frac{\rho k}{\omega}, \tag{3.28}$$

where

$$\alpha^* = \alpha^*_\infty \left(\frac{\alpha^*_0 + \mathrm{Re}_t / R_k}{1 + \mathrm{Re}_t / R_k}\right), \qquad \mathrm{Re}_t = \frac{\rho k}{\mu \omega}$$

$$R_k = 6, \quad \alpha^*_0 = \frac{\beta_i}{3}, \quad \text{and} \quad \beta_i = 0.072.$$

The production of turbulence kinetic energy G_k is given by

$$G_k = \mu_t S^2 , \tag{3.29}$$

and the production of ω, G_ω is given by

$$G_\omega = \alpha \frac{\omega}{k} G_k ,$$

where

$$\alpha = \frac{\alpha_\infty}{\alpha^*}\left(\frac{\alpha_0 + \mathrm{Re}_t / R_\omega}{1 + \mathrm{Re}_t / R_\omega}\right) \quad \text{and} \quad R_\omega = 2.95 .$$

The dissipation of k is given as

$$Y_k = \rho \beta^* f_{\beta^*} k\omega \tag{3.30}$$

where

$$f_{\beta^*} = \begin{cases} 1 & \chi_k \le 0 \\ \dfrac{1+680\chi_k^2}{1+400\chi_k^2} & \chi_k > 0 \end{cases}, \qquad \chi_k = \frac{1}{\omega^3}\frac{\partial k}{\partial x_j}\frac{\partial \omega}{\partial x_j},$$

$$\beta^* = \beta_i^*\left[1 + \zeta^* F(M_t)\right], \quad \beta_i^* = \beta_\infty^*\left(\frac{4/15 + (\mathrm{Re}_t / R_\beta)^4}{1 + (\mathrm{Re}_t / R_\beta)^4}\right),$$

$$\zeta^* = 1.5, \quad R_\beta = 8, \quad \text{and} \quad \beta_\infty^* = 0.09$$

The dissipation of ω is given as

$$Y_\omega = \rho \beta f_\beta \omega^2 \tag{3.31}$$

where

$$f_\beta = \frac{1+70\chi_\omega}{1+80\chi_\omega}, \qquad \chi_\omega = \left|\frac{\Omega_{ij}\Omega_{jk}S_{ki}}{(\beta_\infty^*\omega)^3}\right|,$$

$$\Omega_{ij} = \frac{1}{2}\left(\frac{\partial u_i}{\partial x_j} - \frac{\partial u_j}{\partial x_i}\right), \quad \text{and} \quad \beta = \beta_i\left[1 - \frac{\beta_i^*}{\beta_i}\zeta^* F(M_t)\right].$$

The compressibility function $F(M_t)$ is defined as

$$F(M_t) = \begin{cases} 0 & M_t \le M_{t0} \\ M_t^2 - M_{t0}^2 & M_t > M_{t0} \end{cases}, \tag{3.32}$$

where

$$M_t^2 \equiv \frac{2k}{a^2}, \qquad M_{t0} = 0.25, \quad \text{and} \quad a = \sqrt{\gamma RT}.$$

If the flow is incompressible, $\beta^* = \beta_i^*$, and the model constants are

$$\alpha_\infty^* = 1,\ \alpha_\infty = 0.52,\ \alpha_0 = \frac{1}{9},\ \beta_\infty^* = 0.09,\ \beta_i = 0.072,\ R_\beta = 8,$$

$$R_k = 6,\ R_\omega = 2.95,\ \zeta^* = 1.5,\ M_{t0} = 0.25,\ \sigma_k = 2.0, \text{ and } \sigma_\omega = 2.0.$$

3.2.4 Reynolds Stress Model (RSM)

The Reynolds Stress model (RSM) proposed by Gibson et al. (1978), Launder (1989) and Launder et al. (1975), is more elaborate than the other models mentioned above in that it solves transport equations for the individual Reynolds stress and an equation for the dissipation rate, abandoning the isotropic eddy-viscosity hypothesis. This means that seven additional transport equations have to be solved in 3D. However, the fidelity of the RSM predictions is severely compromised due to the assumptions made in order to close the equations. The Reynolds stress transport equations can be written as

$$\underbrace{\frac{\partial}{\partial x_k}\left(\rho u_k \overline{u_i' u_j'}\right)}_{C_{ij}\equiv\text{convection}} = \underbrace{-\frac{\partial}{\partial x_k}\left[\rho\overline{u_i' u_j' u_k'} + \overline{p\left(\delta_{kj}u_i' + \delta_{ik}u_j'\right)}\right]}_{D_{T,ij}\equiv\text{Turbulent Diffusion}}$$

$$+ \underbrace{\frac{\partial}{\partial x_k}\left[\mu\frac{\partial}{\partial x_k}\left(\overline{u_i' u_j'}\right)\right]}_{D_{L,ij}\equiv\text{Molecular Diffustion}} \underbrace{-\rho\left(\overline{u_i' u_k'}\frac{\partial u_j}{\partial x_k} + \overline{u_j' u_k'}\frac{\partial u_i}{\partial x_k}\right)}_{P_{ij}\equiv\text{Stress Production}}$$

$$- \underbrace{\rho\beta\left(g_i\overline{u_j'\theta} + g_j\overline{u_i'\theta}\right)}_{G_{ij}\equiv\text{Buoyancy Production}} + \underbrace{\overline{p\left(\frac{\partial u_i'}{\partial x_j} + \frac{\partial u_j'}{\partial x_i}\right)}}_{\varphi_{ij}\equiv\text{Pressure Strain}} \tag{3.33}$$

$$- \underbrace{2\mu\overline{\frac{\partial u_i'}{\partial x_k}\frac{\partial u_j'}{\partial x_k}}}_{\varepsilon_{ij}\equiv\text{Dissipation}} - \underbrace{2\rho\Omega_k\left(\overline{u_j' u_m'}\varepsilon_{ikm} + \overline{u_i' u_m'}\varepsilon_{jkm}\right)}_{F_{ij}\equiv\text{Production by System Rotation}}$$

where

$$D_{T,ij} = \frac{\partial}{\partial x_k}\left(\frac{\mu_t}{\sigma_k}\frac{\partial\overline{u_i' u_j'}}{\partial x_k}\right) \text{ and } G_{ij} = \beta\frac{\mu_t}{\text{Pr}_t}\left(g_i\frac{\partial T}{\partial x_j} + g_j\frac{\partial T}{\partial x_i}\right) \tag{3.34}$$

where $\sigma_k = 0.82$.

The turbulence kinetic energy k is computed from

$$k = \frac{1}{2}\overline{u_i' u_i'}, \tag{3.35}$$

and the dissipation tensor ϵ_{ij} is found from

$$\varepsilon_{ij} = \frac{2}{3}\delta_{ij}\left(\rho\varepsilon + 2\rho\varepsilon M_t^2\right) \tag{3.36}$$

where

$$M_t = \sqrt{\frac{k}{a^2}}.$$

The scalar dissipation rate ϵ is computed from

$$\frac{\partial}{\partial x_i}(\rho\varepsilon u_i)=\frac{\partial}{\partial x_j}\left[\left(\mu+\frac{\mu_t}{\sigma_\varepsilon}\right)\frac{\partial\varepsilon}{\partial x_j}\right]C_{\varepsilon 1}\frac{1}{2}(P_{ii}+C_{\varepsilon 3}G_{ii})\frac{\varepsilon}{k}-C_{\varepsilon 2}\rho\frac{\varepsilon^2}{k}, \tag{3.37}$$

and the turbulent viscosity is computed as

$$\mu_t=\rho C_\mu\frac{k^2}{\varepsilon},$$

where $C_\mu=0.09$.

The turbulent heat transfer is modeled from the concept of Reynolds' analogy to turbulent momentum transfer:

$$\frac{\partial}{\partial x_i}[u_i(\rho E+p)]=\frac{\partial}{\partial x_j}\left[\left(k+\frac{c_p\mu_t}{\mathrm{Pr}_t}\right)\frac{\partial T}{\partial x_j}+u_i(\tau_{ij})_{eff}\right], \tag{3.38}$$

where $(\tau_{ij})_{eff}$ is defined as

$$(\tau_{ij})_{eff}=\mu_{eff}\left(\frac{\partial u_j}{\partial x_i}+\frac{\partial u_i}{\partial x_j}\right)-\frac{2}{3}\mu_{eff}\frac{\partial u_i}{\partial x_i}\delta_{ij}. \tag{3.39}$$

3.3 Near wall treatments

The presence of the wall significantly affects turbulent flow field. In the near wall region, the solution variables such as velocities and temperatures have large gradients, and the accuracy of the final numerical solution primarily depends on how successfully the near wall boundary layers are modeled. Unfortunately, most current turbulence models, including the k-ϵ models, are only valid for turbulent core flows far from walls. In order to render these models suitable for wall-bounded flows, a series of empirical functions are introduced in order to resolve the boundary layers.

Two approaches have been proposed for modeling the near-wall region, as shown in figure 3.1. One approach involves the use of semi-empirical formulas in order to bridge the viscosity-affected region between the wall and the fully-turbulent region, thus avoiding the need to modify the turbulence models in order to account for the presence of the wall. Another approach is to modify the turbulence models, and by doing so enable the viscosity-affected region to be resolved all the way to the wall. Since the wall function approach does not need to resolve viscosity-affected near wall region, it saves computational resources substantially. In addition, it has become popular due to its economy, robustness, and reasonable accuracy.

The wall functions that bridge or link the solution variables at the near-wall cells and the corresponding quantities on the wall include formulas for mean velocity and temperature, as well as other scalars and formulas for near-wall turbulent quantities.

3.3.1 The Standard wall functions

The standard wall functions were proposed by Launder and Spalding. The formulas or law-of-the-wall for mean velocity are

$$U^* = \frac{1}{k}\ln(Ey^*), \tag{3.40}$$

where

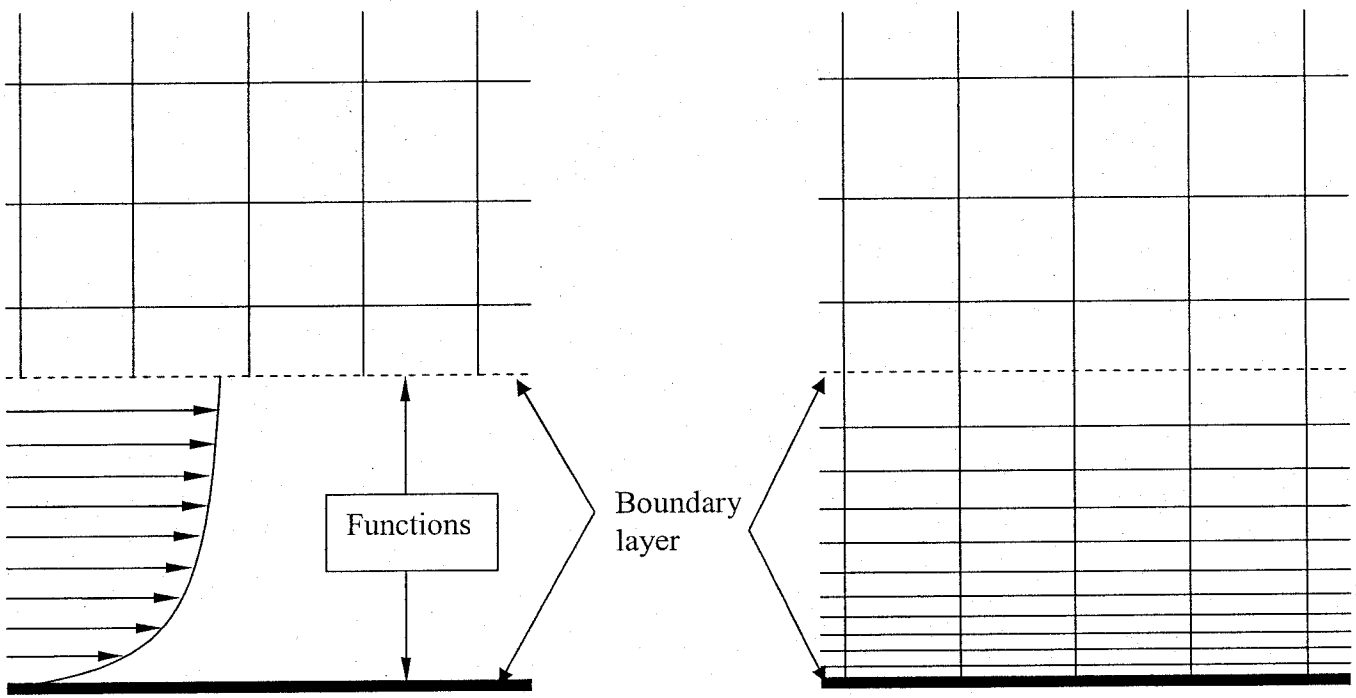

Wall function approach: the boundary layer is not resolved; instead, it is bridged by empirical functions.

Near wall model approach: the boundary layer is resolved all the way to the wall.

Figure 3.1 Difference between wall functions and near wall model approach.

$$U^* \equiv \frac{U_P C_\mu^{1/4} k_P^{1/2}}{\tau_w / \rho}, \tag{3.41}$$

and

$$y^* \equiv \frac{\rho C_\mu^{1/4} k_P^{1/2} y_P}{\mu}. \tag{3.42}$$

The definitions of the other variables are as follows :

k = von Karman constant (= 0.42)

E = empirical constant (= 9.793)

U_P = mean velocity of the fluid at point P

k_P = turbulence kinetic energy at point P

y_P = distance from point p to the wall

μ = dynamic viscosity of the fluid

This logarithmic law for mean velocity is known to be valid for $y^* > 30 \sim 60$. In FLUENT, this log-law is employed when $y^* > 11.225$. Therefore, when $y^* < 11.225$ at the wall-adjacent cells, $U^* = y^*$ is employed.

According to the Reynolds' analogy between momentum and energy transport, a similar logarithmic law for mean temperature is given as

$$T^* \equiv \frac{(T_w - T_P)\rho c_P C_\mu^{1/4} k_P^{1/2}}{\dot{q}} = \begin{cases} \Pr y^* + \frac{1}{2}\rho \Pr \frac{C_\mu^{1/4} k_P^{1/2}}{\dot{q}} U_P^2 & (y^* < y_T^*) \\ \Pr_t \left[\frac{1}{\kappa} \ln(E y^*) + P \right] + & \\ \frac{1}{2}\rho \frac{C_\mu^{1/4} k_P^{1/2}}{\dot{q}} \left[\Pr_t U_P^2 + (\Pr - \Pr_t) U_c^2 \right] & (y^* > y_T^*) \end{cases} \tag{3.43}$$

where $$P = 9.24\left[\left(\frac{\mathrm{Pr}}{\mathrm{Pr}_t}\right)^{3/4} - 1\right]\left(1 + 0.28e^{-0.007\mathrm{Pr}/\mathrm{Pr}_t}\right).$$

The thermal boundary layer thickness y_T^* is computed from the intersection of the linear and logarithmic profiles. In the simulation, the wall temperature T_w or heat flux is computed from the above equations.

The turbulence variables, the production of k and its dissipation rate ϵ, are computed from

$$G_k \approx \tau_w \frac{\partial U}{\partial y} = \tau_w \frac{\tau_w}{\kappa \rho C_\mu^{1/4} k_P^{1/2} y_P}$$

and

$$\varepsilon_P = \frac{C_\mu^{3/4} k_P^{3/2}}{\kappa y_P}$$

At the wall, the boundary condition for k is

$$\frac{\partial k}{\partial n} = 0 \qquad (3.44)$$

where n is the local coordinate normal to the wall. The production of k is assumed to be equal to its dissipation rate ϵ in the wall-adjacent control volume. Note that the solution variables including mean velocity, temperature, species concentration, k, and ϵ are all computed from the wall functions.

3.3.2 The Non-Equilibrium wall functions

The Non-Equilibrium wall functions, a two-layer-based approach, is a little bit different from the standard wall functions in that mean velocity is sensitized to pressure-gradient effects, and a different way of computing the budge of turbulence kinetic energy is used

in the wall-neighboring cells. Therefore, the non-equilibrium functions partly account for non-equilibrium effects which are neglected in the standard wall functions. The functions for mean temperature are the same as in the standard wall function. The mean velocity is sensitized to pressure gradients as

$$\frac{\tilde{U}C_\mu^{1/4}k^{1/2}}{\tau_w/\rho} = \frac{1}{\kappa}\ln\left(E\frac{\rho C_\mu^{1/4}k^{1/2}y}{\mu}\right), \tag{3.45}$$

$$\tilde{U} = U - \frac{1}{2}\frac{dp}{dx}\left[\frac{y_v}{\rho\kappa\sqrt{k}}\ln\left(\frac{y}{y_v}\right) + \frac{y-y_v}{\rho\kappa\sqrt{k}} + \frac{y_v^2}{\mu}\right], \tag{3.46}$$

where the physical viscous sublayer thickness y_v is computed as

$$y_v \equiv \frac{\mu y_v^*}{\rho C_\mu^{1/4}k_P^{1/2}},$$

where $y_v^* = 11.225$.

In computing the budget of turbulence kinetic energy at the wall-adjacent cells, it is assumed that the wall-neighboring cells consist of a viscous sublayer and a fully turbulent layer,

$$\tau_t = \begin{cases} 0, & y < y_v \\ \tau_w, & y > y_v \end{cases}, \qquad k = \begin{cases} \left(\frac{y}{y_v}\right)^2 k_P, & y < y_v \\ k_P, & y > y_v \end{cases}, \qquad \varepsilon = \begin{cases} \frac{2\nu k}{y^2}, & y < y_v \\ \frac{k^{3/2}}{C_l y}, & y > y_v \end{cases},$$

where

$$C_l = \kappa C_\mu^{-3/4}.$$

3.3.3 The Enhanced wall treatment

The Enhanced wall treatment combines a two-layer model with enhanced wall functions. The whole domain is subdivided into a viscosity-affected region and a fully turbulent region by a wall-distance-based turbulent Reynolds number Re_y, defined as

$$\mathrm{Re}_y = \frac{\rho y \sqrt{k}}{\mu} \tag{3.47}$$

where y is the normal distance from the wall at the cell centers. Different turbulence models are used in the fully turbulent region ($\mathrm{Re}_y > \mathrm{Re}_y^*; \mathrm{Re}_y^* = 200$) and in the viscosity-affected near-wall region ($\mathrm{Re}_y < \mathrm{Re}_y^*$). To make the models valid throughout the whole near wall region, including the laminar sublayer, buffer region, and the fully turbulent outer region, a single wall function for the entire wall region is formulated by blending laminar and turbulent functions of the wall:

$$u^+ = e^{\Gamma} u_{lam}^+ + e^{\frac{1}{\Gamma}} u_{turb}^+ \tag{3.48}$$

where $$\Gamma = -\frac{a(y^+)^4}{1+by^+}, \qquad a = 0.01c, \qquad b = \frac{5}{c},$$

$$c = \exp\left(\frac{E}{E''} - 1.0\right), \quad E = 9.793 \quad \text{and} \quad E'' = \frac{E}{f_r}.$$

where f_r is a roughness function. and y^+ is defined as

$$y^+ \equiv \frac{\rho u_\tau y}{\mu}, \tag{3.49}$$

where $$u_\tau = \sqrt{\frac{\tau_w}{\rho_w}}.$$

The enhanced turbulent wall function has been derived as

$$\frac{du^+_{turb}}{dy^+} = \frac{1}{\kappa y^+}\left[S'\left(1-\beta u^+ - \gamma\left(u^+\right)^2\right)\right]^{1/2}, \tag{3.50}$$

where

$$S' = \begin{cases} 1+\alpha y^+ & for\ y^+ < y_s^+ \\ 1+\alpha y_s^+ & for\ y^+ \geq y_s^+ \end{cases}$$

and

$$\alpha \equiv \frac{\nu_w}{\tau_w u^*}\frac{dp}{dx} = \frac{\mu}{\rho^2\left(u^*\right)^3}\frac{dp}{dx}, \quad \beta \equiv \frac{\sigma_t q_w u^*}{c_p \tau_w T_w} = \frac{\sigma_t q_w}{\rho c_p u^* T_w}, \text{ and } \gamma \equiv \frac{\sigma_t\left(u^*\right)^2}{2c_p T_w}.$$

where y_s^+ is the location at which the log-law slope will remain fixed.

The laminar wall function is determined as

$$\frac{du^+_{lam}}{dy^+} = 1+\alpha y^+, \tag{3.51}$$

where the integration of above equation yields

$$u^+_{lam} = y^+\left(1+\frac{\alpha}{2}y^+\right). \tag{3.52}$$

The enhanced thermal wall functions follow the same manner as the profile of u^+:

$$T^+ = e^{\Gamma}T^+_{lam} + e^{\frac{1}{\Gamma}}T^+_{turb}, \tag{3.53}$$

where

$$\Gamma = -\frac{a\left(\mathrm{Pr}\, y^+\right)^4}{1+b\,\mathrm{Pr}^3\, y^+}.$$

3.4 Grid considerations for turbulent flow simulations

Due to turbulence, the numerical results are strongly grid dependent. Thus, special consideration is required during the stage of mesh generation. Generally speaking, sufficiently fine meshes are needed where larger variable gradients exist, such as in regions where the mean flow changes rapidly and in the boundary layer.

When wall functions are employed, it is important to ensure that excessively fine or coarse meshes near the walls are avoided since the log-law is valid for $y^+ > 30$ to 60; that the most desirable value of y^+ is a value close to the lower bound ($y^+ \approx 30$); and that there are at least a few cells inside the boundary layer.

When enhanced wall treatment is employed, the mesh should be able to fully resolve the viscosity affected near wall region. In addition, y^+ at the wall-adjacent cell should be on the order of 1, but a higher y^+ ($y^+ < 4$ to 5) is acceptable as long as it is inside the viscous sublayer. Also, in order to resolve the mean velocity and turbulent quantities in the viscosity affected near wall region ($Re_y < 200$), at least 10 cells are needed in the boundary layer.

The smoothness or successive ratio of the mesh system has a large influence on the final solution and converging rate. Rapid changes in the cell volume between adjacent cells lead to larger truncation errors, causing serious convergence problems. Figure 3.2 shows a typical historical trend of residuals, where the mesh in Case (a) is smoother than that in Case (b). The residuals of Case (a) leveled off after a certain number of iterations and

eventually converged, while the residuals of Case (b) never leveled off, rendering it extremely difficult to judge convergence. Residuals shown in Figure 3.2b indicate very poor quality in the mesh with the successive ratio being too high. In this study, all results presented here have a smooth residual history like that shown Figure 3.2a.

3.5 Calculation procedure

In this study, four different classes of turbulence models have been selected to perform the simulation by solving the Reynolds-averaged Navier-Stokes equations. The performances of these models, namely the Spalart-Allmaras model, the k-ϵ model (including its three variants: standard k-ϵ, RNG k-ϵ, and realizable k-ϵ models), the k-ω model, and Reynolds stress model, as well as the performance of three near wall treatments, namely the standard wall functions, the non-equilibrium wall functions and the enhanced wall treatment, are evaluated. The predictions using these models were validated and compared with the experimental data obtained by Eriksen et al. (1971), Sinha et al. (1991) and Sen et al. (1996). It was found that k-ϵ model with standard wall functions provided the most appropriate predictions. As in the experiments, it is assumed that the flow is incompressible, steady-state turbulent flow.

The CFD package FLUENT 6.0 is used to solve the Navier-Stokes equations for continuity, momentum and energy. This CFD package uses the finite volume method and supports unstructured grids. Fluent stores discrete values of scalar at the cell centers of elements. If face values are required, it will be interpolated from the cell center values, which is accomplished using an upwind scheme. It enables the use of different

discretization schemes and solution algorithms, together with various types of boundary conditions. As part of the same package, a preprocessor, Gambit, is used to generate the required grid for the solver. Different meshes were used at the beginning to determine the optimum grid size and to ensure grid independent solution. The grid contained between 0.4 and 0.8 million cells when the standard wall functions were employed. When the enhanced wall treatment was selected, a grid independent solution and a smooth residual history, as shown in Figure 3.2a, were attained with a grid containing 1.6 million cells. In this study, extremely strict convergence criterions were imposed, where at least 500 additional iterations were performed after the residuals leveled off. Both mass and energy are conserved through the domain. Convergence is assumed when the net mass flux is less than 0.001%, and when the energy imbalance is less than 0.02%.

Unlike the unstructured mesh, with usually tetrahedron elements, the structured mesh, with usually hexahedron elements, cannot be adapted. Therefore, if the solution for y^+ is found to be out of the acceptable range, the mesh has to be discarded and a new one created. The typical procedure to attain a good solution using a structured mesh is outlined in Figure 3.3. Since y^+ is a solution dependent variable and not known a priori, it is pretty clear that it is time consuming to obtain a meaningful solution that meets the near wall requirement. Physically, the boundary layer is comparably very thin. However, it has tremendous influence on the final solution. In the CFD analysis of turbulence flow, its existence is expressed in terms of y^+. Hence, it is critically important to precisely control the near wall mesh y^+ according to the near wall mesh requirement. From this point of view, whenever the parameters such as blowing ratio change, the y^+ will change

and the near wall mesh has to be changed in order to reach a meaningful solution. From this point of view, every mesh corresponds to a unique flow condition. Also, the predictions using any of the turbulence models were critically dependant on y^+, where a value of 34 was mostly used with the standard wall functions. If the enhanced wall treatment is employed, y^+ at the wall-adjacent node was on the order of 1.

(a)

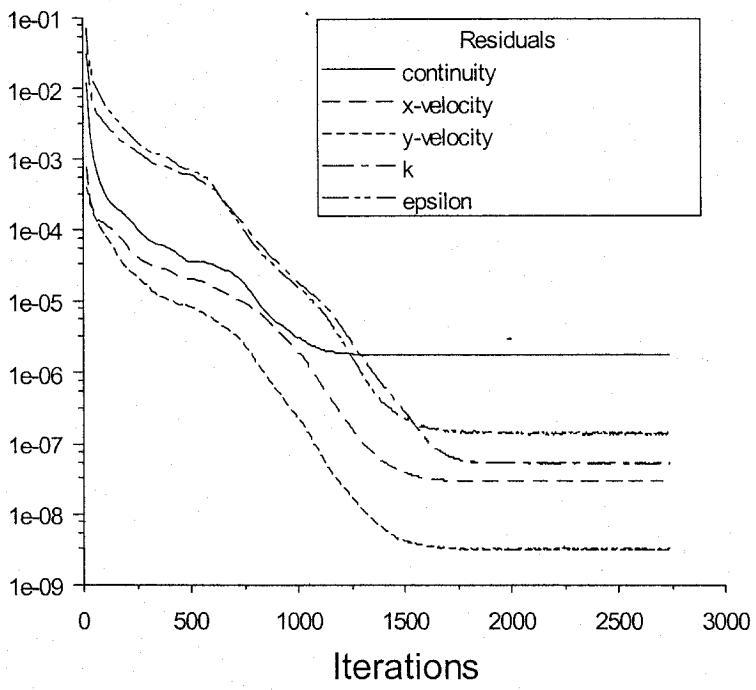

(b)

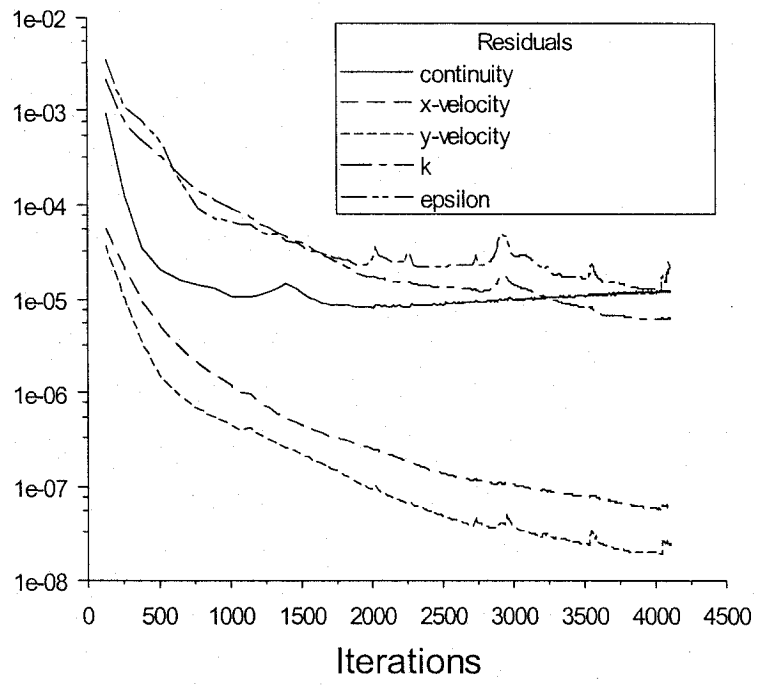

Figure 3.2 Typical residual history in this study, (a) mesh with reasonable successive ratio, (b) mesh with high successive ratio.

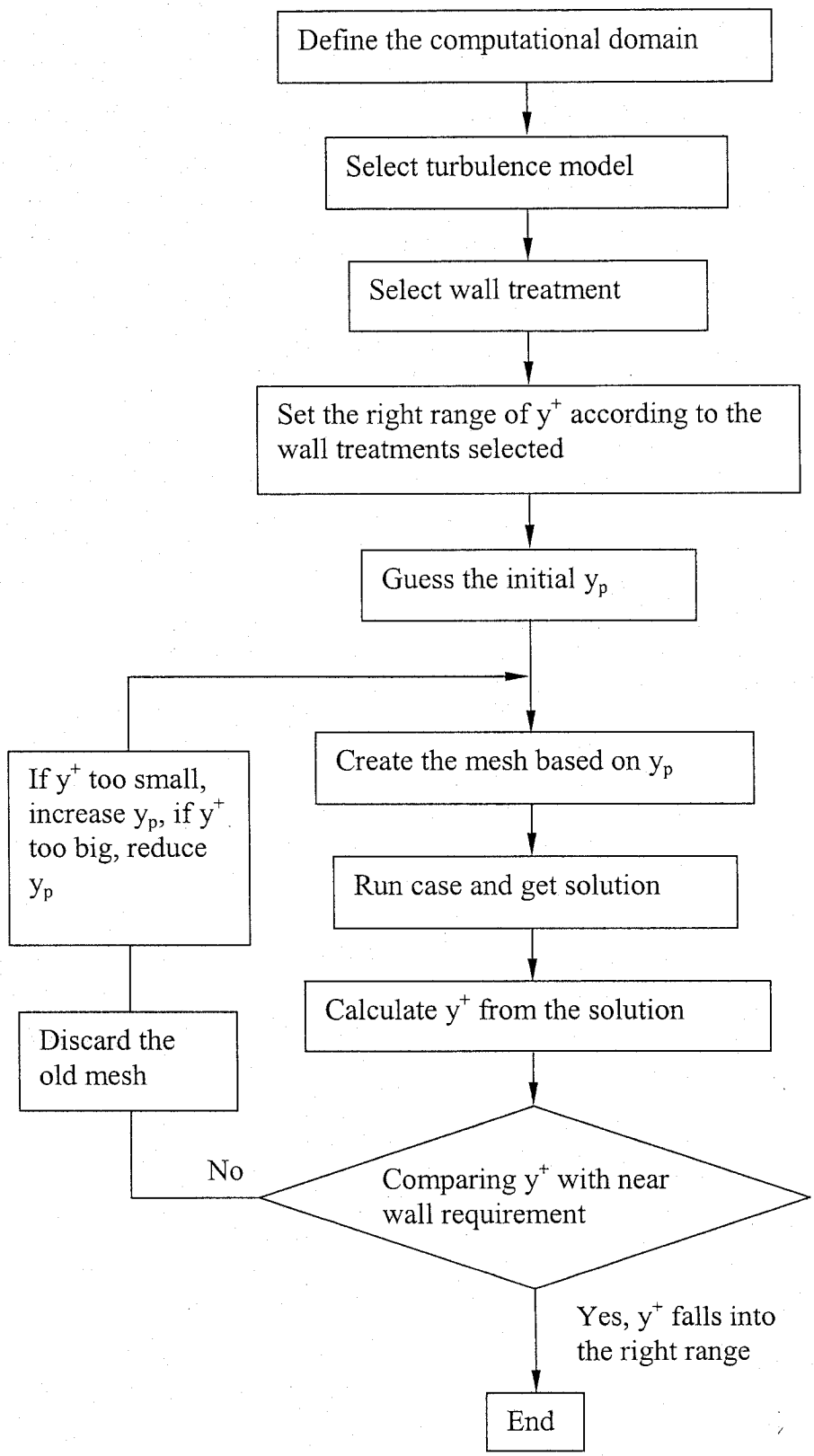

Figure 3.3 Typical procedure to reach a good mesh and a meaningful solution.

Chapter 4

Predictions of Adiabatic Effectiveness

4.1 Geometries and boundary conditions

In the present study, the experimental work of Sinha (1991) and Eriksen (1971) are chosen as the benchmark cases in order to validate the methodology which is used in the new scheme, as well to validate the selected turbulence models. In Eriksen's case, the flow at the exit of jet is fully developed since long tubes (around 1 m) are used, which eliminates some uncertainties introduced by jet exit profiles. In Sinha's case, the material of the testing plate is styrofoam with very low thermal conductivity (0.027 w/m·K), which is significantly lower than the previous testing plate, and can significantly reduce conduction error.

The computational domains and film cooling geometries used in this study are shown in Figures 4.1 ~ 4.4. Each domain consists of an infinite row of film cooling holes in a flat plate, such that the end-wall effects are neglected. The origin of the coordinate system is set at the trailing edge of the jet outlet. The parameters and the geometry in the present computational study are exactly the same as in the experimental study by Sinha (1991) and Eriksen (1971). At the upstream inlet, a velocity inlet condition is applied and at the outlet, a pressure boundary condition is applied. The domain extends 20d from the bottom wall, far enough such that a free slip boundary condition or zero shear stress may be applied. Symmetry boundary conditions are imposed at both the centerline of the jet

and at 1.5d plan, stream wise. Preliminary simulations show that the results are exactly the same when the computational domain extends either 1.5d, 3d or 6d pitches in the spanwise direction. At the bottom wall, as well as the other walls, an adiabatic wall boundary condition with no-slip was imposed. Typical mesh is shown in figure 4.5 and figure 4.6. If the geometry is simple like the Sinha case – short jet with plenum, structured mesh is used. If the geometry becomes complicated like the new scheme, unstructured mesh is used only in the areas with irregular shape.

4.2 Eriksen case

The test parameters are shown in Table 4.1. Figure 4.7 shows the performance of different turbulence models in terms of adiabatic effectiveness on the centerline at m = 1. Both the k-ω model and Spalart-Allmaras model underpredicted the effectiveness in the near hole region. The Reynolds-Stress model underpredicts the effectiveness from x/d = 10 to 60. Although the standard k-ϵ model seems to perform slightly better than the realizable k-ϵ model in the near hole region, it barely captures the jet liftoff effect. Hence, it was determined that the realizable k-ϵ model overall yields the realistic results. Figure 4.8 shows the effect of three different wall treatments with the realizable k-ϵ model, namely the standard wall functions, non-equilibrium wall functions and enhanced wall treatment. In contrast to the commonly accepted notion that the enhanced wall treatment gave better results, the three different wall treatments essentially yielded the same results provided that the near wall mesh requirement was met. The standard wall functions were selected for the subsequent simulations since the enhanced wall treatment requires a finer

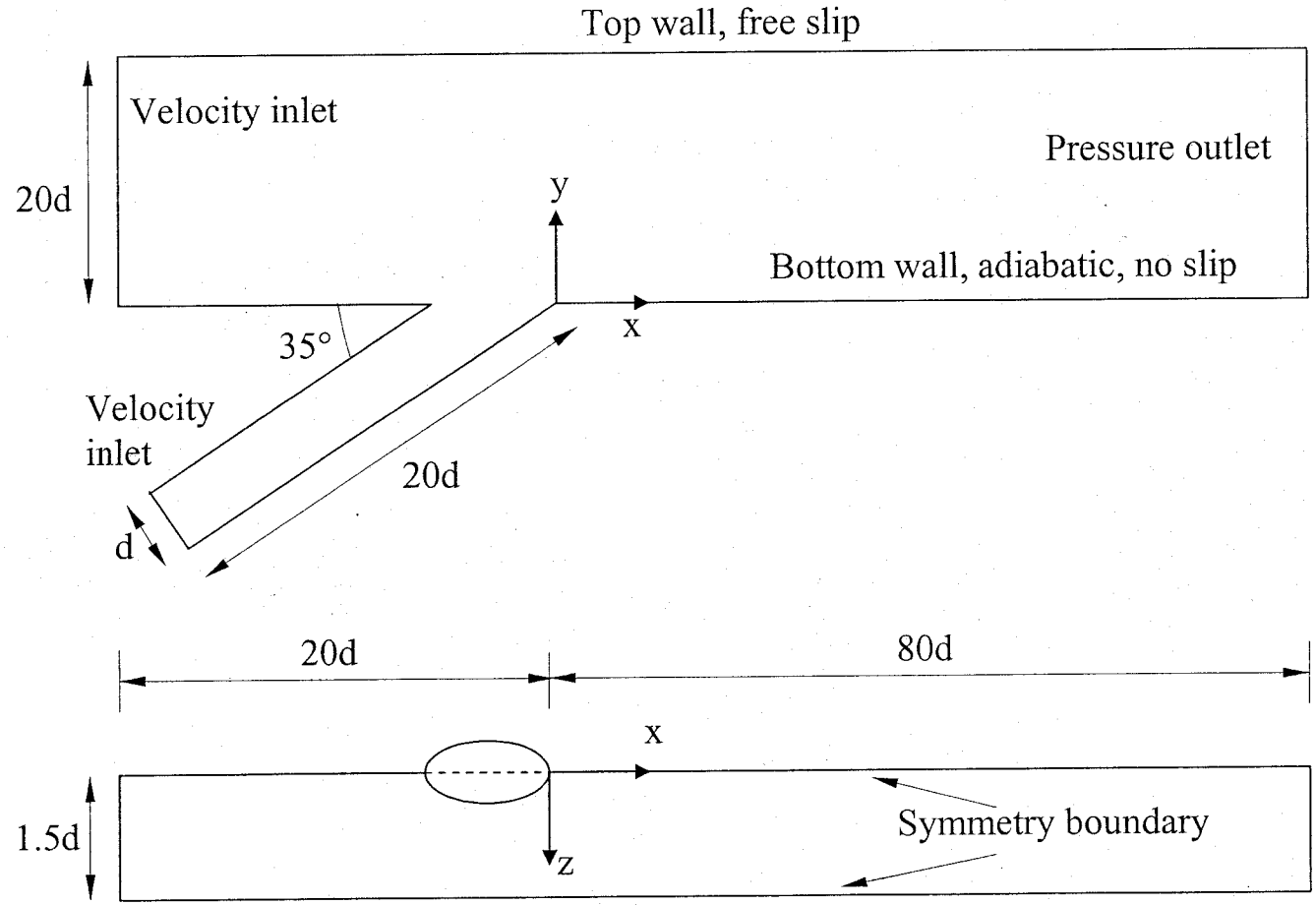

Figure 4.1 Geometry of Eriksen case showing the computational domain and the boundary conditions (d = 0.0118m).

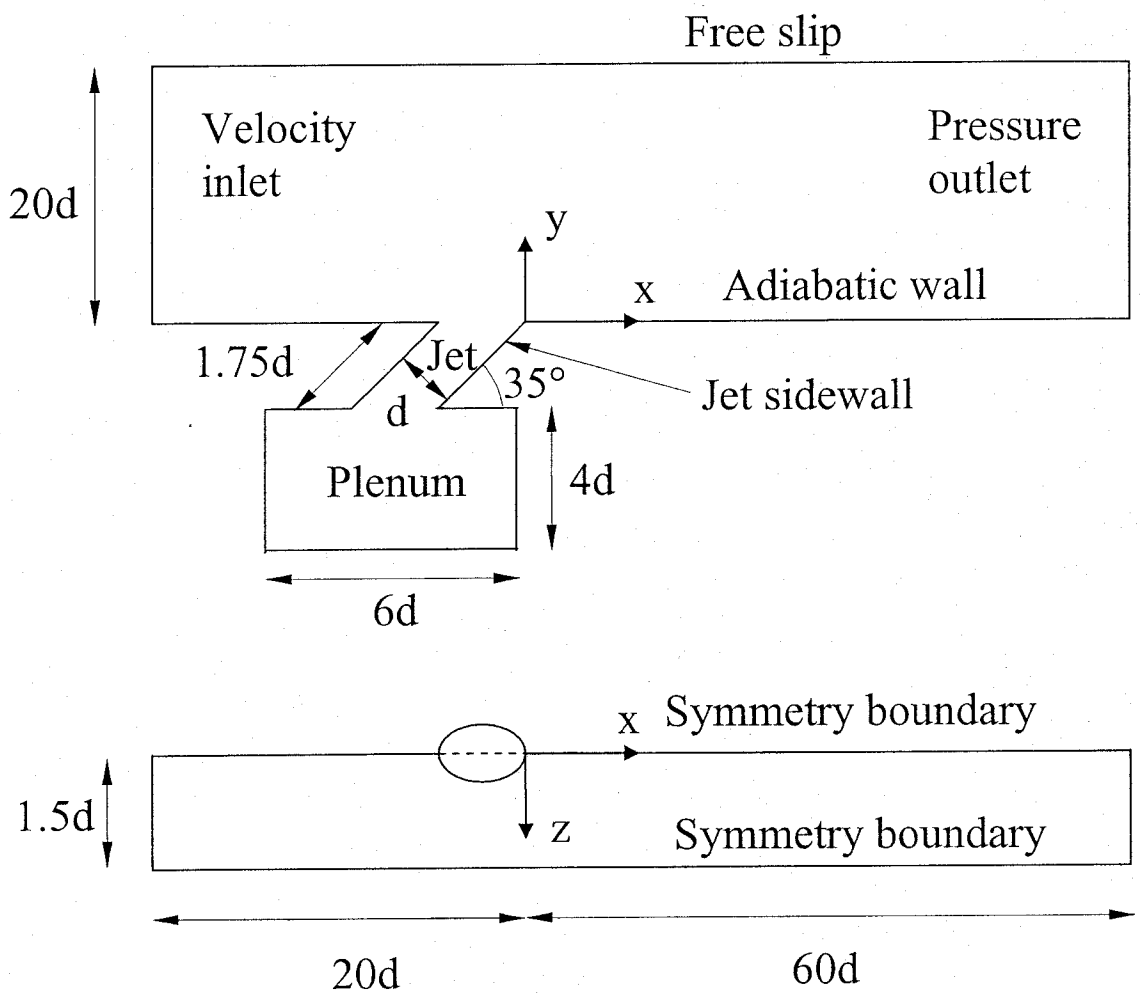

Figure 4.2 Geometry and computational domain of Sinha case (d = 0.0127m).

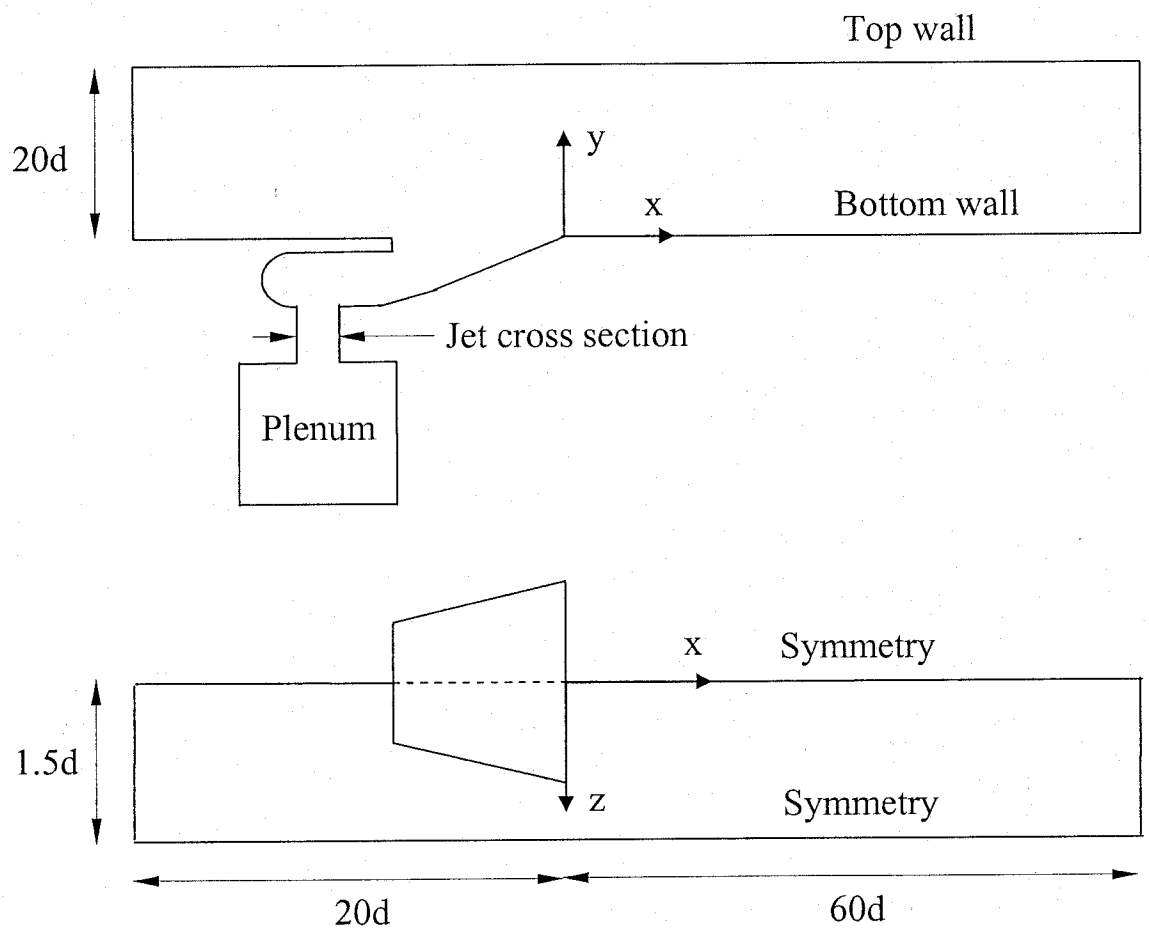

Figure 4.3 Geometry of the new scheme showing the computational domain.

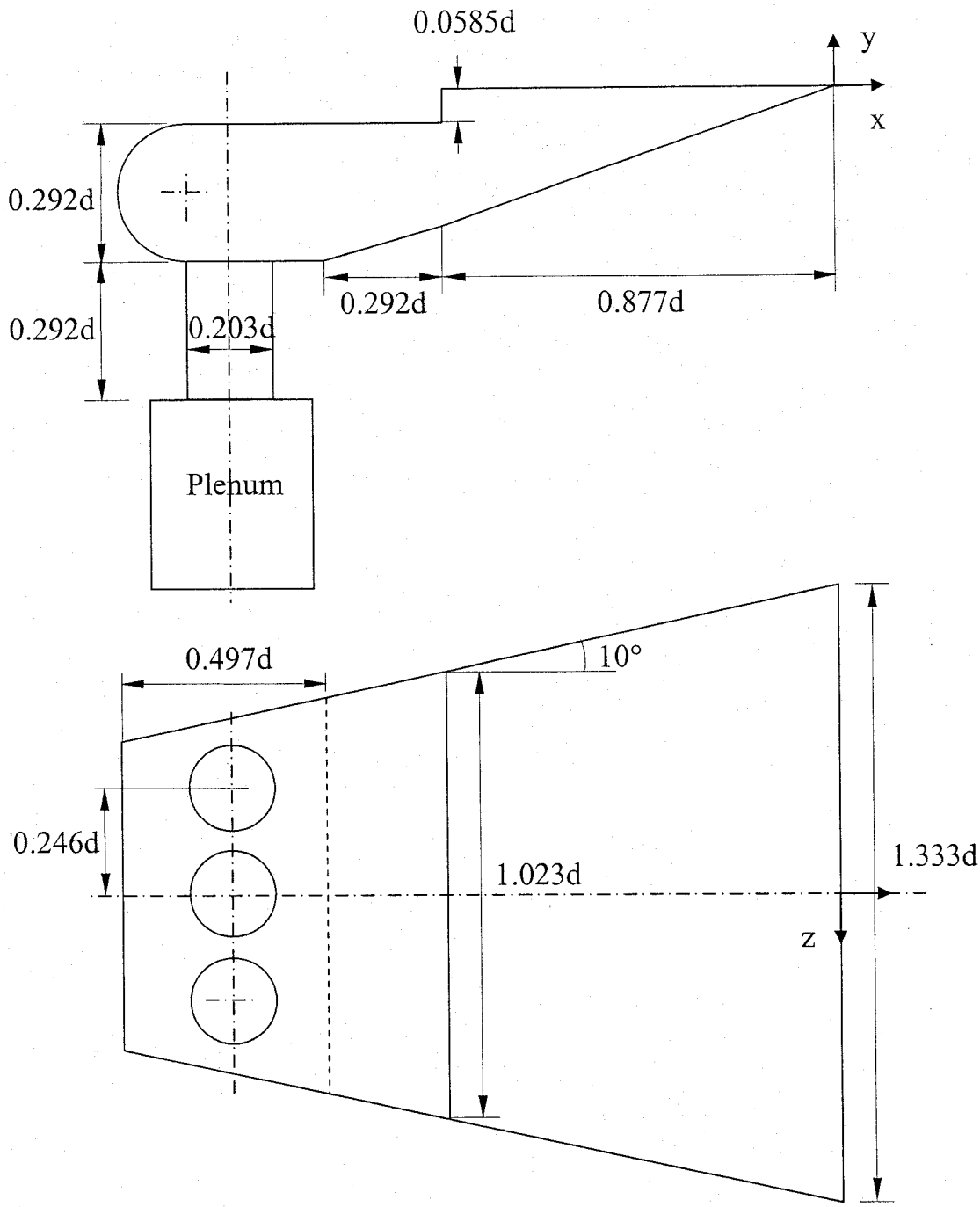

Figure 4.4 Geometry of the jet section of the new scheme.

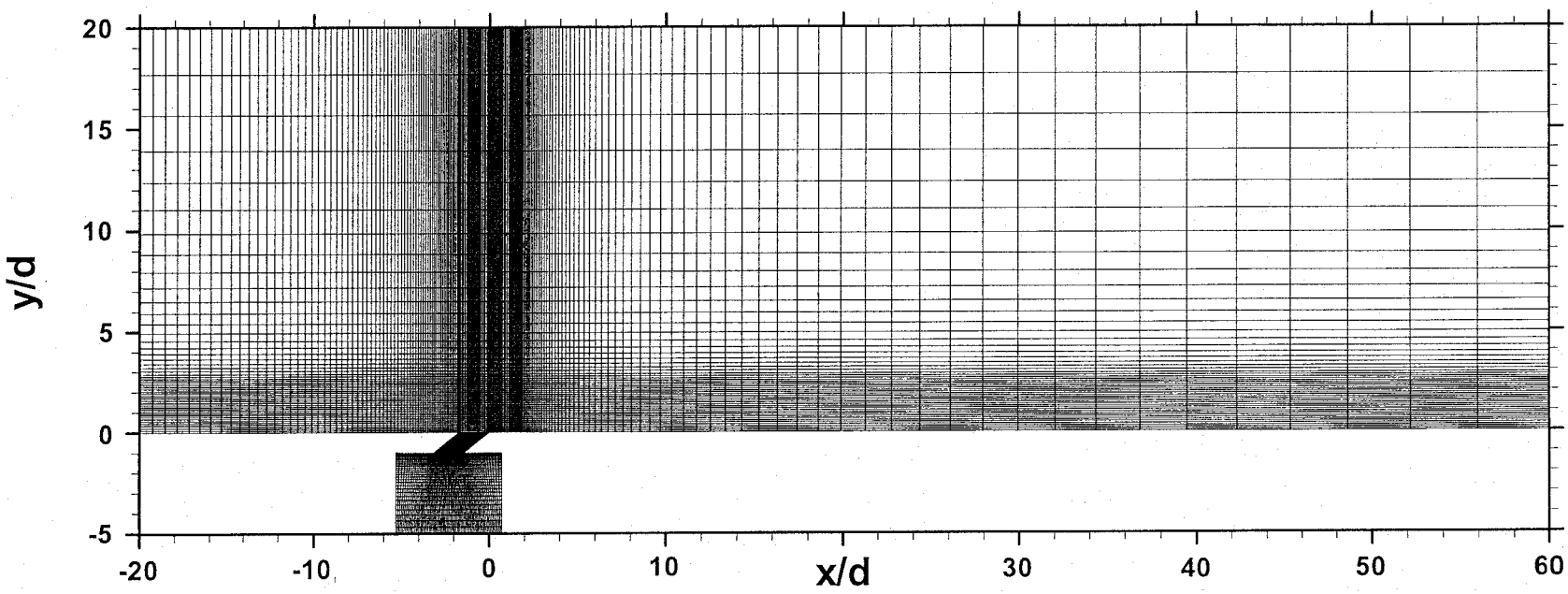

Figure 4.5 Typical mesh for the Sinha case.

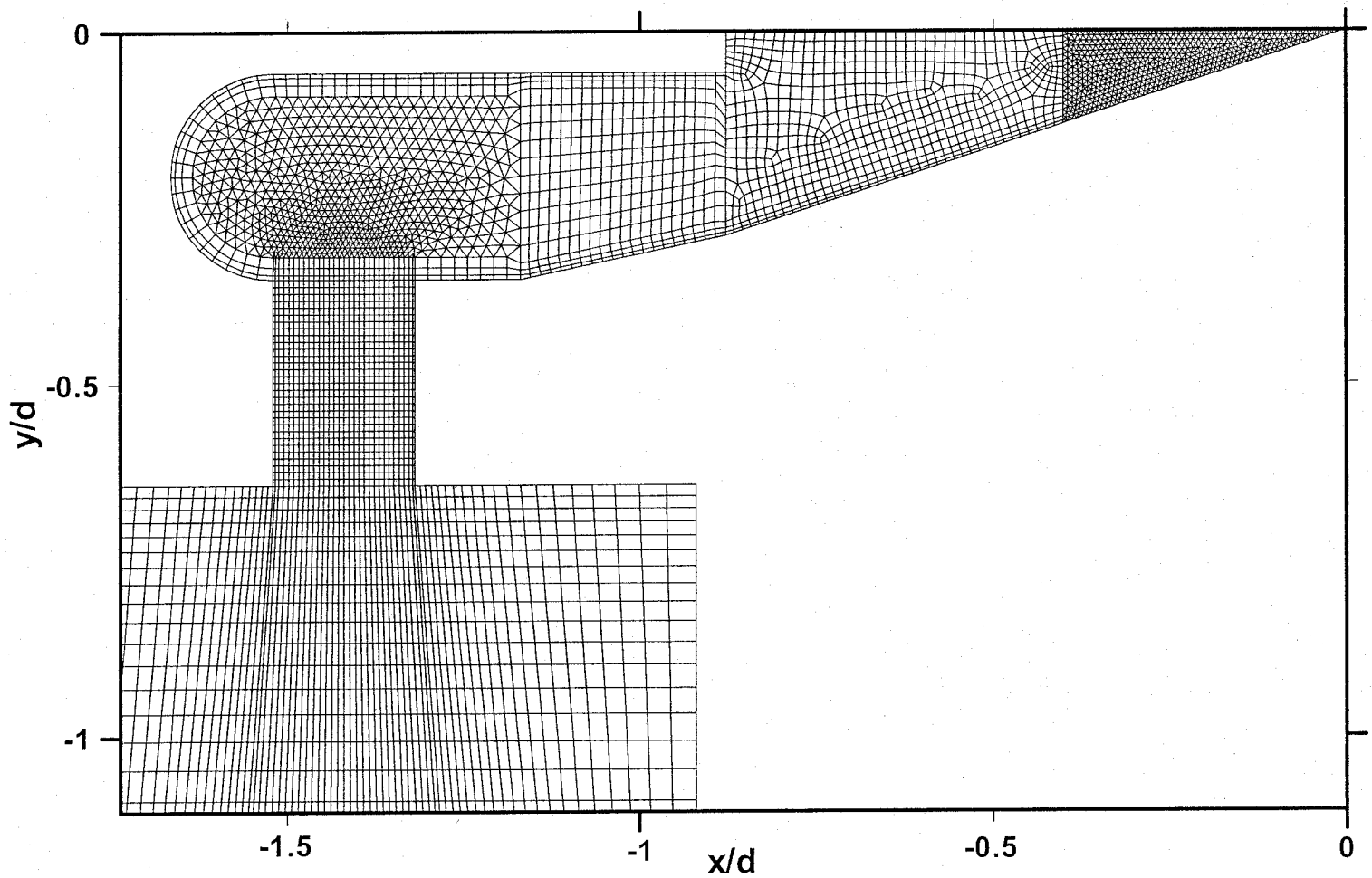

Figure 4.6 Typical mesh in the jet section of the new scheme.

Table 4.1 Experimental parameters for Eriksen (1971) case – η

d (m)	0.0118
Re_D (based on d)	0.44×10^5
U_∞ (m/s)	61
T_∞ (K)	300
U_j (m/s)	70.238
T_j (K)	355

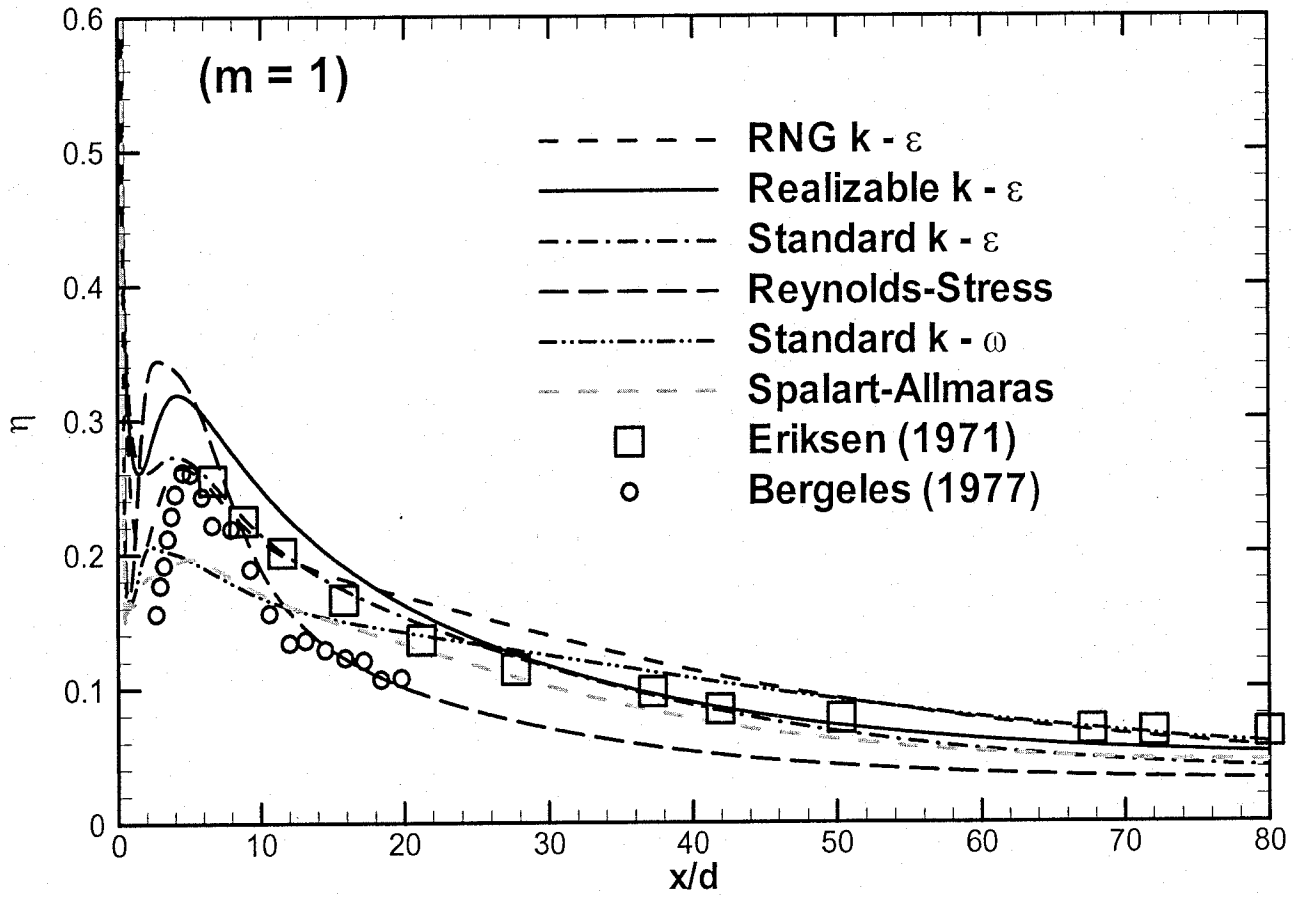

Figure 4.7 The performance of turbulence models with the experimental data of Eriksen (1971) and Bergeles (1977).

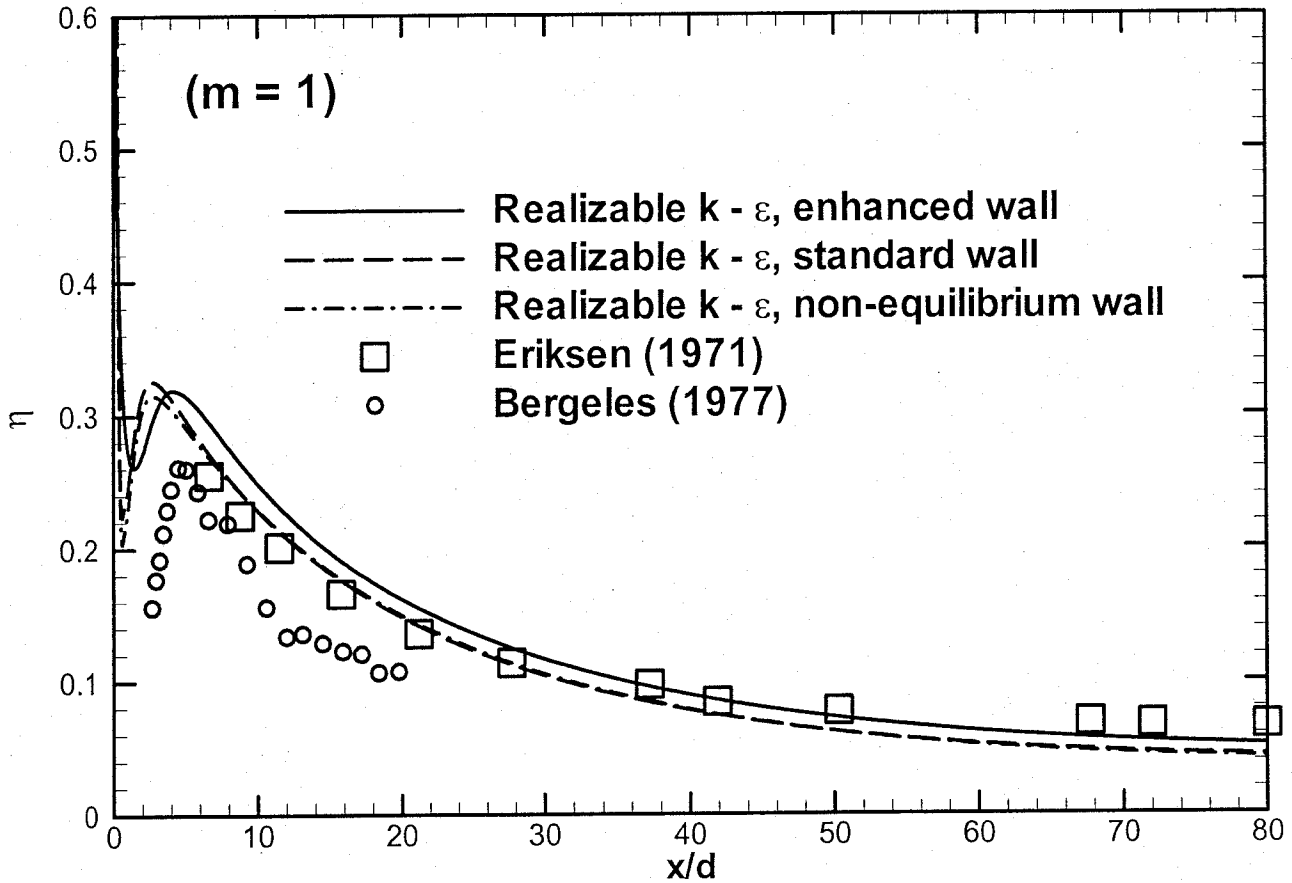

Figure 4.8 The effect of wall treatment on η prediction.

mesh in the near wall region, which is costly in computational time and, at the end, does not necessarily give a more accurate solution.

As shown in Figure 4.8, the jet liftoff effect was clearly captured; the minimum value of effectiveness occurred at x/d = 2, and the maximum value occurred at x/d = 4, which is confirmed by the experimental data given by Bergeles (1977). Close examination reveals that the point of the maximum effectiveness value at x/d = 4 matched very well with Bergeles (1977) because a heat-mass transfer analogy technique was employed instead of measuring the local wall temperature. In addition, the values of film cooling effectiveness were obtained by measuring at the plate surface the concentration of a tracer of helium introduced into the secondary air supply, thus eliminating conduction error.

4.3 Sinha case

In comparison with the Eriksen case, with long jets and no plenum, the Sinha case, with a short hole and plenum, is more complex and more realistic in jet engines. As mentioned above, this case has been compared with numerical prediction by many researchers over the years, such as Leylek (1993), Mulugeta (1996), Ferguson (1998), Walters (2000), Kapadia (2003), Immarigeon (2004) etc. All these papers documented that at low blowing ratio of less than 0.5, their prediction agreed well with the experimental data. However, at a higher blowing ratio such as 1, the most significant disagreement occurred immediately downstream of the jet exit, with an error as much as 100%, as shown in Figure 4.9. At a higher blowing ratio, the jets will lift off from the surface and penetrate into the main stream, causing the deterioration of protection. All previous works fail to

capture the jet liftoff and this could be attributed to either the deficiency of turbulence models, the use of isotropic eddy viscosity models, the presence of a recirculation region, or the use of wall functions. In the present study, a more rigorous methodology is employed and the jet liftoff effect, at high blowing ratios, is clearly captured for the first time, to the best of authors' knowledge. During this study, all the cases by Sinha et al. (1991) have been tested and consistent results have been obtained. The experimental parameters are shown in Table 4.2 ~ 4.4.

Figure 4.10 shows the comparison between the experimental data and the prediction of centerline effectiveness at D.R. = 2 and m = 1, as well as the relative performance of the three variants of k-ϵ models. The realizable k-ϵ model yielded the best results. The standard k-ϵ model completely missed the jet liftoff effect for this geometry. The RNG k-ϵ model considerably underpredicted the effectiveness in the near hole region, although it did capture the jet liftoff. The figure also shows that the results for the non-equilibrium wall functions option are identical to that of the standard wall functions.

Figure 4.11 shows the performance of different turbulence models at D.R. = 1.6 and m = 1. Again realizable k-ϵ model outperforms all the other turbulence models, as in the Eriksen case. Standard k-ϵ missed the jet liftoff effect completely, while the k-ω model barely captures it. The RNG k-ϵ, Spalart-Allmaras, and Reynolds-stress models all significantly underpredicted the effectiveness in the near hole region from x/d = 2 to 12, although all turbulence models captured the correct trend. At D.R. = 1.6 and m = 0.9, and D.R.=1.2 and m = 0.78, excellent agreement between the experimental data and the

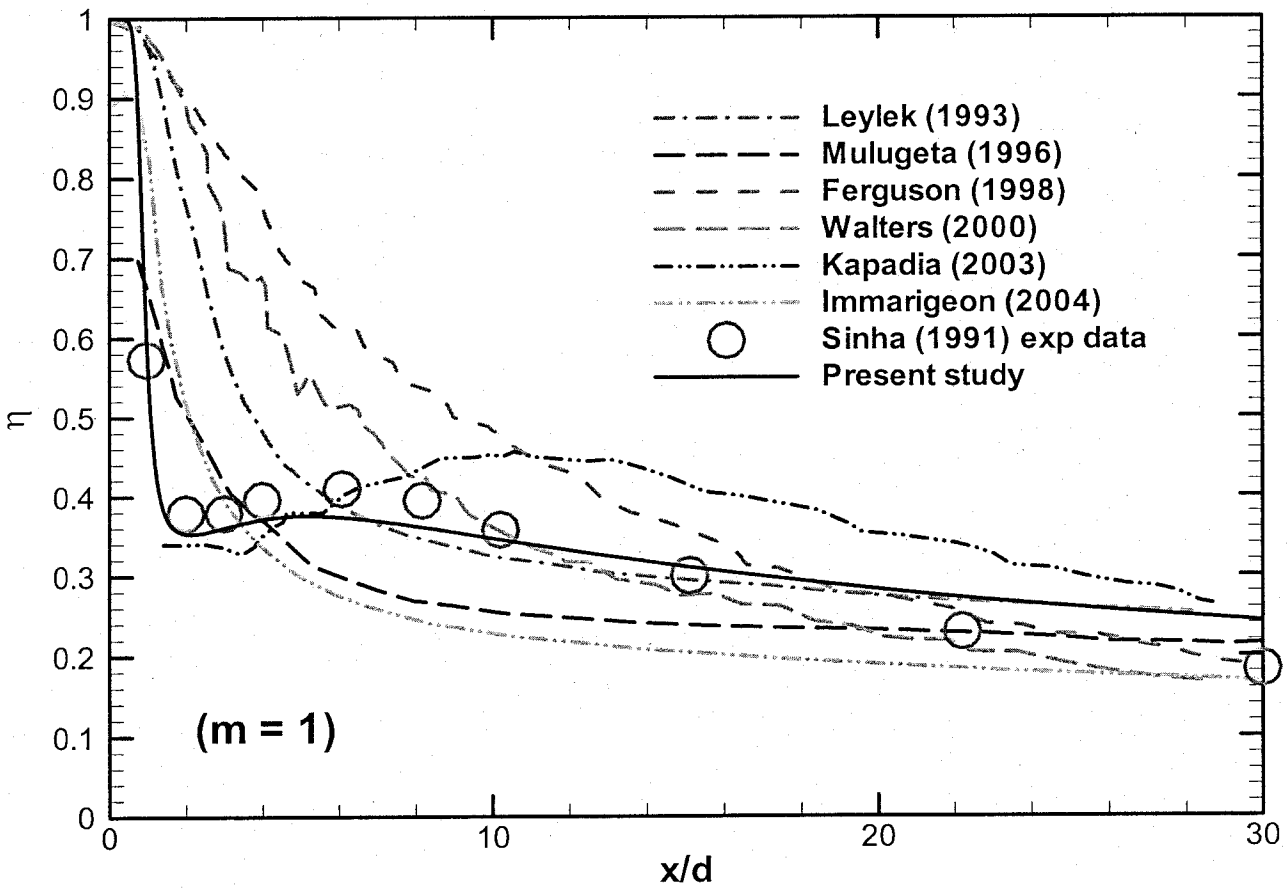

Figure 4.9 Present and previous predictions for Sinha (1991) experimental data.

Table 4.2 Experimental parameters for Sinha (1991) case – at $\rho_\infty/\rho_j = 2.0$

Density Ratio $\rho_\infty/\rho_j = 2.0$						
	U_∞ (m/s)	T_∞ (K)	U_j (m/s)	T_j (K)	V.R.	I
m = 1.0	20	300	10	150	0.5	0.5
m = 0.8	20	300	8	151.1	0.4	0.32
m = 0.5	20	300	5	150	0.25	0.125

Table 4.3 Experimental parameters for Sinha (1991) case – at $\rho_\infty/\rho_j = 1.6$

Density Ratio $\rho_\infty/\rho_j = 1.6$						
	U_∞ (m/s)	T_∞ (K)	U_j (m/s)	T_j (K)	V.R.	I
m = 1.0	20	300	12.5	190.4	0.625	0.625
m = 0.9	20	300	11.2	189.7	0.56	0.5
m = 0.8	20	300	10	190.4	0.5	0.4
m = 0.57	20	300	7	187.6	0.35	0.2

Table 4.4 Experimental parameters for Sinha (1991) case – at $\rho_\infty/\rho_j = 1.2$

Density Ratio $\rho_\infty/\rho_j = 1.2$						
	U_∞ (m/s)	T_∞ (K)	U_j (m/s)	T_j (K)	V.R.	I
m = 1.0	20	300	16.6	249.2	0.83	0.83
m = 0.78	20	300	13	250	0.65	0.5
m = 0.6	20	300	10	250	0.5	0.3
m = 0.5	20	300	8.4	252.4	0.42	0.208
m = 0.25	20	300	4.16	249.7	0.208	0.05

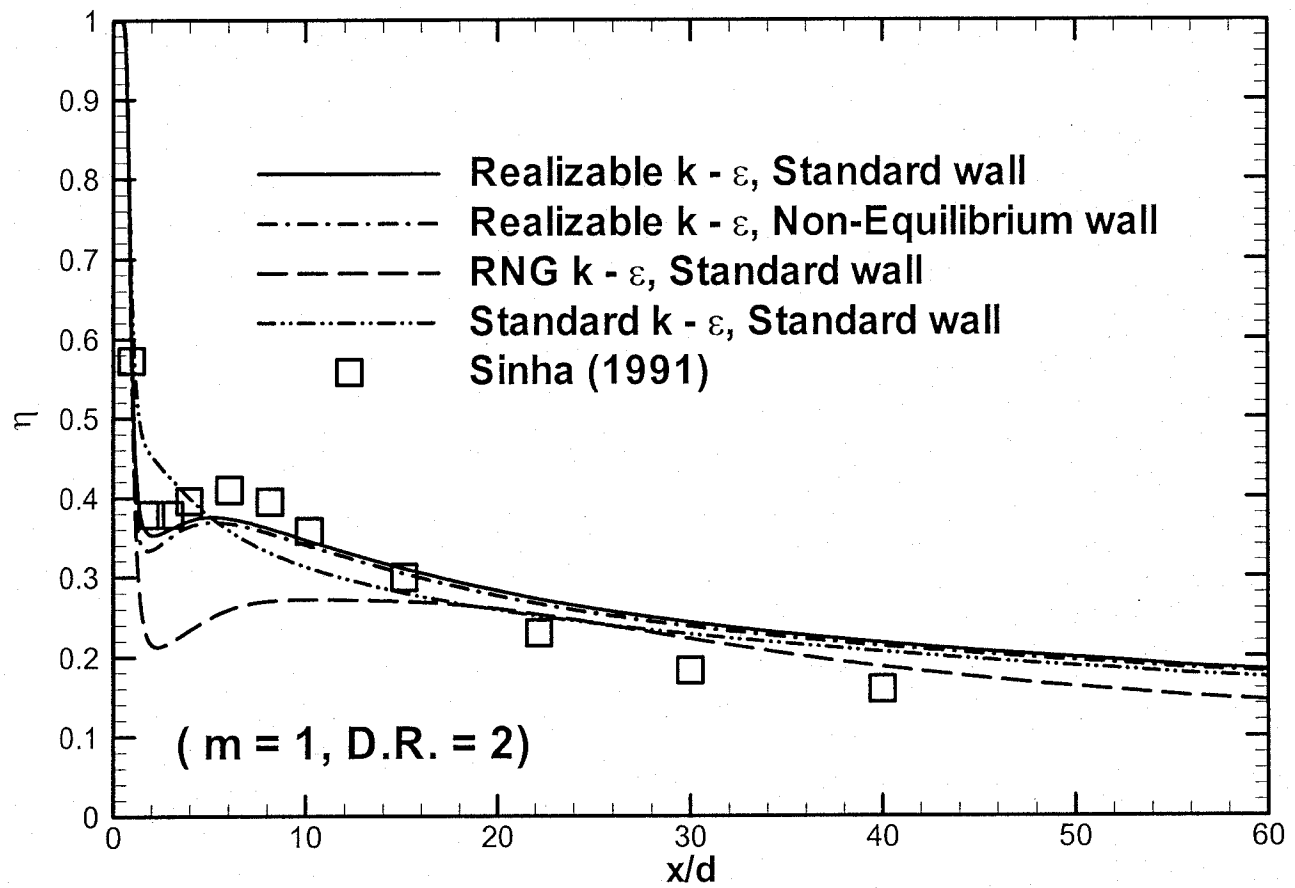

Figure 4.10 The performance of different wall treatments with Sinha (1991) experimental data.

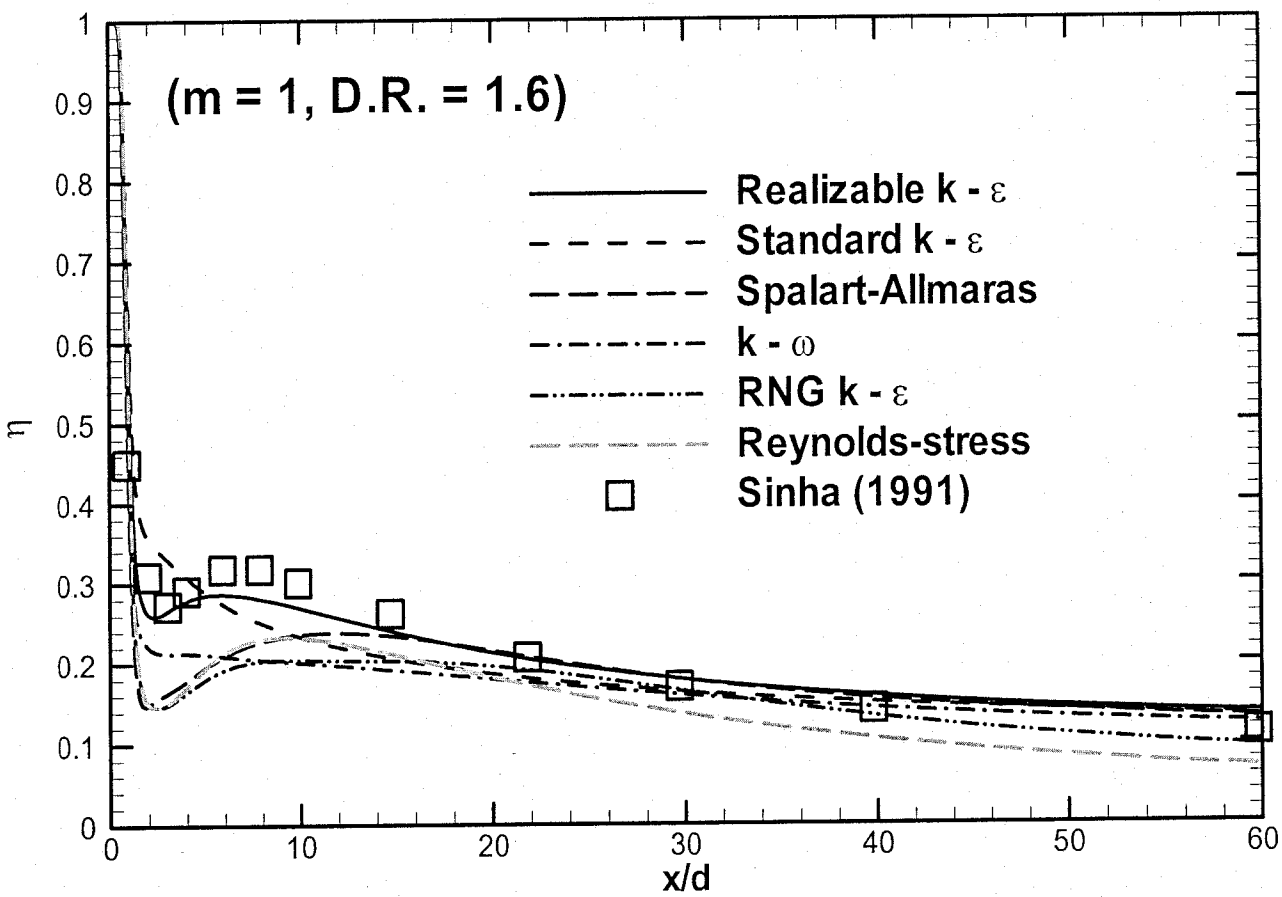

Figure 4.11 The performance of turbulence models with the experimental data of Sinha (1991).

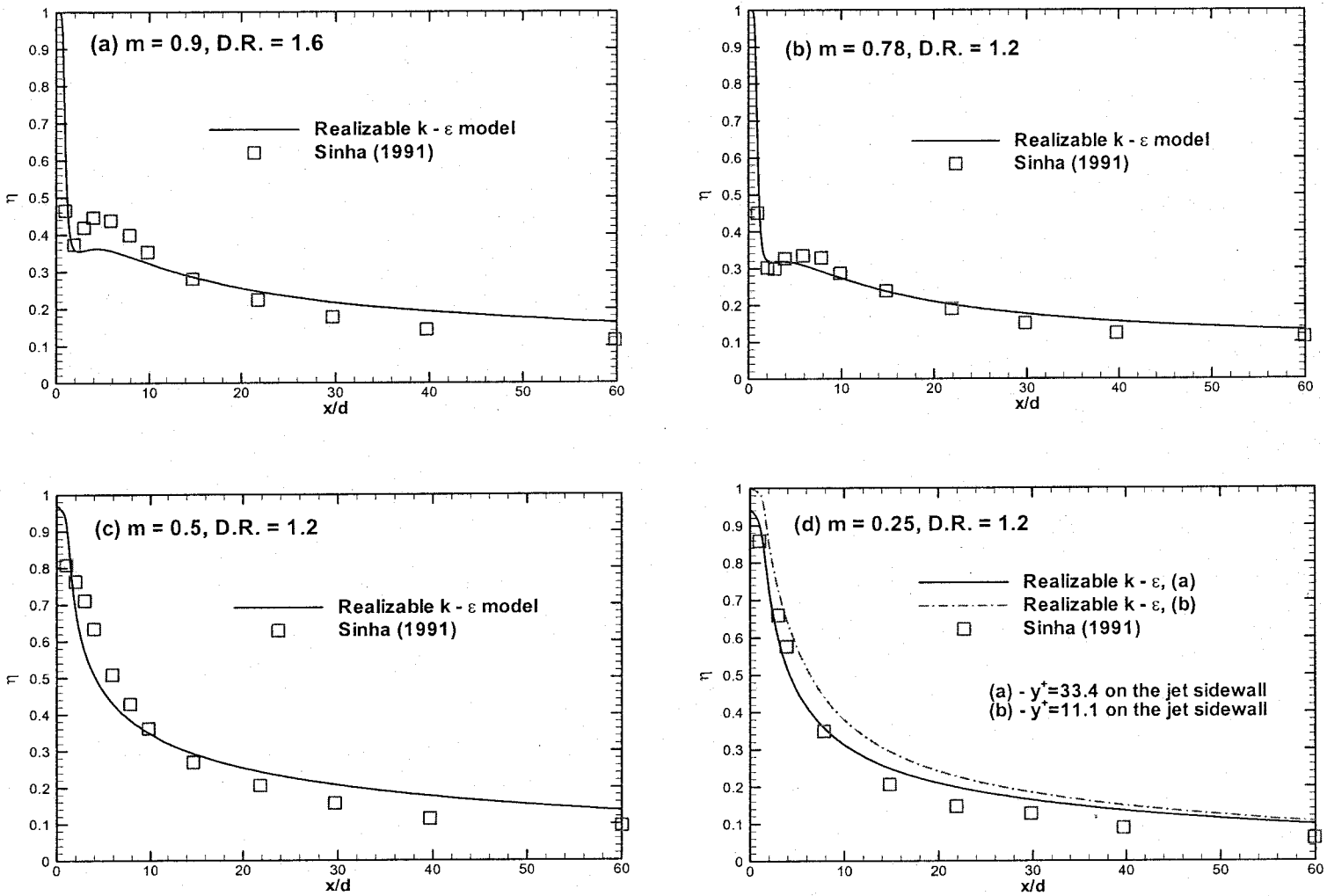

Figure 4.12 Predictions of η at different cooling parameters.

predictions was obtained with the jet liftoff unquestionably captured, as shown in Figure 4.12a and b. At low blowing ratio of D.R. = 1.2 and m = 0.5, and D.R. = 1.2 and m = 0.25, the jets remained attached to the surface, and excellent agreement is shown in Figure 4.12c and d. Figure 4.12d shows that the solution is sensitive to the near wall mesh (y^+). In these two cases, the area averaged y^+ on the bottom test surface is maintained constant at 34 while all other parameters remained the same. Also, the area averaged y^+ on the jet sidewall, which is a very small part of the whole domain, was different between the two cases, where Case (a) had a y^+ value of 33.4 while Case (b) had a y^+ value of 11.1 on the jet sidewall surface. The difference of the centerline effectiveness between these two cases would show that the boundary layer has a tremendous influence on the final solution.

Figure 4.13 shows the local effectiveness in the spanwise direction. The prediction agreed very well with the experimental data. Contrary to the popular thought that current turbulence models systematically underpredict the adiabatic effectiveness in the spanwise direction, it seems the prediction would match the experimental data better if conduction error on the testing surface is taken into account in the experimental work, which to date has been neglected. Therefore, if the current turbulence models did underpredict the adiabatic effectiveness in the spanwise direction, the underprediction is not as severe as previously thought as long as all experimental error is taken into account. The Sinha's case further confirms that the present methodology is fully capable of capturing the jet liftoff effect and can consistently give accurate results with density ratio ranging from 1.2

to 2.0 and blowing ratio ranging from 0.25 to 1.0, both in the centerline and in the spanwise direction. The possible reasons of capturing this correct trend are given below.

1. Structured meshes perform better than unstructured counterparts. Recent research has favored unstructured meshes, with usually tetrahedral elements, since it is easy to generate and can be easily adapted to concentrate more nodes in areas of large gradients as well as adjust the near wall mesh according to the value of y^+. However, it is extremely difficult to control the distribution of the nodes and the truncation error is considerably larger than the hexahedral mesh. As a result, a large part of the nodes are placed in some areas with small gradients, resulting in unnecessarily finer meshes, which is a waste of numerical resource. Consequently, in the near hole region, the mesh is too coarse to resolve the wake of recirculation. Another drawback of unstructured mesh is the numerical diffusivity, which can cause a serious error. The structured mesh, on the other hand, is more difficult to create and can not be adapted. Thus, if the y^+ is not appropriate to meet the near wall mesh requirement, the mesh must be discarded and a new one created. However, the high fidelity of the solution and the high accuracy of structured mesh is incomparable and worth the extra effort.
2. The y^+ issue has to be taken seriously. The present turbulence models are empirical or semi-empirical, and for the most part are only valid in the turbulence core flow far away from the boundary layer. Within the boundary layer, which has an extremely significant effect on the final solution, the

current turbulence models are not valid. Therefore, a series of empirical relations are brought in to bridge that gap to reach closure. Hence, in order for the solution to be physically meaningful, a certain requirement, namely y^+, has to be satisfied. Figure 4.14 shows the typical contour of y^+ on the testing surface in this study. The value of y^+ falls in the range of 30~60 and the area averaged y^+ is 34 on the bottom wall when standard wall functions are employed. Figure 4.14b shows the Sinha case and 4.14c shows the new scheme. When enhanced wall treatment is selected, the area averaged y^+ on the wall is 2.7, as is the case for the Eriksen case shown in Figure 4.14a. Figure 4.12d shows the effect of y^+ on the final solution. Thus, the solution is very sensitive to y^+.

3. The selection of computational domain is very important. During the course of the present study, the selection of the height of the computational domain definitely has some effect on the solution. Since a height of 10d did not seem sufficient, a height of 20d was tested, and it was found that the results given by 30 and 40d high geometry were identical to that of the 20d high one. Kim (1992) selected 7.5d high, Tyagi (1999) 5d high, Hale (1999) 6d, Hoda (2000) 5d, while most of the others selected 10d high in the open literature. This can partly explain the large descrepancies between the experimental data and their predictions in the immediate near hole region. If the height of the duct is too low, and the free slip or zero shear stress boundary conditions are imposed on the top wall, the flow will be squeezed in the vertical direction. Thus, the simulations cannot emulate the jets correctly, as in the experiments.

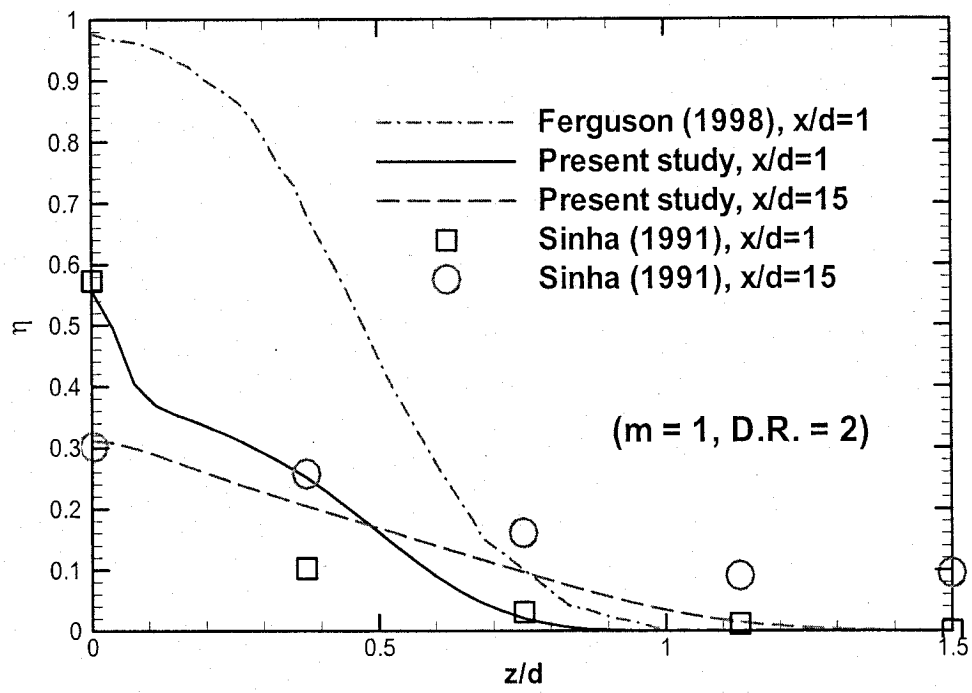

a.

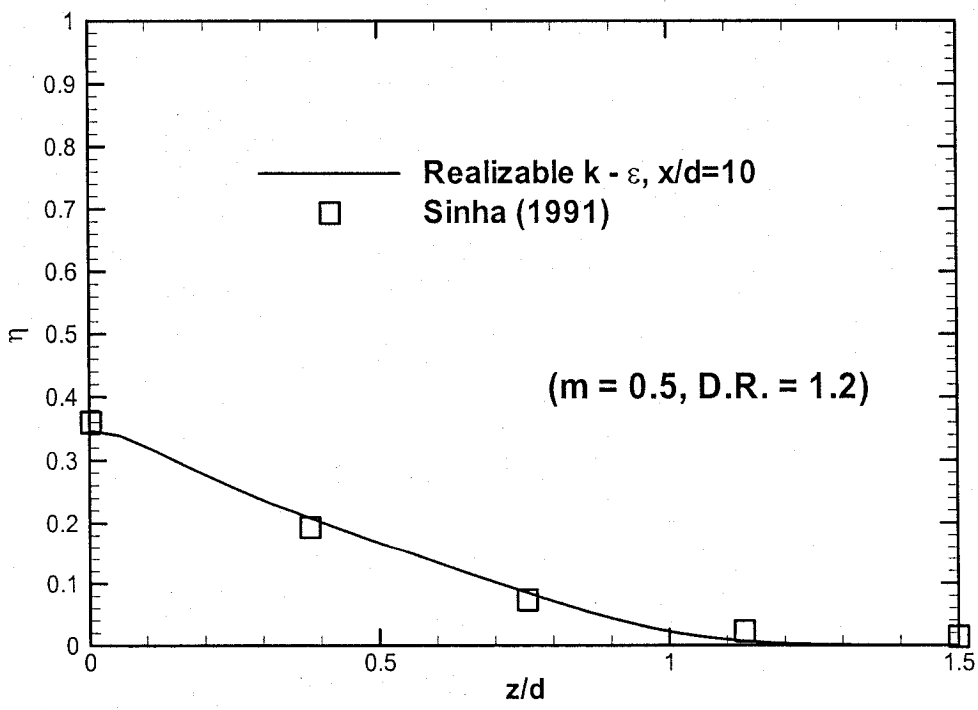

b.

Figure 4.13 Predictions of η in the spanwise direction.

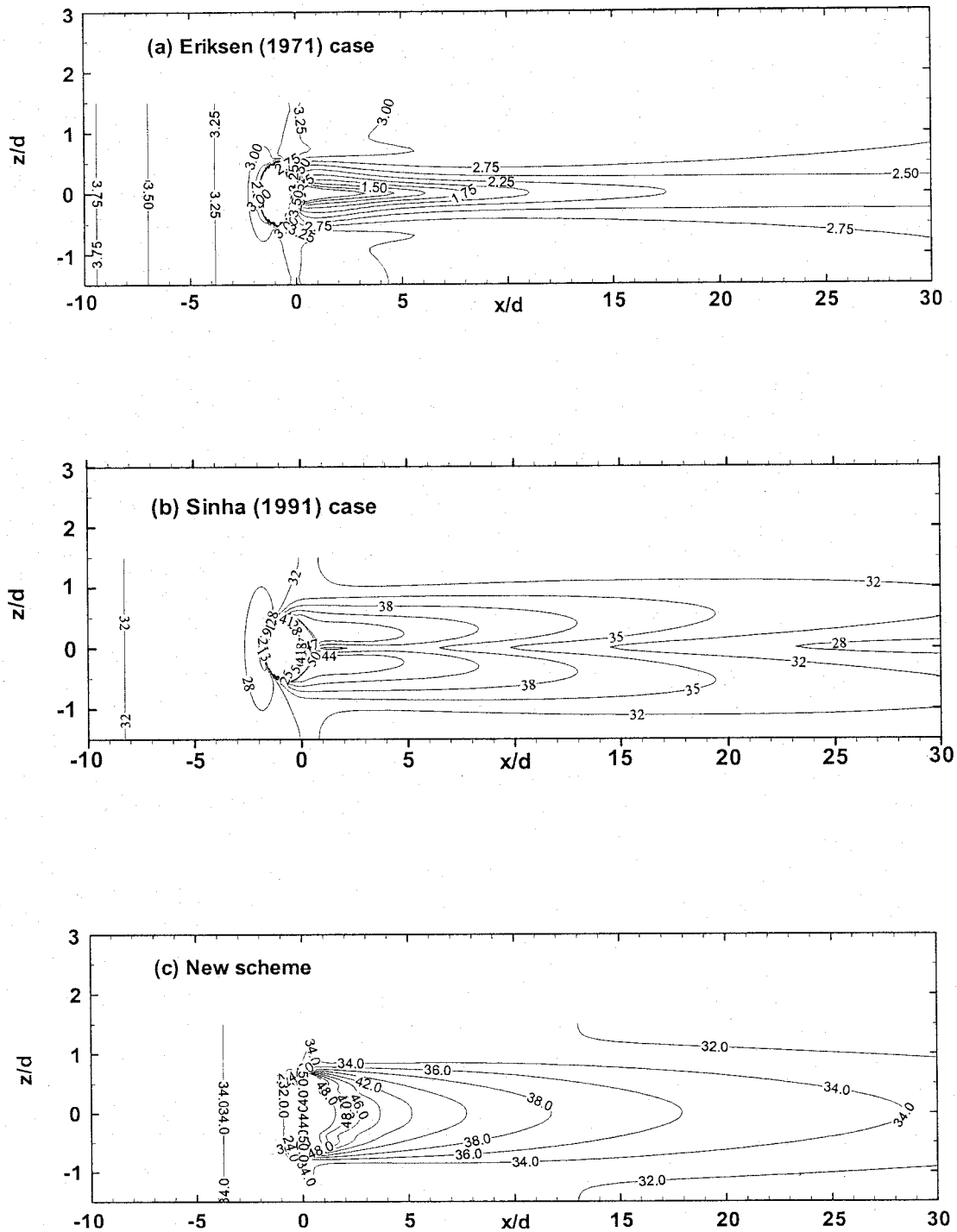

Figure 4.14 Typical contours of y^+ value on the bottom wall.

In these two benchmark cases, one considers very simple long jets, while the other considers short jets and a plenum. It seems that the prediction of the Eriksen case is in better agreement to the experimental results than the Sinha case due to the strong coupling between the mainstream flow and jets. The Sinha case is associated with some uncertainties caused by the plenum, but overall, the prediction compares very well with the experimental data. Using the present methodology, the realizable k-ϵ model with standard wall functions gives accurate results consistently when different geometries at different density ratios and different blowing ratios were considered. Thus, in the new scheme, the realizable k-ϵ model with standard wall functions was selected to perform the simulations. Results are following.

4.4 New scheme

Since there is no experimental data available for the new scheme, shown in Figures 4.3 and 4.4 for comparison purposes, the dimension of the new scheme (d = 0.03620m) is specifically defined such that the area of the jet cross section of the new scheme is equal to that in the Sinha case(d = 0.0127m). This means that at the same blowing ratio used in the Sinha case, the same amount of coolant will pass through the jet hole of the new scheme. Thus, at the same blowing ratio with the same amount of coolant being used and with all the other parameters remaining the same, the performance of the new scheme will be compared with that of Sinha case. The results of two cases will be presented, i.e. m = 1 and 0.5 at D.R. = 2. The test parameters are shown in Table 4.5.

Figure 4.15a shows the centerline effectiveness at m = 1 and D.R. = 2, in the Sinha case, the jet liftoff from the surface causes a sharp drop in effectiveness immediately down stream of injection. However in the new scheme, the jets still remain attached to the surface and the effectiveness gradually decreases in the streamwise direction. At x/d around 5, both schemes give the same centerline effectiveness. In the region of x/d < 5, the new scheme gives much higher centerline effectiveness than the traditional cylindrical jets due to jet liftoff effect. Since the new scheme renders the coolant more uniform in the spanwise direction, the rarefied coolant yields slightly lower centerline effectiveness than the traditional cylindrical holes further downstream after x/d = 5. Figure 4.15b shows the centerline effectiveness at m = 0.5. At blowing ratio of 0.5, the traditional cylindrical jets remain attached to the surface. However, the coolant issued from the exit of the new scheme is more uniform. Consequently, the centerline effectiveness is lower than the cylindrical jets due to the fact that the coolant is stretched thin in the spanwise direction after injection. The advantage of the new scheme is shown clearly in the effectiveness distribution in the spanwise direction presented in Figure 4.16. Along the x/d = 1 line, from z/d = 0 to 0.6, the local effectiveness of the new scheme is almost constant and much higher than that of the traditional cylindrical holes. At x/d = 15, due to turbulence, the coolant mixed with the mainstream, resulting in approximately equal effectiveness for both the new scheme and the cylindrical jets. However, the effectiveness of the new scheme is still more uniform than the traditional cylindrical jets. Figure 4.17 compares the contours of effectiveness on the test surface for both Sinha case and the new scheme at m = 1. It can be seen that the new scheme gives more uniform protection than the cylindrical jets.

Table 4.5 Test parameters for the new scheme – η

	m = 1	m = 0.5
d (m)	0.03620	0.03620
U_∞ (m/s)	20	20
T_∞ (K)	300	300
U_j (m/s)	10	5
T_j (K)	150	150

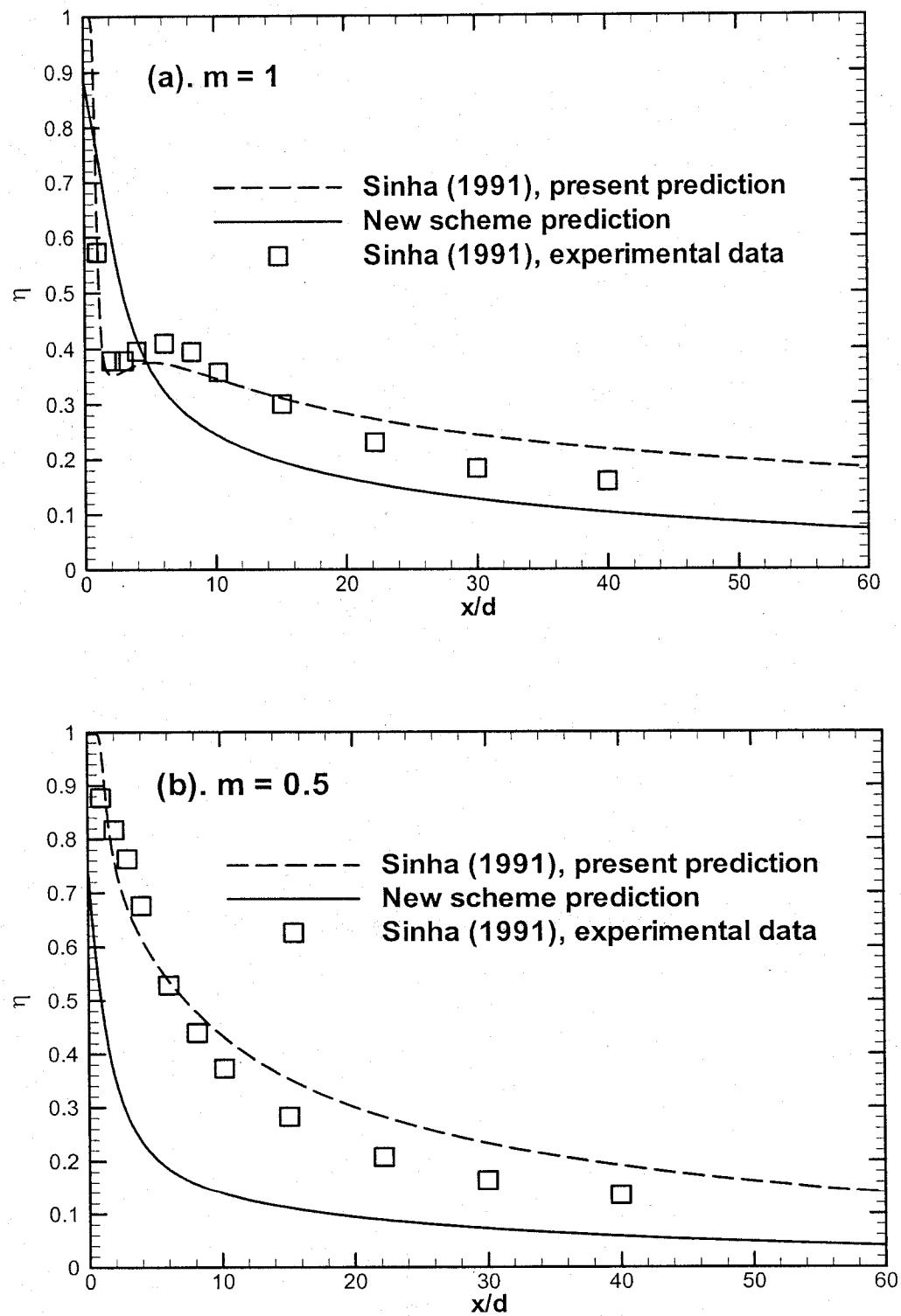

Figure 4.15 Centerline effectiveness for the new scheme showing the jet remain attached to the testing surface at m=1.

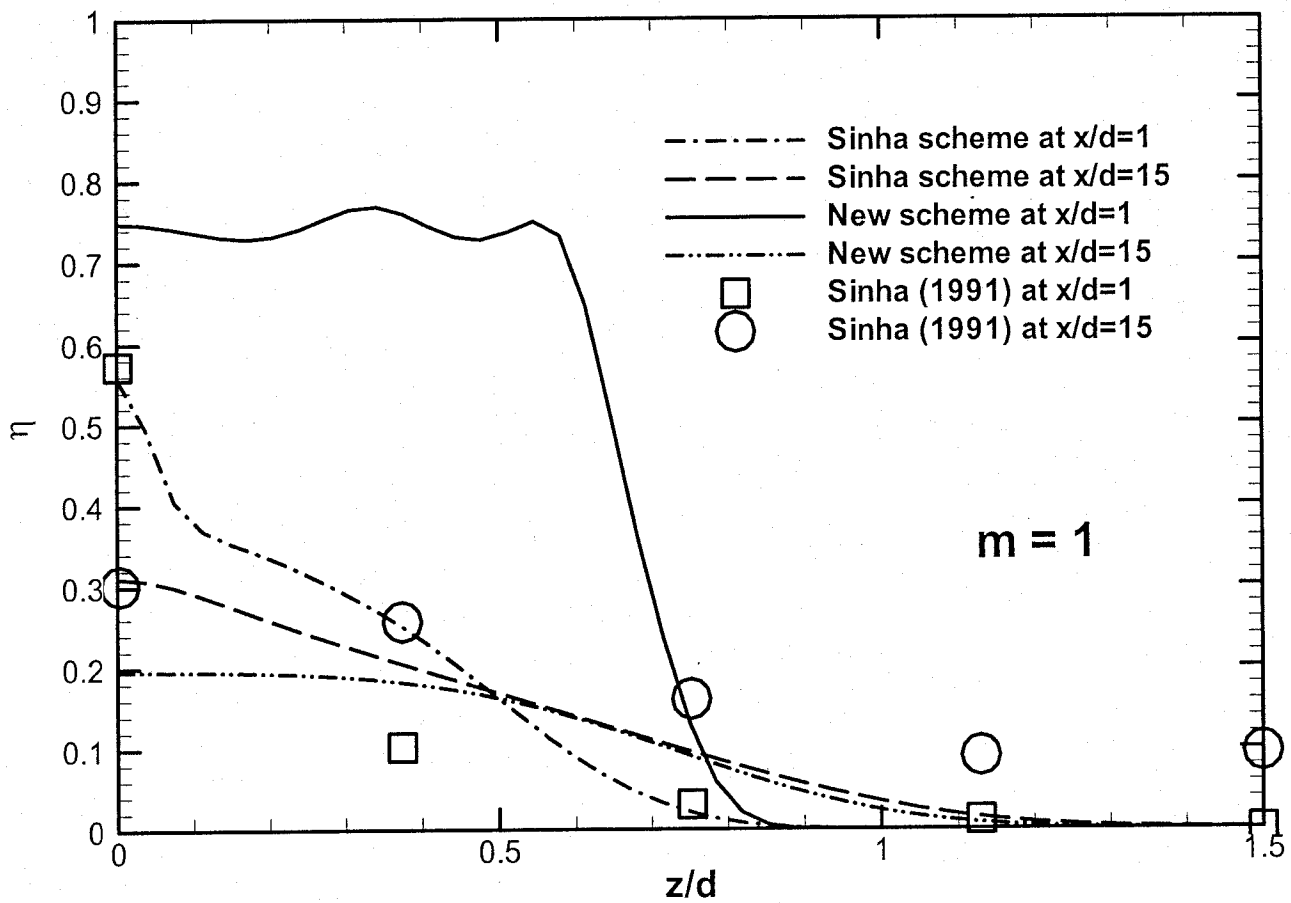

Figure 4.16 Comparison of the local spanwise effectiveness for the new scheme with the standard scheme of Sinha (1991).

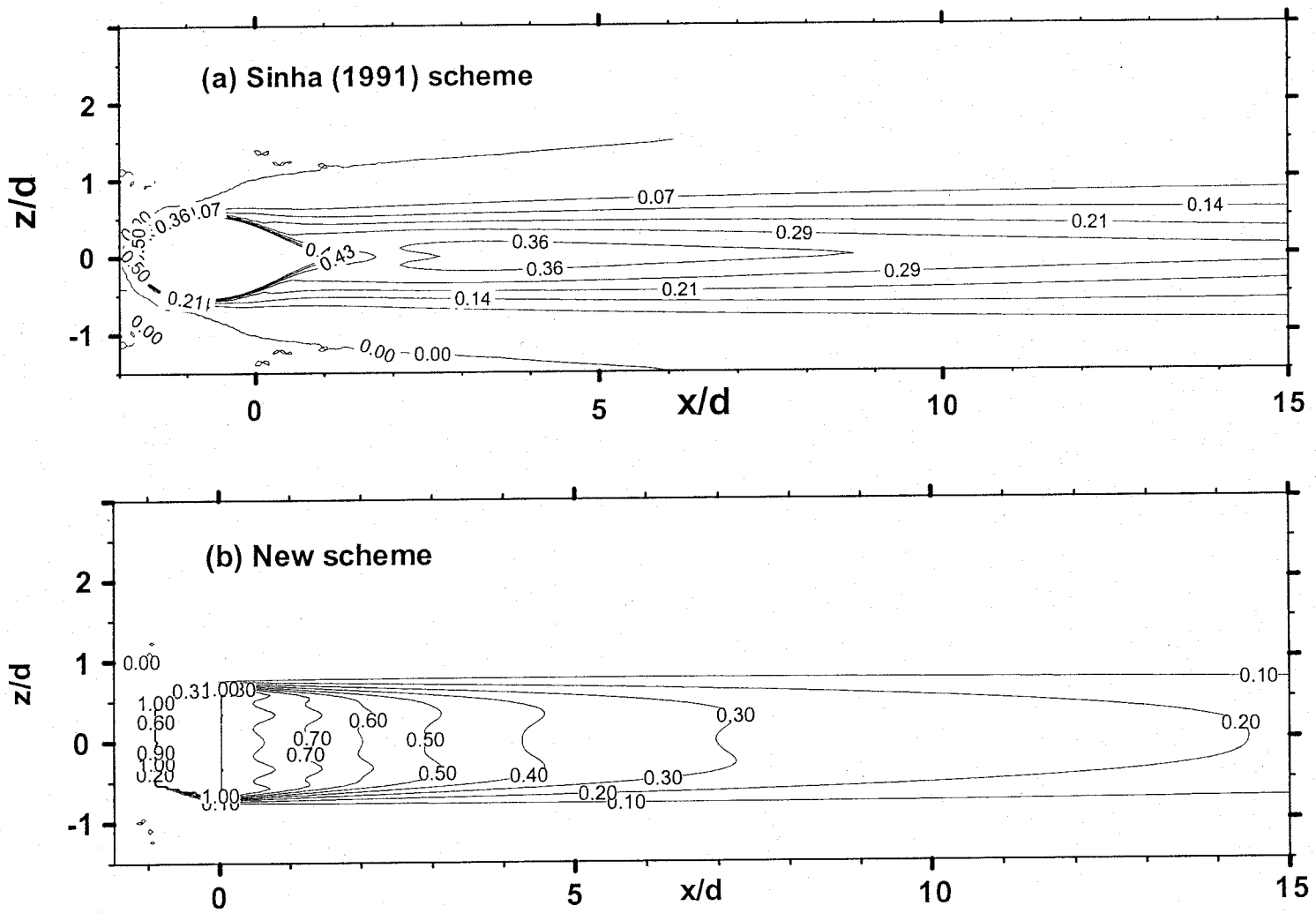

Figure 4.17 Contour of adiabatic effectiveness on the bottom wall.

For the two cases, both at m = 1 and 0.5, the new scheme give more uniform effectiveness than the traditional cylindrical hole, especially at higher blowing ratios since the traditional cylindrical jet lifts off from the surface. Thus the new scheme will efficiently eliminate the presence of hot or cold spots on the protected surface, and significantly reduce thermal stress level on the turbine blade and elongate the expected service life of the engine. In the new scheme, the coolant remains attached to the surface for all blowing ratios tested from 0.5, 1, 3, 6, to 20, and even at 50. However, at a blowing ratio of 50, the velocity in the jet cross section becomes supersonic, and so the incompressible assumption ceases to be valid. Thus, the simulation at blowing ratio of 50 has no physical meaning except for the purpose of showing whether or not the jets will lift off. With this new scheme, no matter how high the blowing ratio is, the possibility of jet liftoff is completely eliminated, which will significantly reduce the disturbance to the mainstream and reduce the efficiency penalty. The only drawback is that as the coolant become more uniform after injection, the coolant has more surface area directly in contact with the hot mainstream when compared to the traditional cylindrical hole. Therefore, it is possible that some coolant could dissipate into the hot mainstream, which will reduce the protection effect slightly.

Figure 4.18 shows the comparison of the velocity vectors at the cross section of x/d = 2 for both Sinha case and the new scheme. There is usually a strong horse-shoe vortex pair associated with the traditional cylindrical jets since there is strong interaction between the jet and the mainstream causing the hot mainstream to tuck in below the jets and thus deteriorating the jet performance. However, in the new case, there are four very weak

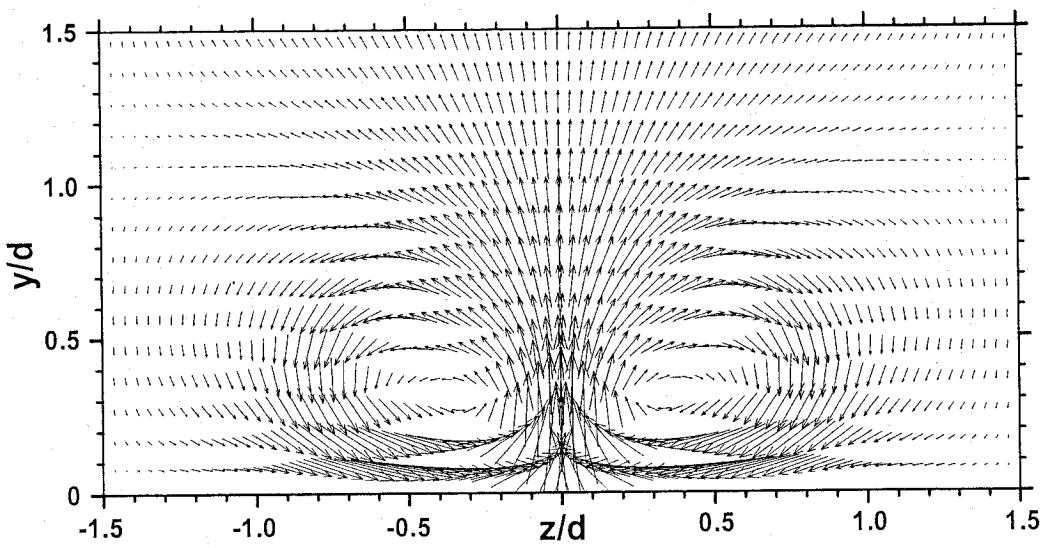

a. Sinha (1991) scheme

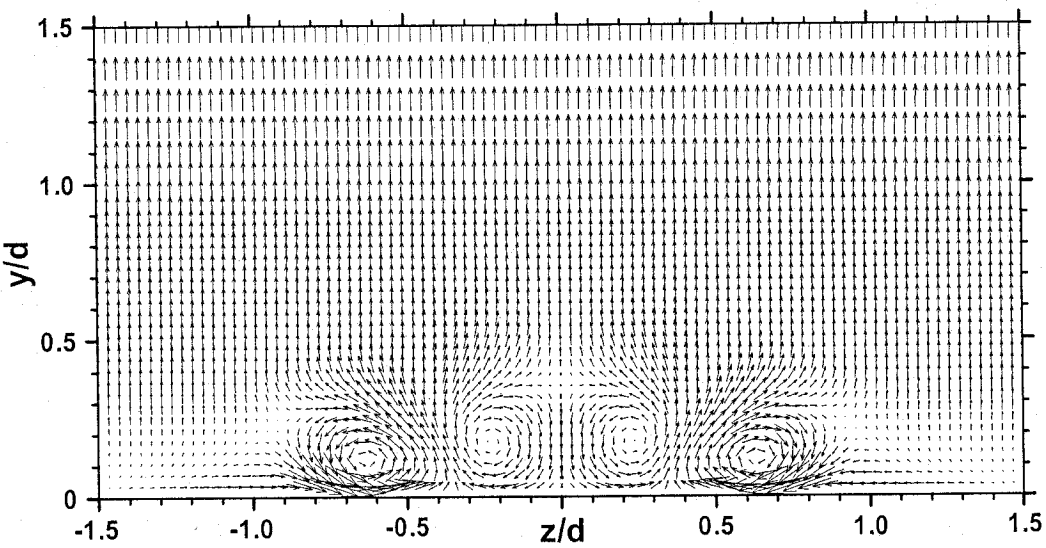

b. new scheme

Figure 4.18 Velocity vectors at the cross section of x/d = 2.

vortices created by the interaction between the mainstream and the coolant after injection due to the momentum being considerably reduced after passing diffused section of the jet. The presence of the weak vortices results in more uniform velocity in the x-direction and the coolant forms a smooth blanket over the surface, providing more efficient protection against the hot mainstream.

Chapter 5

Predictions of Heat Transfer Coefficient

5.1 Geometries and boundary conditions

In the experiments intended for measurement of adiabatic effectiveness, there is no need of construction of a constant heat flux, thus insulating materials like Styrofoam can be used to make the test surface, which can reduce conduction error significantly, the main reason that all the results of adiabatic effectiveness from different researchers are similar to one another. However, in order to measure the heat transfer coefficient, a constant heat flux condition on the bottom wall is required and the manner in which the constant heat flux plate is constructed has a significant effect on the temperature distribution on the bottom surface. This explains why there are large discrepancies between experimental results given by different researchers (as shown in Figure 5.1). The present study will show that the conduction errors on the test surface are much larger than believed in previous experimental investigations.

Usually a very thin plate such as stainless steel sheet was used to cover the bottom wall and was heated underneath by electrical wire. On one hand a material with high thermal conductivity is desirable so the heat could conduct without loss across the sheet and into the flow where it is generated; on the other hand heat conduction in the lateral direction can create a big error for it will make the heat flux not uniform any more. In this study, the heat conduction on the test surface will be considered in the simulations by modeling

conjugate heat transfer. In order to validate the methodology which will be used for the new scheme, the experimental works of Eriksen et al. (1971) and Sen et al. (1996) have been chosen as the benchmark cases. Eriksen et al.'s case consisted of a very simple long jet without plenum, where the flow at the exit of jet was fully developed since long tubes (around 1 m) were used, thus eliminating uncertainties introduced by jet exit profiles. In Sen et al.'s case, a short jet with plenum was used, which represents real engine applications more closely.

The computational domains and film cooling geometries used in this study are: (a). for both Eriksen case and the new scheme – the same as figure 4.1, 4.3, 4.4. (b). for Sen case see Figure 5.2. The parameters and the geometries of the two benchmark cases in the present computational study are exactly the same as in experimental studies by Eriksen et al. (1971) and Sen et al. (1996). At the bottom wall, from the point of upstream inlet to the starting point of the constant heat flux, an adiabatic wall boundary condition with no-slip is applied. From the starting point of the heat flux to outlet of the duct, a constant heat flux is imposed. On the other walls, same as shown in figure 4.1 ~ 4.3. Therefore, constant heat flux boundary condition is applied only on the test surface section, downstream of the injection. In the open literature, most of the researchers such as Brittingham (2000), Ferguson (1998) applied constant heat flux boundary condition in their heat transfer simulations on the whole bottom wall, however, in the experimental study with which their results are compared, only the test surface downstream of the jet is instrumented with heater.

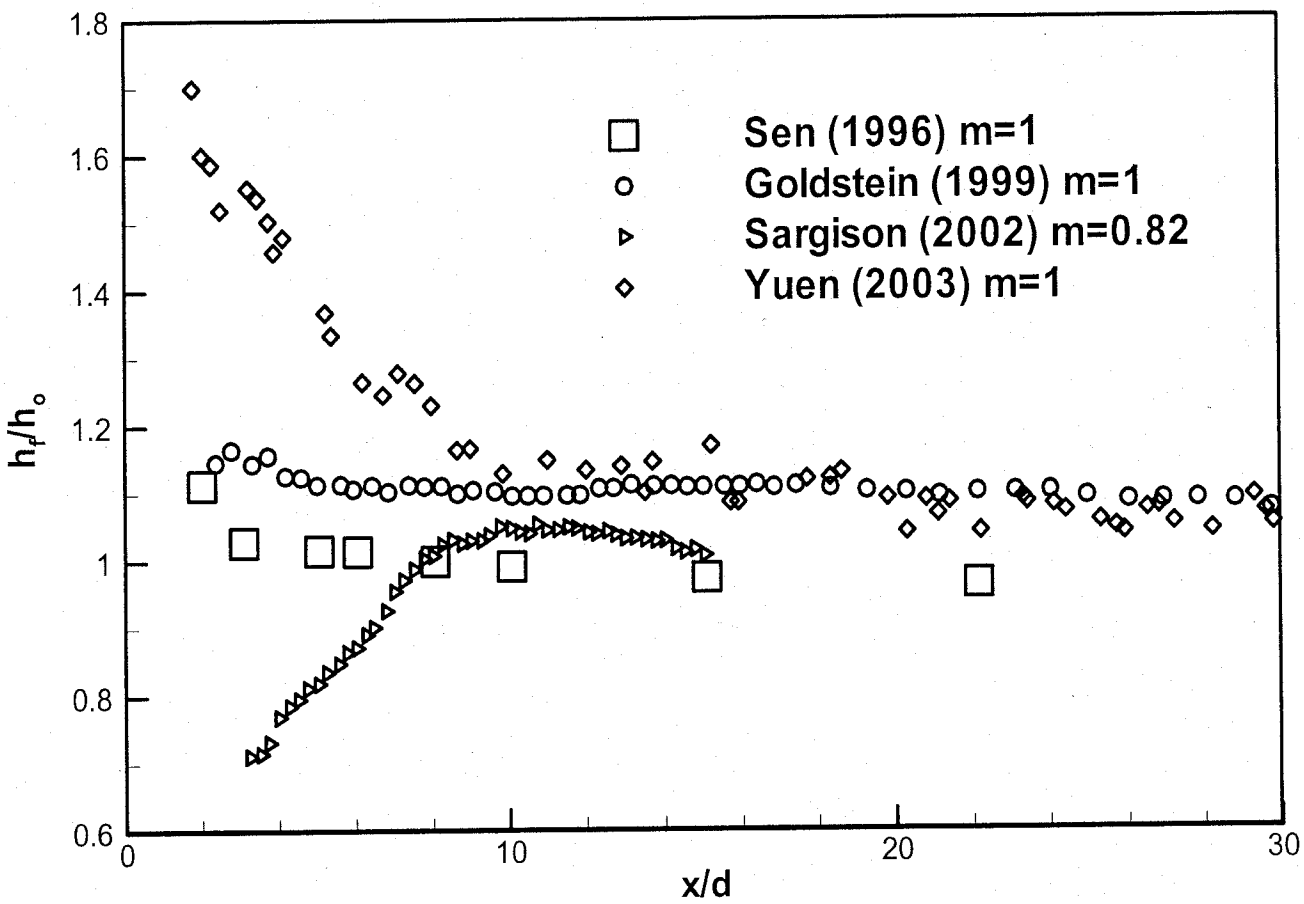

Figure 5.1 Disparities between experimental data of h given by different researchers on traditional cylindrical hole.

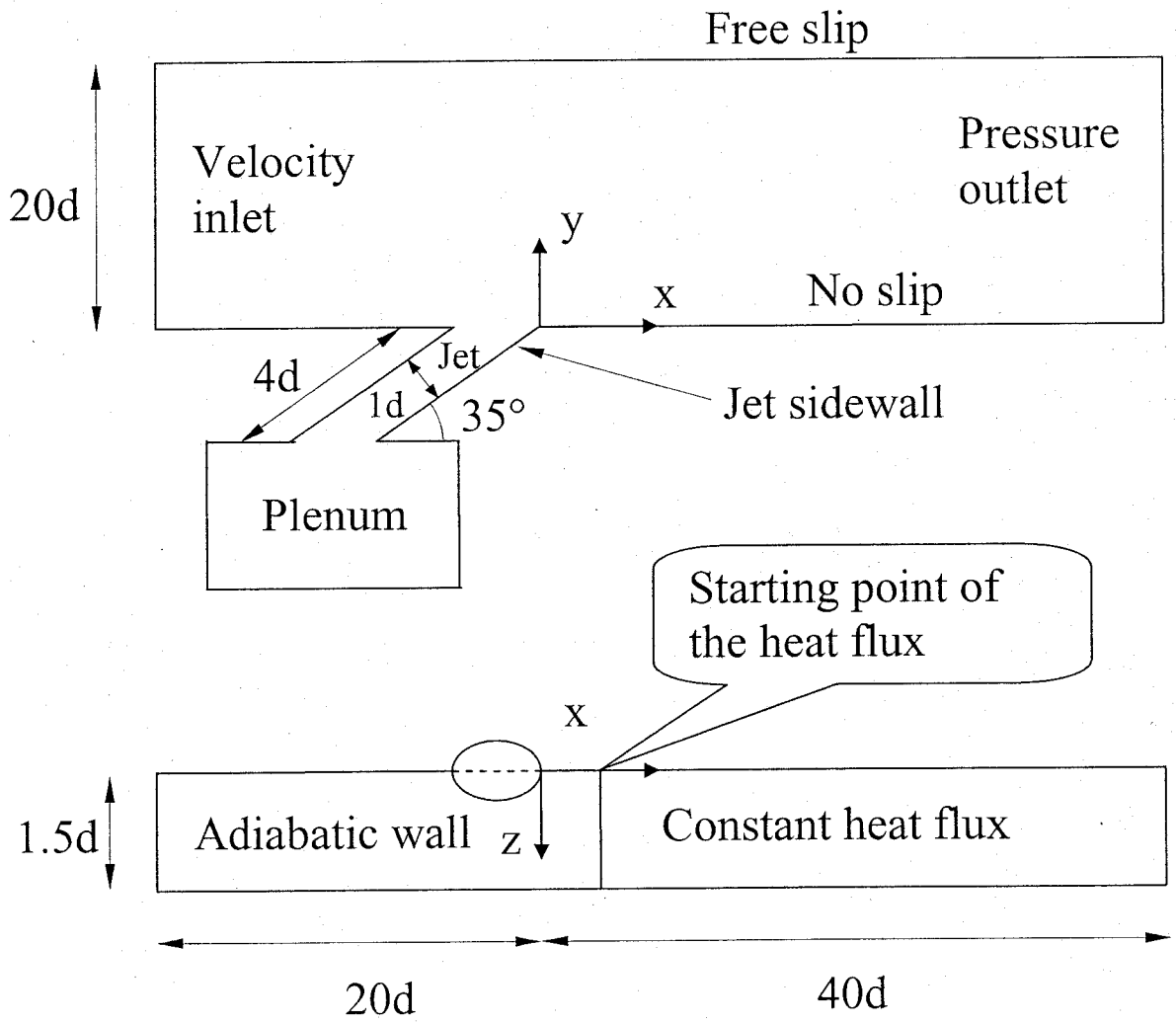

Figure 5.2 Geometry and computational domain for Sen (1996) case (d = 0.0111m).

5.2 Eriksen (1971) case

The test parameters are shown in Table 5.1. Figure 5.3 shows the performance of different turbulence models in terms of normalized heat transfer coefficient on the centerline at m = 1 and $Re_D = 0.22 \times 10^5$ for the Eriksen et al. (1971) case. The Reynolds-Stress model gives very good prediction in the region of x/d < 14 beyond which it under predicts the heat transfer coefficient significantly. Both k-ω model and Spalart-Allmaras model slightly under predicts the heat transfer coefficient in the near hole region of x/d < 15 and slightly over predicts the heat transfer coefficient in the region of x/d > 20. The k-ϵ model slightly under predicts the heat transfer coefficient in the near hole region of x/d < 15 as well, however, beyond this region it gives excellent result. Figure 5.4 shows the performance of the 3 variants of k-ϵ model, Realizable, RNG and Standard k-ϵ models. Although all of them give good prediction with the error less than 10%. The RNG k-ϵ model seems to slightly overpredict the heat transfer coefficient beyond x/d of 15, while the realizable k-ϵ model gives the correct trend. The standard k-ϵ model predicts the heat transfer coefficient the best in the region of x/d > 20. Hence, it was concluded that both the realizable k-ϵ model and standard k-ϵ model give realistic results, which are very close to each other.

Figure 5.5 shows the performance of three different wall treatments with the same standard k-ϵ model, namely the standard wall functions, the non-equilibrium wall functions, and the enhanced wall treatment. Contrary to the commonly accepted notion that two-layer based wall treatment gives better results, the three different wall treatments essentially yielded the same results provided that the near wall mesh requirement was

Table 5.1 Experimental parameters for Eriksen (1971) case – h

	m = 1	m = 0.2	m = 0.1
d (m)	0.0118	0.0118	0.0118
Re_D (based on d)	0.22×10^5	0.23×10^5	0.44×10^5
U_∞ (m/s)	29.234	30.563	58.469
T_∞ (K)	300	300	300
U_j (m/s)	28.971	5.96	5.788
T_j (K)	300	300	300
q (W/m^2)	1290	1290	1990

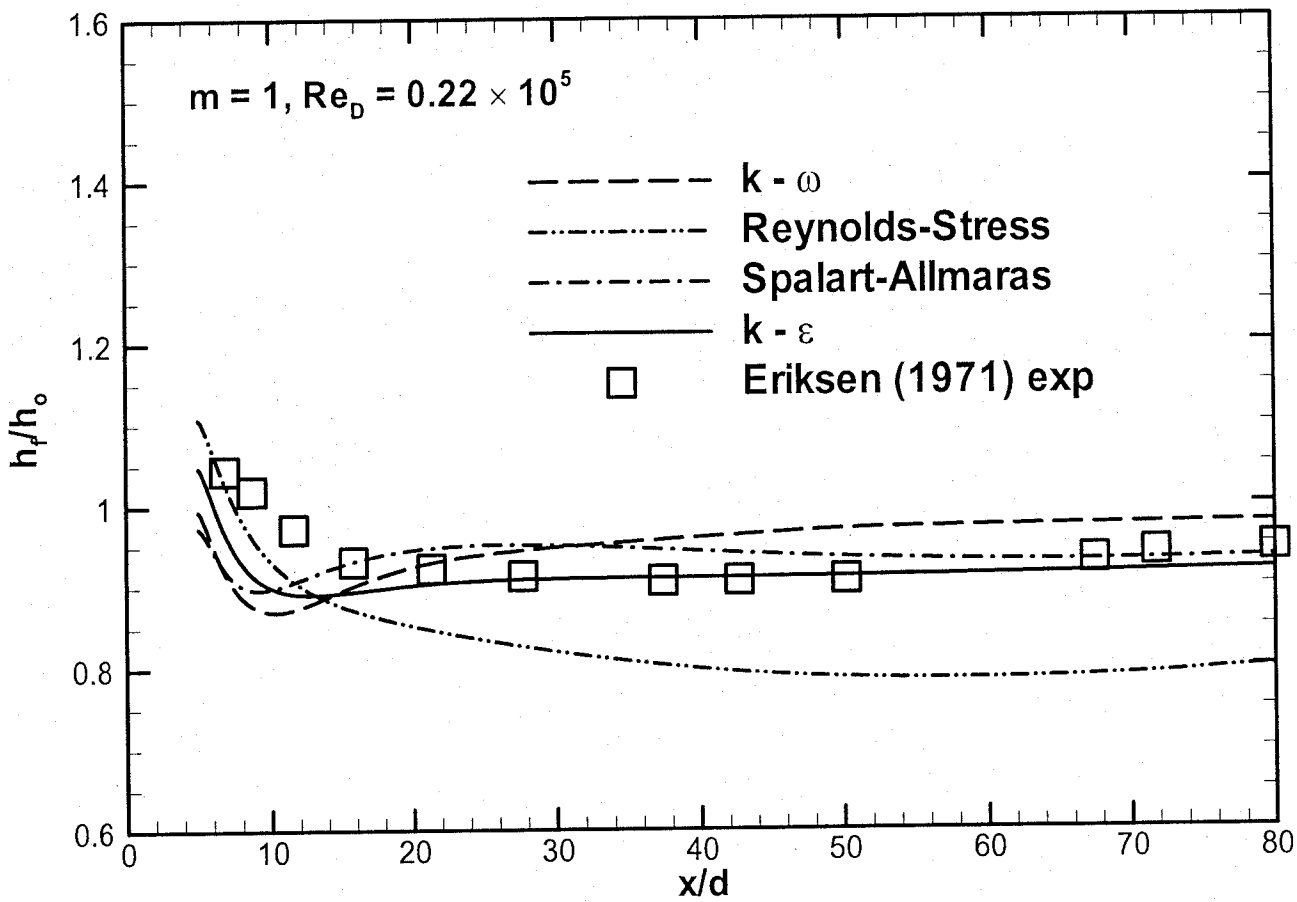

Figure 5.3 The performance of turbulence models with the experimental data of Eriksen (1971)

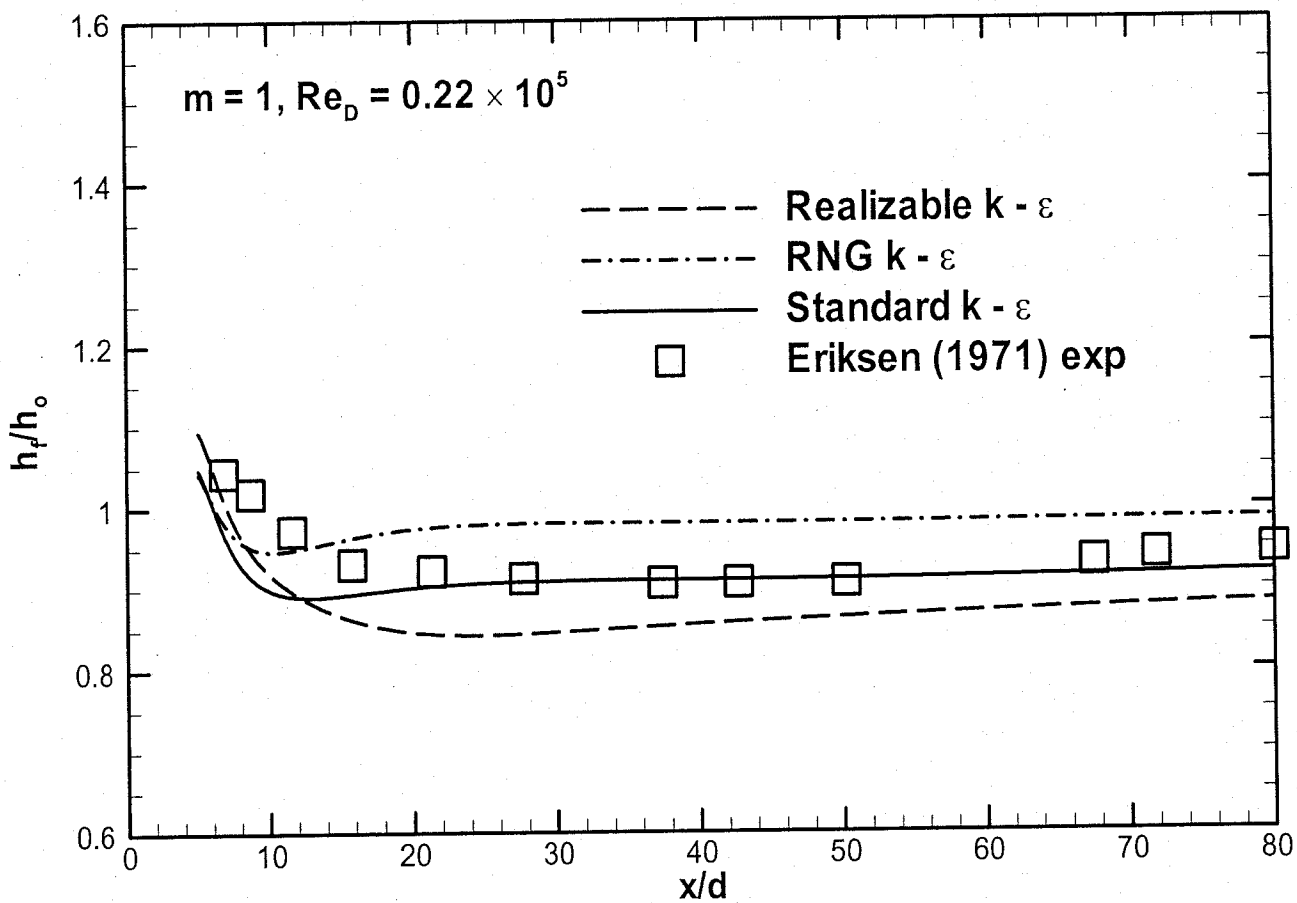

Figure 5.4 The performance of 3 variants of k-ϵ turbulence models with the experimental data of Eriksen (1971)

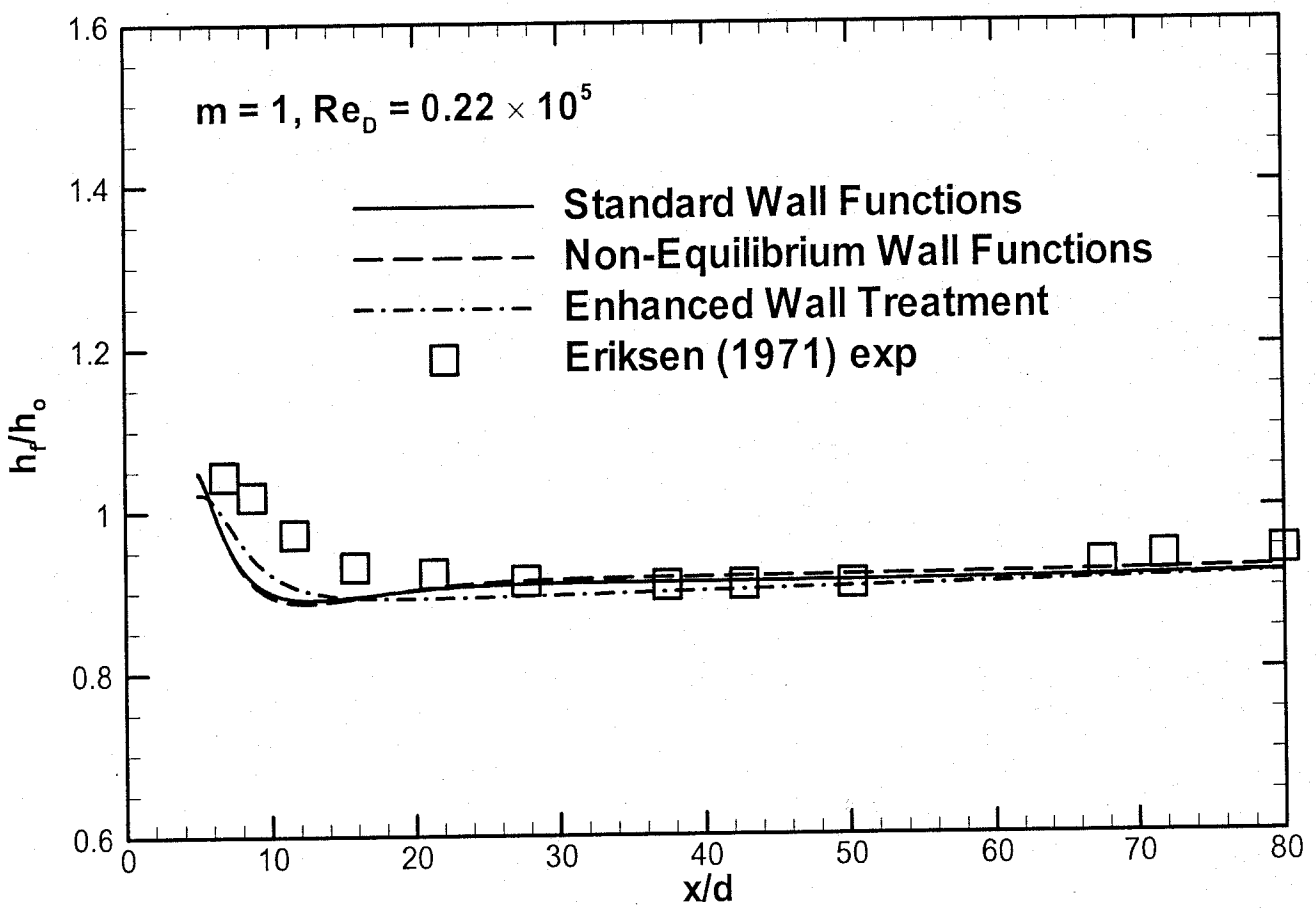

Figure 5.5 The performance of different wall treatments with Eriksen (1991) experimental data.

met. For blowing ratio of 1, it has been demonstrated that both realizable and standard k-ϵ model outperform the other turbulence models, though it is hard to decide which one is better. Since the enhanced wall treatment needs a very fine near wall mesh, thus rendering it numerically expensive, wall functions will be mainly employed since they require less computational resources. Therefore, the two k-ϵ turbulence models combined with wall functions have been chosen to carry out the simulations of the remaining cases.

Figure 5.6 shows the comparison between prediction and experimental data for the heat transfer coefficient at the centerline for different cooling parameters. The results given by both realizable k-ϵ model and standard k-ϵ model are similar and agree well with the experimental data. Around the starting point of the heat flux plate the heat transfer coeffiient is underpredicted, which can be explained by conduction error since the temperature gradient will be very large. Figure 5.7 shows the predictions on the spanwise direction at different cooling parameters, and it can be seen that the predictions agree well with the experimental data.

5.3 Sen (1996) case and the new scheme

Since there is no experimental data available for the new scheme, shown in Figures 4.3 and 4.4, the dimension of the new scheme (d = 0.03163m) is specifically defined such that the area of the jet cross section of the new scheme is equal to that in the Sen et al. case (d = 0.0111m). This means that at the same blowing ratio used in the Sen et al. (1996) case, the same amount of coolant will pass through the jet hole of the new scheme. Thus, at the same blowing ratio with the same amount of coolant being used and

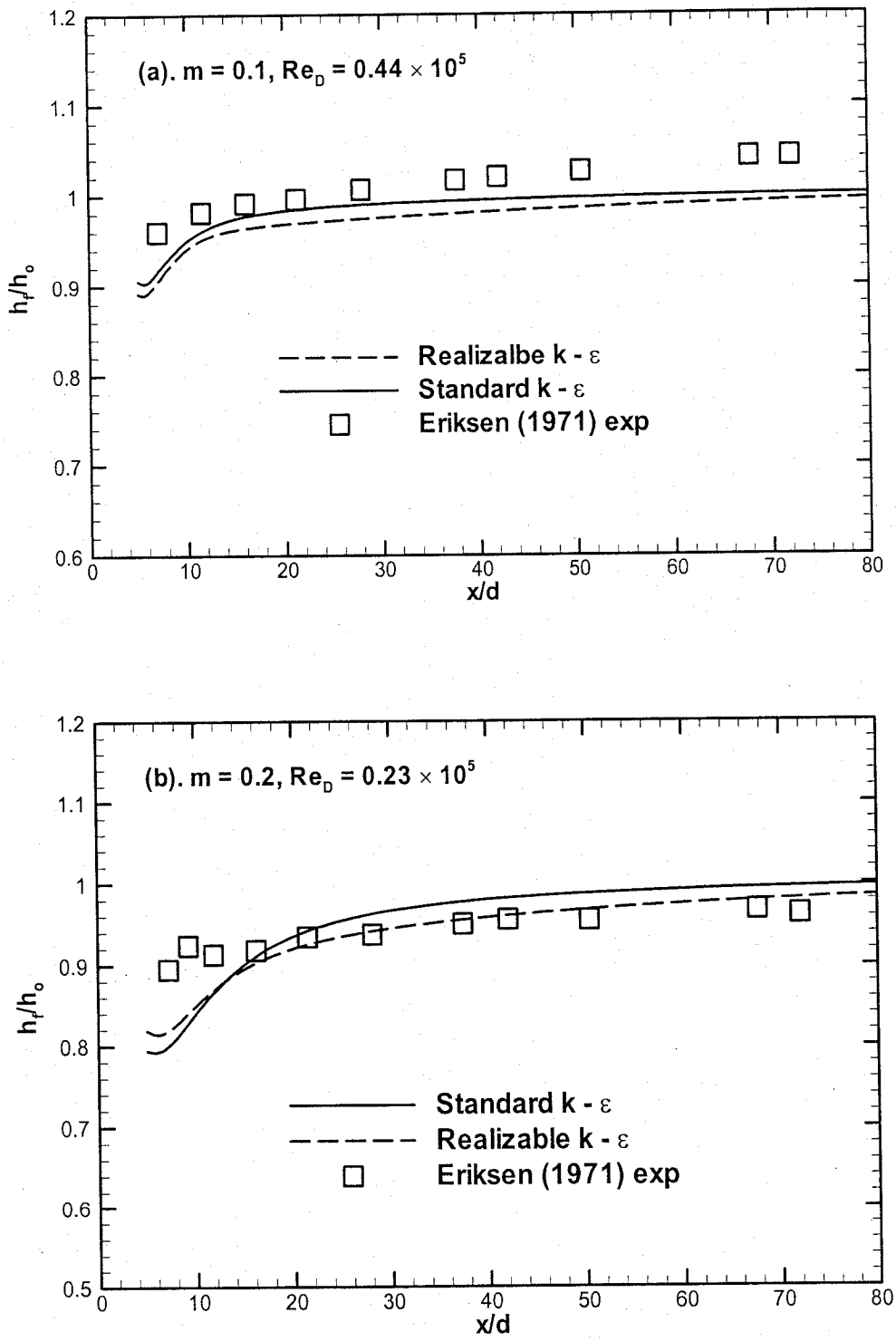

Figure 5.6 Predictions of h at different cooling parameters.

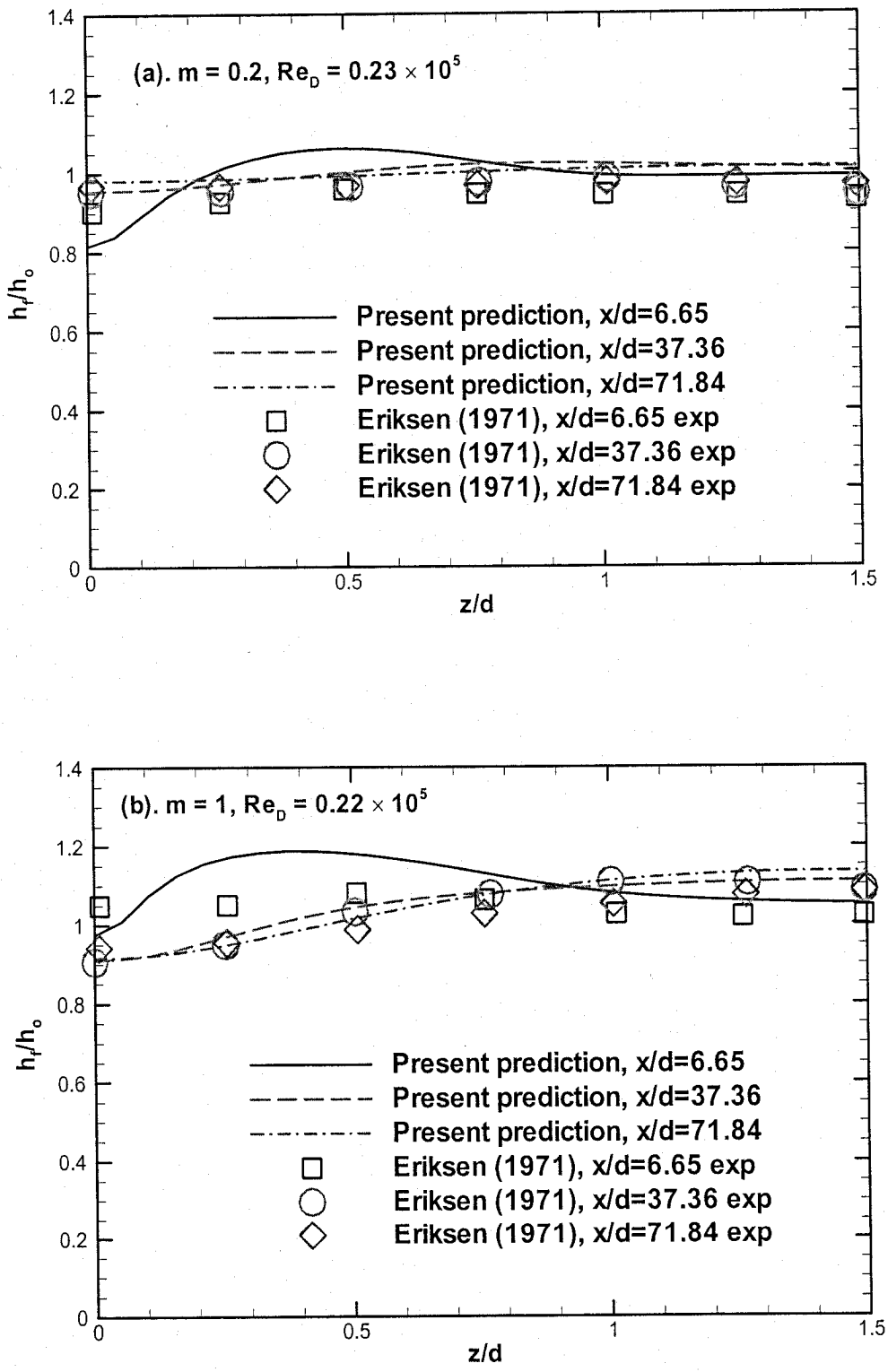

Figure 5.7 Predictions of h in the spanwise direction.

with all the other parameters remaining the same, the performance of the new scheme will be compared with that of Sen et al. (1996). The results of two cases will be presented, i.e. m = 1 and 0.5. The test parameters for Sen (1996) were shown in Table 5.2, the new scheme in Table 5.3.

Figure 5.8 shows how a grid independent solution is obtained. Four grids with different number of nodes are created and four cases are run with the same y^+ value on the wall, including the testing surface and jet sidewall, while all other parameters remain the same. As the number of the nodes increases, the solutions become asymptotically close to the final solution. After the number of the mesh reaches 373160 cells, any further increase in the number of the cells produces only negligible changes in the final results, and so a grid independent solution has been obtained.

The performance of standard k-ϵ model and realizable k-ϵ model for the Sen et al. (1996) scheme is shown in Figure 5.9. Based on Sen et al.'s experimental data, the standard k-ϵ model seems to give better prediction of the heat transfer coefficient despite the fact that these two predictions are close to within 6%. At blowing ratio of 1, the jets undergo liftoff from the surface causing the mainstream to tuck below the jets. It should be noted that when the temperature of the jet and mainstream are identical, as was the case for the experimental study, the effect of jet liftoff on the temperature distribution will not be as dramatic. Also shown in Figure 5.9 is the prediction of Ferguson (1998), and it can be seen that the prediction of the present study remains closest to the experimental data, especially in the near hole region.

Table 5.2 Experimental parameters for Sen (1996) case – h

	m = 1	m = 0.5
d (m)	0.0111	0.0111
Re_D (based on d)	7000	7000
U_∞ (m/s)	10	10
T_∞ (K)	300	300
U_j (m/s)	10	5
T_j (K)	300	300
q (W/m^2)	4000	4000

Table 5.3 Test parameters for the new scheme – h

	m = 1	m = 0.5
d (m)	0.03163	0.03163
U_∞ (m/s)	10	10
T_∞ (K)	300	300
U_j (m/s)	10	5
T_j (K)	300	300
q (W/m^2)	4000	4000

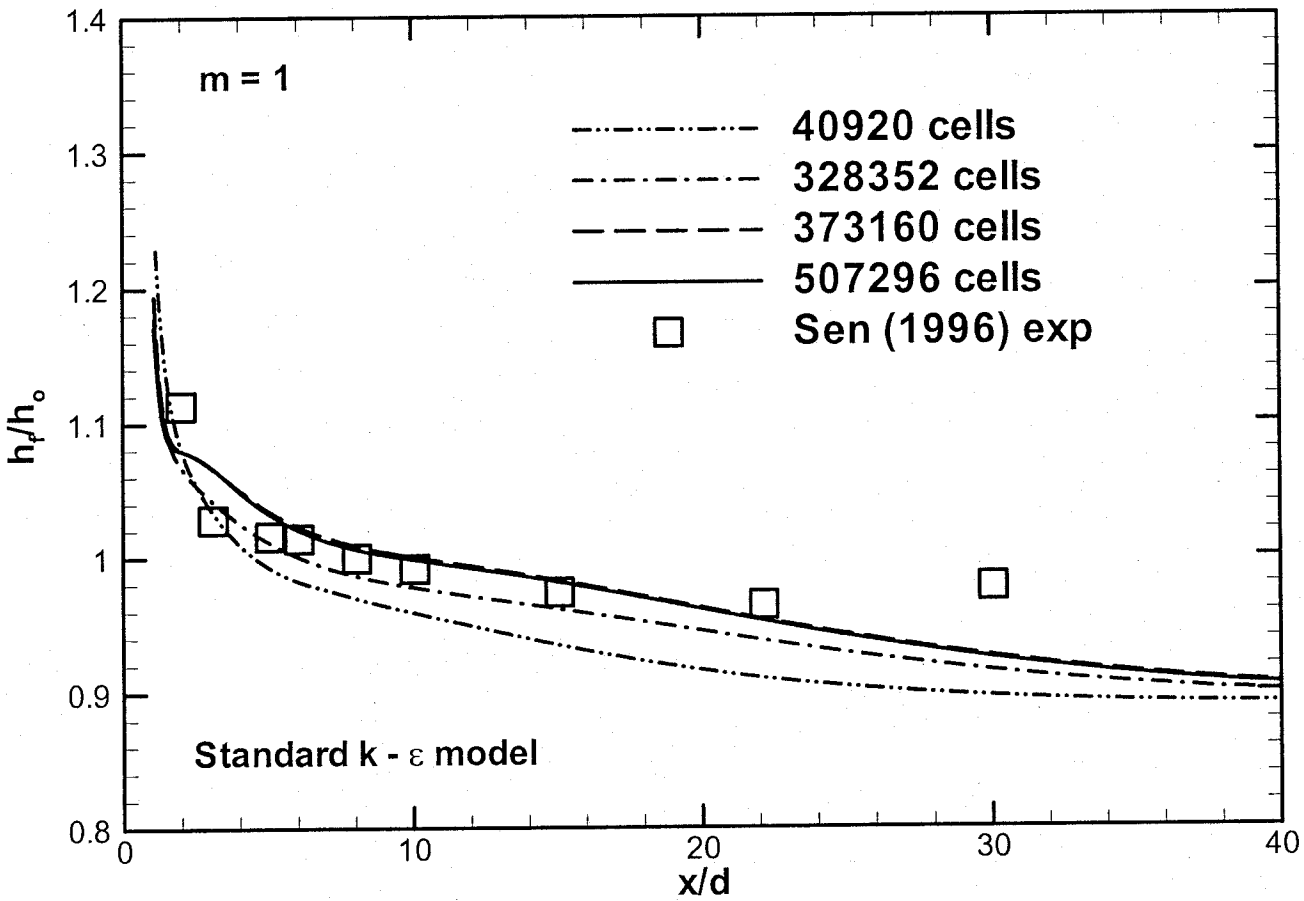

Figure 5.8 After the grid increases to 373160 cells, further increasing the cell number produces negligible change in the final solution.

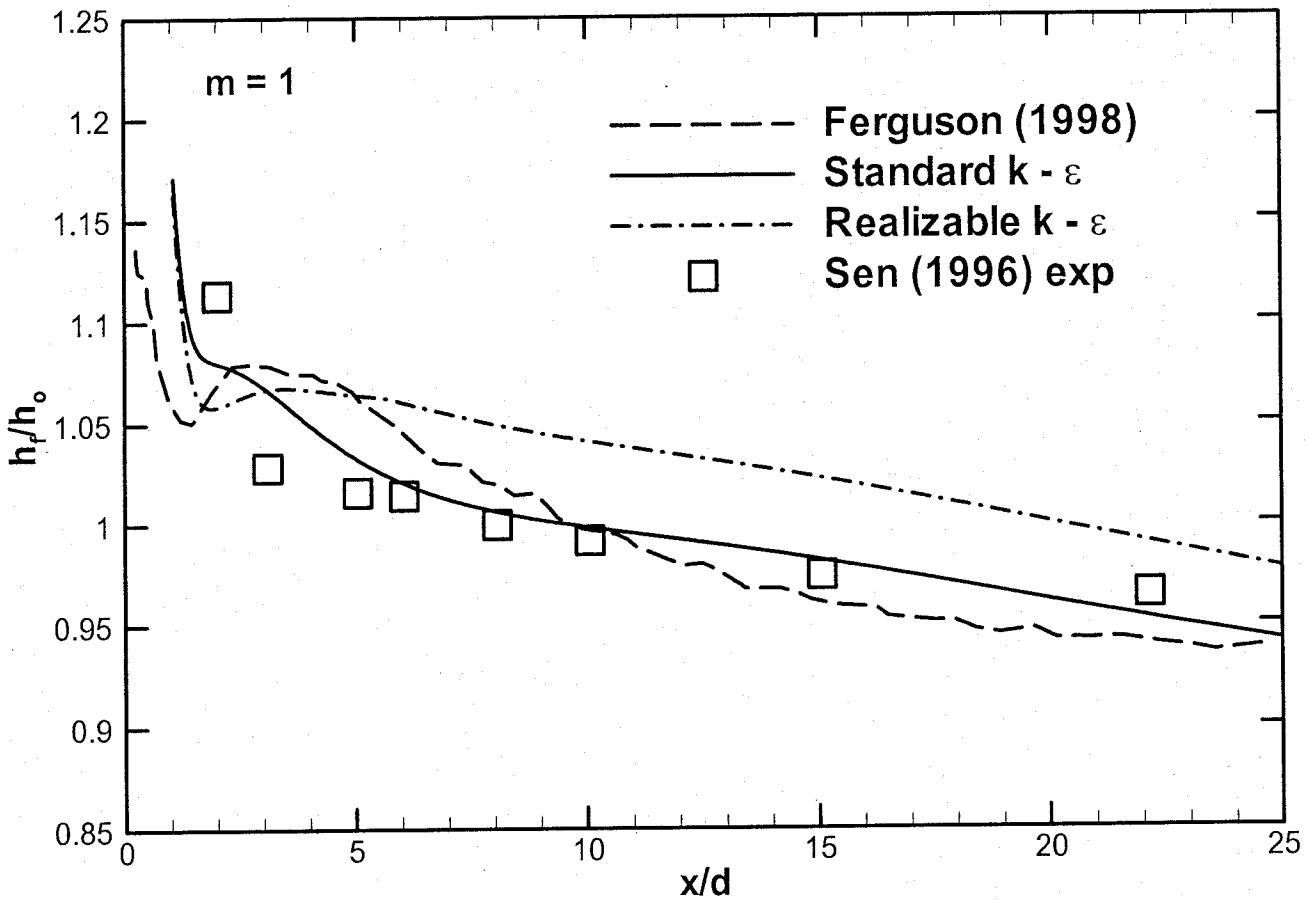

Figure 5.9 The performance of 2 k-ϵ turbulence models with the experimental data of Sen (1996) and previous predictions.

Figure 5.10 compares the predictions of the centerline h_f/h_o of the Sen et al. case (1996) and the new scheme with experimental data of Sen et al. (1996). At m = 1, in the Sen et al. (1996) scheme, the jets lift off from the testing surface, causing a substantial rise in heat transfer immediately after the injection, and the prediction agrees very well with the experimental data. In the new scheme at m = 1, the jets remain attached to the surface, therefore the heat transfer with jets is slightly lower than that without jets in the near hole area of around x/d < 8, as shown in Figure 5.10a, indicating better protection than traditional cylindrical holes. Beyond x/d of 8, due to turbulence, the diluted coolant dissipates into the mainstream and the h_f/h_o approaches 1 in the new scheme. For the Sen et al. (1996) scheme, the jets reattach to the surface causing h_f/h_o to decrease slightly. At m = 0.5, the jets in both the Sen et al. (1996) scheme and the new scheme remain attached to the protected surface. The heat transfer in the new scheme is slightly higher than that of the traditional cylindrical scheme due to the dilution effect of the diffusion section in the jet of the new scheme, as shown in Figure 5.10b.

The predictions of local heat transfer in the new scheme are shown in Figure 5.11. At m = 1, as shown in Figure 5.11a, the new scheme gives lower heat transfer coefficient than the traditional cylindrical hole due to the jet liftoff effect in the near hole region, especially in the area of z/d < 0.8. In the other area of z/d > 0.8, both schemes produce a heat transfer level of close to 1. At m = 0.5, the h_f/h_o lingers around 1 since both schemes do not undergo jet liftoff, as shown in Figure 5.11b.

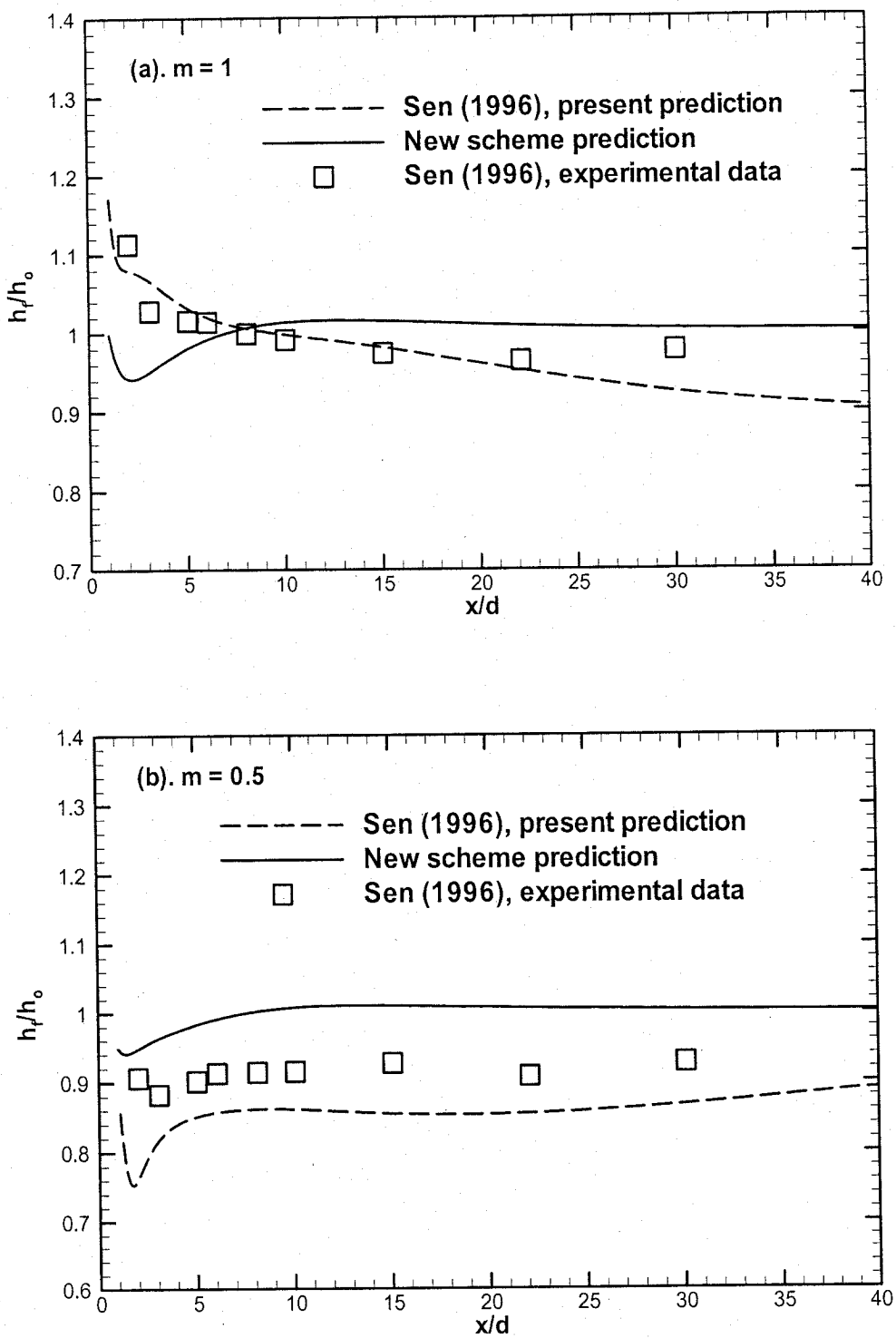

Figure 5.10 Centerline h for the new scheme showing the new scheme giving lower h in the near hole region at high blowing ratio of 1.

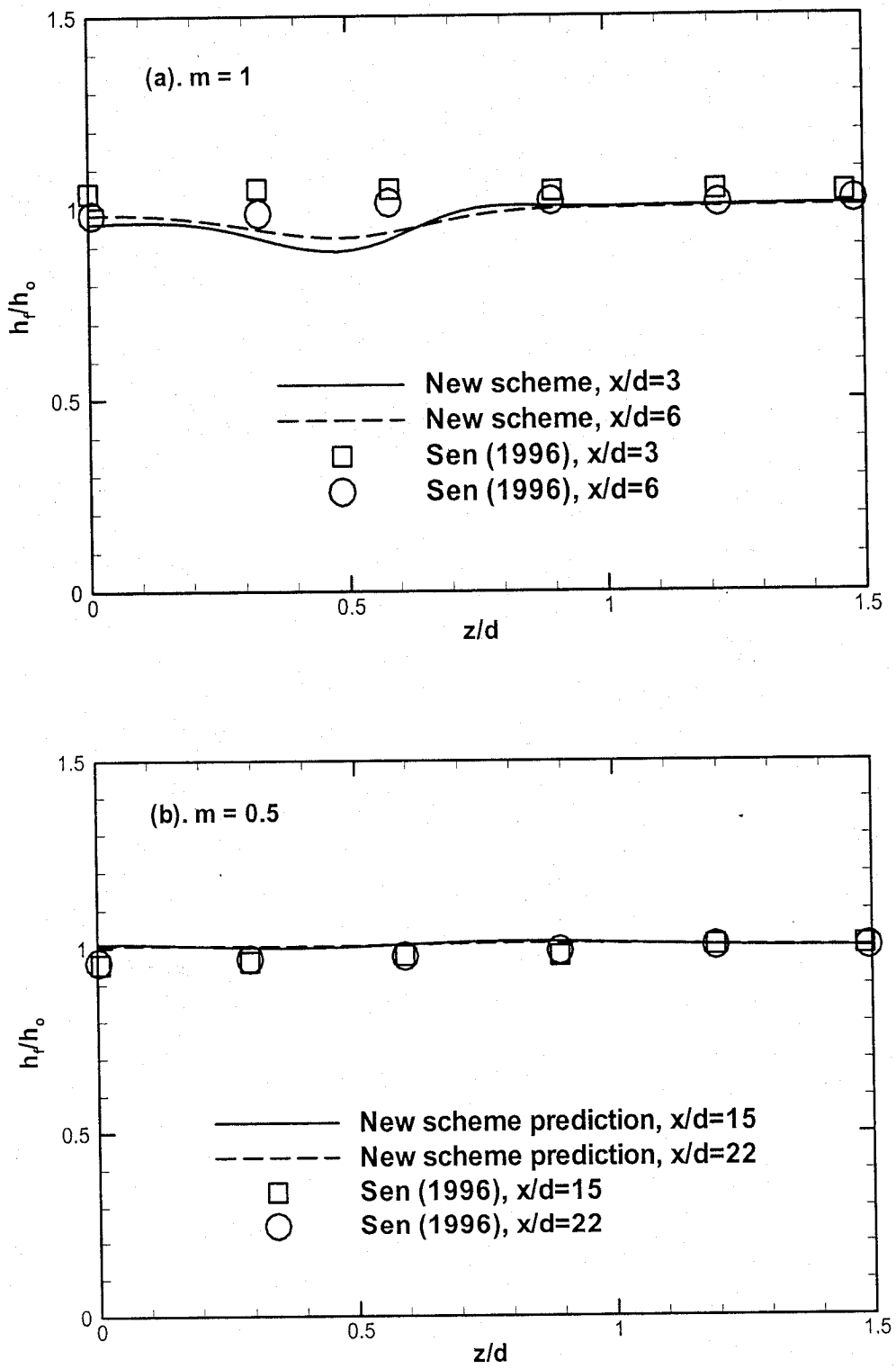

Figure 5.11 Comparison of the local spanwise h for the new scheme with the standard scheme of Sen (1996).

Figure 5.12 compares the predictions which include conjugate heat transfer with those that do not. The prediction without conjugate heat transfer shows that the heat transfer in the spanwise direction is over predicted around z/d = 0.5, and this can be attributed to heat conduction error in the test plate which has not been taken into account. Considerable improvement in the prediction of h_f/h_o in the spanwise direction is achieved when conjugate heat transfer was taken into account. On the other hand, there is little difference between them on the centerline heat transfer in the streamwise direction (results not shown here). Thus, the thickness and the properties of the material, mainly thermal conductivity of the heater, have been shown to affect the final solution significantly, however these values were not available in the work of Sen et al. (1996). As a result, assumed values have been used in the simulations with conjugate heat transfer in order to tentatively obtain a solution. The details of the simulations with the conjugate heat transfer are not given in the present study. Figure 5.13 shows the predictions of heat transfer coefficient on the test surface for the new scheme at different blowing ratio, namely m = 1 and m = 0.5.

It has been shown in the open literature that in the traditional cylindrical hole scheme, the gradient of adiabatic temperature in the spanwise direction is significantly larger than that of streamwise direction. Therefore, there will be a huge driving force of heat conduction on the testing surface in the spanwise direction which tends to move energy from the high temperature end to the low temperature end. This heat conduction error in the spanwise direction causes the boundary condition of constant heat transfer on the testing surface to be no longer valid. As a result, the prediction in the spanwise direction deviates largely

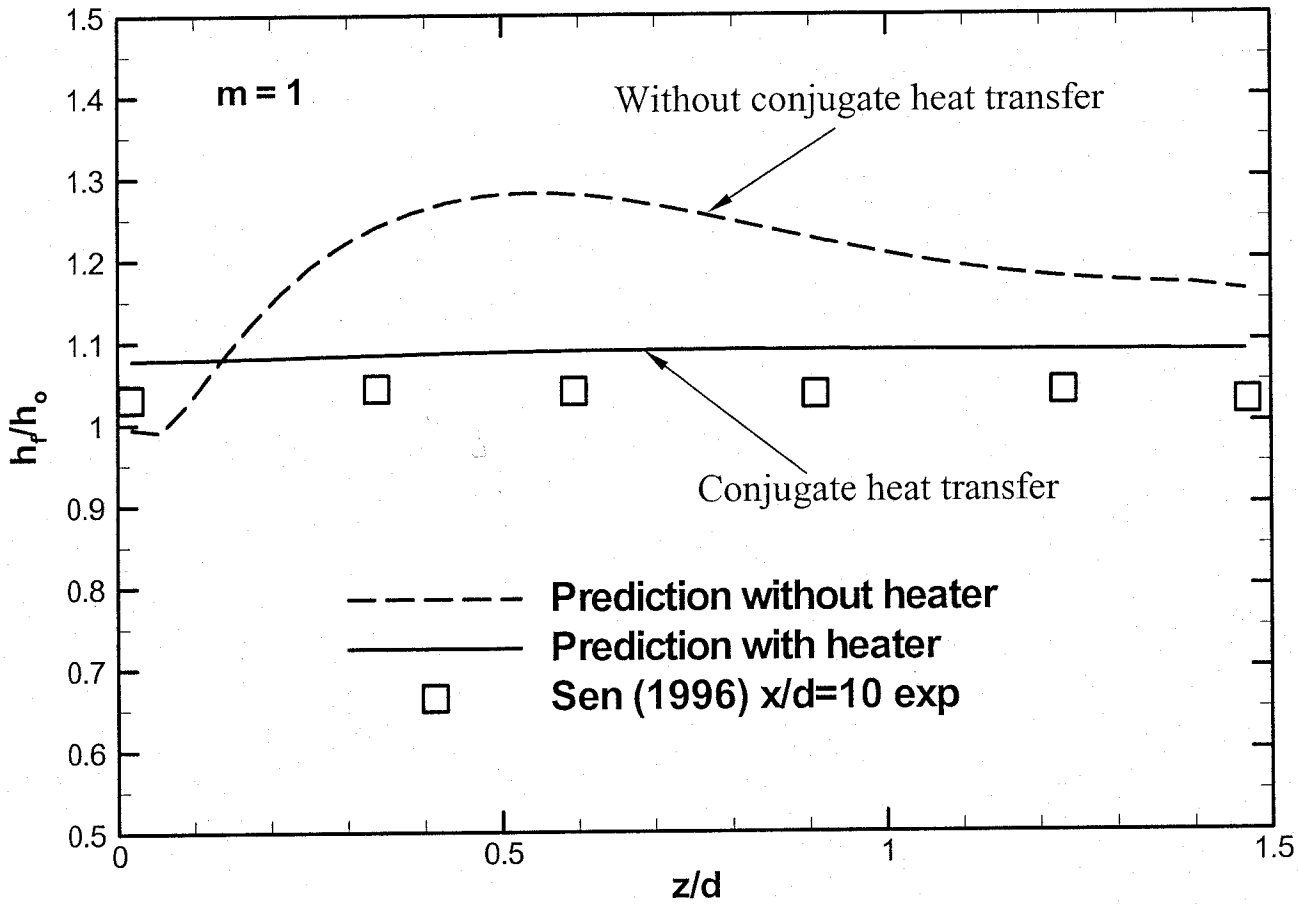

Figure 5.12 The improvement on prediction of h in the local spanwise direction by modeling conjugate heat transfer (with heater).

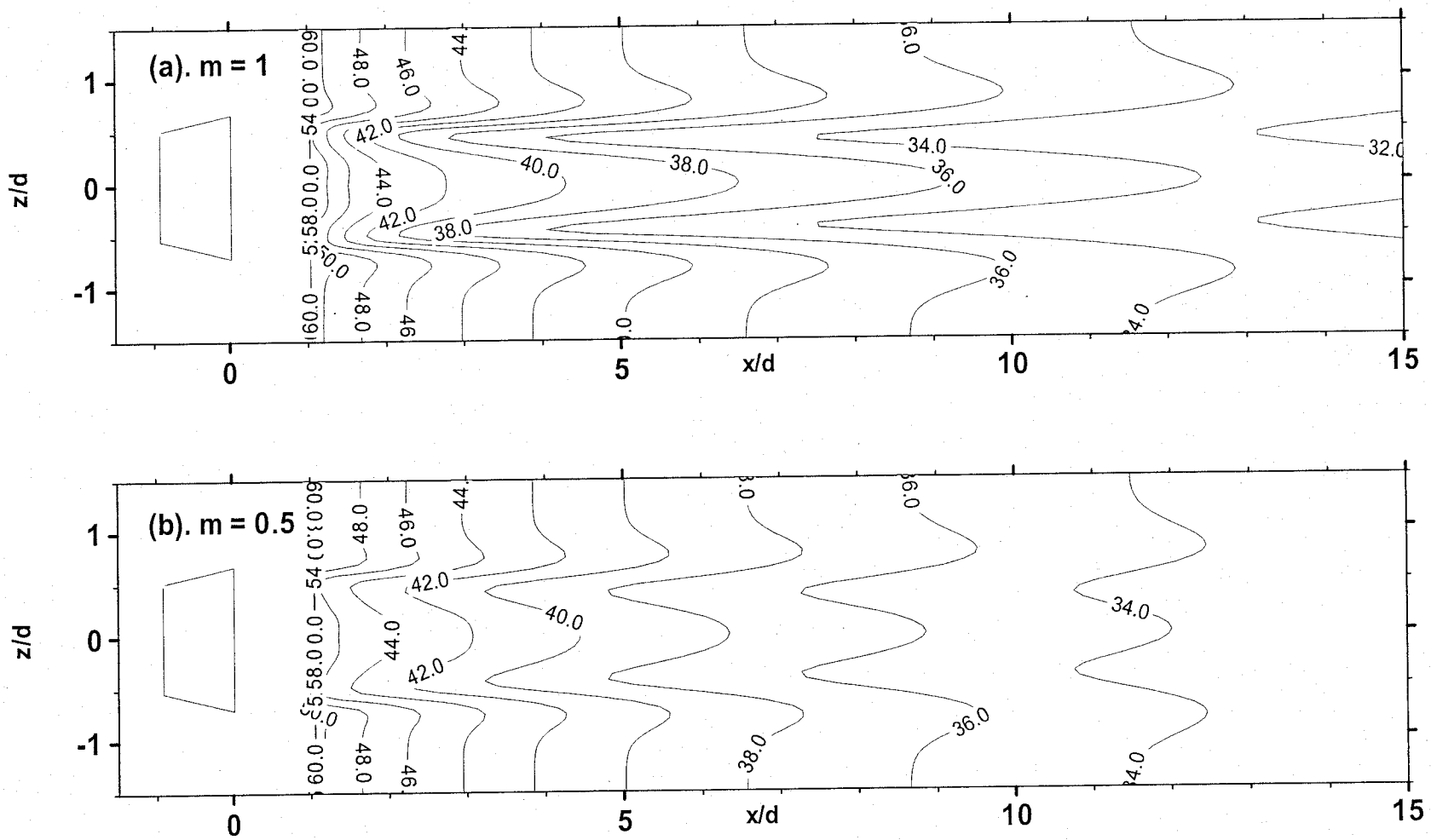

Figure 5.13 Contours of h ($W/m^2 \cdot K$) on the test surface at different blowing ratio.

from the experimental data, especially in the area of from z/d = 0.2 to 0.8 where a large temperature gradient exits. Again, the current turbulence models are unfairly being blamed for this disparity in the open literature.

Chapter 6

Conclusions and Future Directions

6.1 Adiabatic effectiveness

In the present study, the performances of different turbulence models as well as different wall treatments have been evaluated. Simulations of two different benchmark cases have been performed and excellent agreement between the predictions and available experimental data has been shown. The methodology, fully established in the two benchmark simulations, has been applied to a novel cooling scheme, and its results are compared with those of the cylindrical hole. The new scheme combines in-hole impingement cooling with traditional downstream film-cooling for improved cooling capabilities. It was determined that the proposed cooling scheme can prevent coolant lift-off much better than standard round holes. The key conclusions are:

- The jet liftoff effect can be captured by current turbulence models when a high quality mesh system is applied. The y^+ issue has to be taken seriously since it has more significant effects on the solution than the turbulence model and wall treatment combined.
- The proposed cooling scheme can completely eliminate the possibility of jet liftoff and provide more uniform protection over the surface. It can efficiently reduce the presence of hot spots in the blade and significantly reduce thermal stress.

6.2 Heat transfer coefficient

An extensive investigation has been carried out to evaluate the performance of different turbulence models as well as the different wall treatments in film cooling simulations. Systematic simulations of two different benchmark cases have been performed and good agreement between the predictions and available experimental data has been shown. This study has shown that if used with care, CFD can be successfully employed with the current turbulence models in order to predict the correct levels of heat transfer. The following summarizes the findings.

- Contrary to the notion that isotropic turbulence models such as the k-ϵ models are not adequate for modeling jet-in-crossflow, the k-ϵ model actually gave superior predictions than those obtained from the Reynolds Stress model, which is supposed to be an anisotropic turbulence model. All the wall treatments, including standard wall functions, non-equilibrium wall functions, and two-layer zonal or enhanced wall treatment essentially give the same results as long as the near wall mesh requirements were met, although two-layer zonal model has been shown to perform better by other researchers. This conclusion indicates that any effort to use the two-layer zonal model or enhanced wall treatment in order to attain more accurate results is doomed to fail from the beginning in view of the fact that all wall treatments are empirical functions and all empirical functions are very similar to each other.
- The conduction error on the test surface in experimental work intended for the measurement of the heat transfer coefficient is considerably larger than believed

by the technical community. This explains why different researchers obtained different measurements for the heat transfer coefficient from different configurations of the constant heat flux test plate. Modeling conjugate heat transfer by considering the effect of heat conduction in the testing plate can yield more realistic results, especially in the spanwise direction.

- The proposed cooling scheme gave considerably lower heat transfer coefficient at the centerline in the near hole region when compared to the traditional cylindrical hole, especially at high blowing ratio where traditional cylindrical hole undergoes liftoff. The heat transfer coefficient is much lower in the spanwise direction as well, thus providing more efficient protection over the surface.

6.3 Future directions

The results presented in this study provide important insights for future computational studies of film cooling. Prior to this study, it was commonly believed that the current turbulence models were not capable of capturing the jet liftoff effect in the traditional cylindrical hole scheme, which is the most fundamental problem of film cooling and has been studied extensively in the open literature. Turbulence models and the quality of the numerical grid have a tremendous effect on the final solution. The quality of the mesh has such a big role in determining the solution that the performance of turbulence models could be completely masked. As a result, a poor quality mesh could accidentally produce excellent results. Thus, CFD practitioners must make sure that consistent results have been obtained before drawing any conclusion. It is entirely possible that the current

turbulence models have been unfairly blamed for not being able to predict some phenomenon when, in reality, they would have if the model was set up properly.

Since the reliability of the experimental data of heat transfer coefficient in the open literature is questionable, new experiments specifically intended for validating numerical models need to be conducted, in which more details of the constant heat flux plate, such as the thickness and properties of the heater, considered to be of minor importance by the previous researchers, must be given. The existence of the thin heater is supposed to generate the constant heat flux boundary condition, but it is extremely difficult to model in the numerical simulations due to its extremely thin thickness compared with the diameter of the jets. A thicker heater, with the thickness on the order of the radius of the jets, is easier to model in the simulations when modeling conjugate heat transfer, and is therefore highly recommended. Moreover, the performance of the new scheme on curved surface will certainly be different than that on the flat plate and this should be studied in the future. Finally, since adiabatic and constant heat flux boundary conditions are not realistic conditions for real turbine blades, the modeling of conjugate heat transfer problem is inevitable in the simulations of real engine application since the heat conduction within the blades cannot be ignored, given that they are typically fabricated from highly conductive materials such as titanium or aluminum alloy.

References

Ajersch, P., J-M Zhou, S. Ketler, M. Salcudean, I. S. Gartshore, "Multiple jets in a crossflow: detailed measurements and numerical simulations," ASME Paper No. 95-GT-9, 1995.

Al-Hamadi, A. K., B. A. Jubran, G. Theodoridis, "Turbulence Intensity Effects on Film Cooling and Heat Transfer from Compound Angle Holes with Particular Application to Gas Turbine Blades", Energy Convers. Mgmt, Vol. 39, No. 14, pp. 1449-1457, 1998.

Amer, A. A., B. A. Jubran, M. A. Hamdan, "Comparison of Different Two-equation Turbulence Models for Prediction of Film Cooling from Two Rows of Holes", Numerical Heat Transfer, Part A, Vol. 21, pp. 143-162, 1992.

Ammari, H. D., N. Hay, D. Lampard, "The Effect of Density Ratio on the Heat Transfer Coeffcient from a Film-Cooled Flat Plate", Journal of Turbomachinery, Vol.112, pp.444-450, 1990.

Andreopoulos, "Measurements in a jet-pipe flow issuing perpendicularly into a cross stream," J. Fluid Eng., Vol. 104, pp. 493-499, 1982.

Azad, G. S., J.C. Han, S. Teng , R. Boyle, "Heat Transfer and Pressure Distributions on a Gas Turbine Blade Tip", ASME Journal of Turbomachinery, Vol.122, pp.717-724, 2000.

Baldauf, S., M. Scheurlen, A. Schulz, S. Wittig, "Heat Flux Reduction from Film Cooling and Correlation of Heat Transfer Coefficients from Thermographic Measurements at Enginelike Conditions", Journal of Turbomachinery, Vol. 124, pp. 699-709, 2002.

Bergeles, G., A. D. Gosman, B. E. Launder, "Near-Field Character of a Jet Discharged through a Wall at 30° to a Mainstream", AIAA Journal, Vol. 15, No. 4, pp. 499-504, 1977.

Bergeles, G., A. D. Gosman, B. E. Launder, "The turbulent jet in a cross stream at low injection rates: a three-dimensional numerical treatment," Numerical Heat Transfer, Vol. 1, pp. 217-242, 1978.

Berhe, M. K., S. V. Patankar, "A Numerical Study of Discrete-Hole Film Cooling", ASME Paper No. 96-WA/HT-8, 1996.

Boyce, M. P., "Gas Turbine Engineering Handbook", Gulf Professional Publishing, Boston, Chap. 9, pp. 356, 2002.

Brittingham, R. A., J. H. Leylek, "A Detailed Analysis of Film Cooling Physics: Part IV - Compound - Angle Injection With Shaped Holes", Journal of Turbomachinery, Vol. 122, pp. 133-145, 2000.

Burd, S. W., R. W. Kaszeta, T. W. Simon, "Measurements in Film Cooling Flows: Hole L/D and Turbulence Intensity", ASME Journal of Turbomachinery, Vol. 120, pp. 791 - 798, 1998.

Cho, H. H., D. H. Rhee, B. G. Kim, "Enhancement of Film Cooling Performance Using a Shaped Film Cooling Hole with Compound Angle Injection", JSME International Journal, Series B, Vol. 44, No. 1, pp. 99-110, 2001.

Cutbirth, J. M., D. G. Bogard, "Thermal Field and Flow Visualization Within the Stagnation Region of a Film-Cooled Turbine Vane", Journal of Turbomachinery, Vol. 124, pp. 200-206, 2002.

Demuren, A. O., and W. Rodi, "Three-dimensional calculation of film cooling by a row of jets," Proceedings of the Fifth GAMM-Conference on Numerical Methods in Fluid Mechanics, pp. 49-56, 1983.

Di Ai, P. P. Ding, P. H. Chen, "The selection criterion of injection temperature pair for transient liquid crystal thermography on film cooling measurements", International Journal of Heat and Mass Transfer, Vol. 44, pp. 1389-1399, 2001.

Dibelius, G. H., R. Pitt, and B. Wen, "Numerical Prediction of Film Cooling Effectiveness and the Associated Aerodynamic Losses with a Three-Dimensional Calculation Procedure," ASME Paper No. 90-GT-226, 1990.

Dittmar, J., A. Schulz, S. Wittig, " Assessment of Various Film-Cooling Configurations Including Shaped and Compound Angle Holes Based on Large-Scale Experiments", Journal of Turbomachinery, Vol. 125, pp. 57-64, 2003.

Ekkad, S. V., J. C. Han, H. Du, "Detailed Film Cooling Measurements on a Cylindrical Leading Edge Model: Effect of Free-Stream Turbulence and Coolant Density", Journal of Turbomachinery, Vol. 120, pp. 799-807, 1998.

Eriksen, V. L., "Film Cooling Effectiveness and Heat Transfer with Injection through Holes", Ph.D. Dissertation, University of Minnesota, 1971.

Ferguson, J. D., D. K. Walters, J. H. Leylek, "Performance of Turbulence Models and Near-Wall Treatments in Discrete Jet Film Cooling Simulations", ASME Paper 98-GT-438, 1998.

FLUENT 6.1 Documentation, User's Guide, Chapter – 8, 10, 11. Fluent Inc., 2003.

Fukuyama, Y., F. Otomo, M. Sato, Y. Kobayashi, H. Matsuzaki, "Prediction of vane surface film cooling effectiveness using compressible Navier-Stokes procedure and k-ϵ turbulence model with wall function," ASME Paper No. 95-GT-25, 1995.

Garg, V. K., and Rigby, D. L., "Heat Transfer on a Film-cooled Rotating Blade – Effect of Hole Physics," Int. J. Heat and Fluid Flow, Vol. 20, pp. 10-25, 1999.

Garg, V. K., "Modeling Film-cooled Flow Characteristics at the Exit of Shower-head Holes," Int. J. Heat and Fluid Flow, Vol. 22, pp. 134-142, 2001.

Garg, V. K., "Heat Transfer Research on Gas Turbine Airfoil at NASA GRC," Int. J. Heat and Fluid Flow, Vol. 23, pp. 109-136, 2002.

Gartshore, I., M. Salcudean, I. Hassan, "Film Cooling Injection Hole Geometry: Hole Shape Comparison for Compound Cooling Orientation", AIAA Journal, Vol. 39, No. 8, pp. 1493-1499, 2001.

Gibson, M. M., B. E. Launder, "Ground Effects on Pressure Fluctuations in the Atmospheric Boundary Layer", J. Fluid Mech., Vol. 86, pp. 491-511, 1978.

Goldstein, R. J., E. R. G. Eckert, J. W. Ramsey, "Film Cooling with Injection through Holes: Adiabatic Wall Temperatures Downstream of a Circular Hole", Journal of Engineering for Power, Series A, Vol. 90, pp. 384-395, 1968.

Goldstein, R. J., T. Yoshida, "The Influence of a Laminar Boundary Layer and Laminar Injection on Film Cooling Performance", Journal of Heat Transfer, Vol. 104, pp. 355-362, 1982.

Goldstein, R. J., P. Jin, R. L. Olson, "Film Cooling Effectiveness and Mass/Heat Transfer Coefficient Downstream of One Row of Discrete Holes", Journal of Turbomachinery, Vol. 121, pp. 225-232, 1999.

Goldstein, R. J., P. Jin, "Film Cooling Downstream of a Row of Discrete Holes With Compound Angle", Journal of Turbomachinery, Vol. 123, pp. 222-230, 2001.

Gritsch, M., A. Schulz, S. Wittig, "Effect of Crossflows on the Discharge Coefficient of Film Cooling Holes with Varying Angles of Inclination and Orientation", Journal of Turbomachinery, Vol. 123, pp. 781-787, 2001.

Gritsch, M., A. Schulz, S. Wittig, "Effect of Internal Coolant Crossflow on the Effectiveness of Shape Film-Cooling Holes", Journal of Turbomachinery, Vol. 125, pp. 547-554, 2003.

Hale, C. A., "An Experimental and Numerical Study of the Hydrodynamics and Surface Heat Transfer Associated with Short Film Cooling Holes Fed by a Narrow Plenum," PhD. Dissertation, Purdue University, 1999.

Hale, C. A., M. W. Plesniak, S. Ramadhyani, "Film Cooling Effectiveness for Short Film Cooling Holes Fed by a Narrow Plenum", Journal of Turbomachinery, Vol. 122, pp. 553-557, 2000.

Harrington, M. K., M. A. McWaters, D. G. Bogard, C. A. Lemmon, K. A. Thole, "Full-Coverage Film Cooling With Short Normal Injection Holes", Journal of Turbomachinery, Vol. 123, pp. 798-805, 2001.

Hoda, A., S. Acharya, M. Tyagi, "Reynolds Stress Transport Model Predictions and Large Eddy Simulations for Film coolant Jet in Crossflow", ASME Paper 2000-GT-249, 2000.

Hyams, D. G., McGovern, K. T., and Leylek, J. H., "Effects of Geometry on Slot-jet Film Cooling Performance," ASME Paper 96-GT-187, 1996.

Hyams, D. G., J. H. Leylek, "A Detailed Analysis of Film Cooling Physics: Part III-Streamwise Injection with Shaped Holes", Journal of Turbomachinery, Vol. 122, pp. 122-132, 2000.

Immarigeon, A. A., "Advanced Impingement/Film-Cooling Schemes for High-Temperature Gas Turbine – Numerical Study", MSc. Thesis, Concordia University, 2004.

Jung, I. S., J. S. Lee, "Effects of Orientation Angles on Film Cooling Over a Flat Plate: Boundary Layer Temperature Distributions and Adiabatic Film Cooling Effectiveness", Journal of Turbomachinery, Vol. 122, pp. 153-160, 2000.

Kapadia, S., S. Roy, "Detached Eddy Simulation of Turbine Blade Cooling", AIAA Paper 2003-3632, 2003.

Kim, S. W., T. J. Benson, "Calculation of a Circular Jet in Crossflow with a Multiple-Time-Scale Turbulence Model", Int. J. Heat Mass Transfer, Vol. 35, No. 10, pp. 2357-2365, 1992.

Kim, Y. J., S. M. Kim, "Influence of Shaped Injection Holes on Turbine Blade Leading Edge Film Cooling", International Journal of Heat and Mass Transfer, Vol. 47, pp. 245-256, 2004.

Kohli, A., D. G. Bogard, "Effects of Hole Shape on Film Cooling With Large Angle Injection", ASME Paper 99-GT-165, 1999.

Lakehal, D., "Near-wall Modeling of Turbulent Convective Heat Transport in Film Cooling of Turbine Blades with the Aid of Direct Numerical Simulation Data," ASME Journal of Turbomachinery, Vol. 124, pp. 485-498, 2002.

Lam, C. K. G., K. A. Bremhorst, "Modified Form of the k-ϵ Model for Predicting Wall Turbulence," J. Fluids Eng., Vol. 103, pp. 456-460, 1981.

Launder, B. E., D. B. Spalding, "Lectures in Mathematical Models of Turbulence", Academic Press, London, England, 1972.

Launder, B. E., D. B. Spalding, "The Numerical Computation of Turbulent Flows", Computer Methods in Applied Mechanics And Eegineering, Vol. 3, pp. 269-289, 1974.

Launder, B. E., G. J. Reece, and W. Rodi, "Progress in the Development of a Reynolds-Stress Turbulence Closure", J. Fluid Mech., Vol. 68(3), pp. 537-566, 1975.

Launder, B. E., "Second-Moment Closure: Present... and Future?", Inter. J. Heat Fluid Flow, Vol. 10(4), pp. 282-300, 1989.

Leylek, J. H., R. D. Zerkle, "Discrete-Jet Film Cooling: A Comparison of Computational Results with Experiments", ASME Paper 93-GT-207, 1993.

Li, X., J. L. Gaddis, T. Wang, "Mist/Steam Heat Transfer in Confined Slot Jet Impingement", Journal of Turbomachinery, Vol. 123, pp. 161-167, 2001.

McGovern, K. T., and Leylek, J. H., "A Detailed Analysis of Film Cooling Physics Part 2. Compound-Angle Injection with Cylindrical Holes," ASME Paper 97-GT-270, 1997.

Maiteh, B. Y., B. A. Jubran, "Influence of mainstream flow history on film cooling and heat transfer from two rows of simple and compound angle holes in combination", International Journal of Heat and Fluid Flow, Vol. 20, pp. 158-165, 1999.

Mayhew, J. E., J. W. Baughn, A. R. Byerley, "The Effects of Free-Stream Turbulence on Film Cooling Adiabtaic Effectiveness", International Journal of Heat and Fluid Flow, Vol. 24, pp.669-679, 2003.

Medic, G., P. A. Durbin, "Toward Improved Prediction of Heat Transfer on Turbine Blades", Journal of Turbomachinery, Vol. 124, pp. 187-192, 2002.

Mulugeta, K. B., S. V. Patankar, "A Numerical Study of Discrete-Hole Film Cooling", ASME Paper 96-WA/HT-8, 1996.

Nasir, H., S. Acharya, S. Ekkad, "Improved film cooling from cylindrical angled holes with triangular tabs : effect of tab orientations", International Journal of Heat and Fluid Flow, Vol. 24, pp.657-668, 2003.

Patankar, S. V., D. K. Basu, S. A. Alpay, "Prediction of the Three-Dimensional Velocity Field of a Deflected Turbulent Jet," Journal of Fluids Engineering, Vol. 99, pp. 758-762, 1977.

Pedersen, D. R., E. R. G. Eckert, R. J. Goldstein, "Film Cooling With Large Density Differences Between the Mainstream and the Secondary Fluid Measured by the Heat-Mass Transfer Analogy", Journal of Heat Transfer, Vol. 99, pp. 620-627, 1977.

Rhee, D. H., Lee, Y. S. Lee, H. H. Cho, "Film Cooling Effectiveness and Heat Transfer of Rectangular-shaped Film Cooling Holes," ASME Paper No. GT-2002-30168, 2002.

Rodi, W., "Experience with two-layer models combining the k-ϵ with a one-equation model near the wall", AIAA-91-0216, 1991.

Sargison, J. E., S. M. Guo, M. L. G. Oldfield, G. D. Lock, A. J. Rawlinson, "A Converging Slot-Hole Film-Cooling Geometry – Part I: Low-Speed Flat-Plate Heat Transfer and Loss", Journal of Turbomachinery, Vol. 124, pp. 453-460, 2002.

Sathyamurthy, P., S. V. Patankar, "Prediction of film cooling with lateral injection," Heat Transfer in Turbulent Flow, pp. 61-70, 1990.

Saumweber, C., A. Schulz, S. Wittig, "Free-Stream Turbulence Effects on Film Cooling With Shaped Holes", Journal of Turbomachinery, Vol. 125, pp. 65-72, 2003.

Schmidt, D. L., B. Sen, D. G. Bogard, "Effects of Surface Roughness on Film Cooling", ASME Paper 96-GT-299, 1996.

Schönung, B., W. Rodi, "Prediction of Film Cooling by a Row of Holes With a Two-Dimensional Boundary-Layer Procedure," Journal of Turbomachinery, Vol. 109, pp. 579-587, 1987.

Sen, B., B. Tech., "Effect of Injection Hole Geometry, High Freestream Turbulence, and Surface Roughness on Film Cooling Heat Transfer", Ph.D. Dissertation, The University of Texas at Austin, 1995.

Sen, B., D. L. Schmidt, D. G. Bogard, "Film Cooling With Compound Angle Holes: Heat Transfer", Journal of Turbomachinery, Vol. 118, pp. 800-806, 1996.

Shih, T.-H., W. W. Liou, A. Shabbir, Z. Yang, and J. Zhu, "A New k-ϵ Eddy-Viscosity Model for High Reynolds Number Turbulent Flows - Model Development and Validation", Computers Fluids, Vol. 24(3), pp. 227-238, 1995.

Sinha, A. K., D. G. Bogard, M. E. Crawford, "Film-Cooling Effectiveness Downstream of a Single Row of Holes with Variable Density Ratio", Journal of Turbomachinery, Vol. 113, pp. 442-449, 1991.

Son, C., D. Gillespie, P. Ireland, G. Dailey, "Heat Transfer and Flow Characteristics of an Engine Representative Impingement Cooling System", Transactions of the ASME, vol. 123, pp. 154-160, 2001.

Spalart, P., S. Allmaras, "A one-equation turbulence model for aerodynamic flows", Technical Report AIAA-92-0439, American Institute of Aeronautics and Astronautics, 1992.

Taslim, M.E., L. Setayeshgar, S.D. Spring, "An Experimental Evaluation of Advanced Leading Edge Impingement Cooling Concepts", ASME Journal Of Turbomachinery, vol.123, pp.147-153, 2001.

Tyagi, M., S. Acharya, "Large Eddy Simulations of Rectangular Jets in Crossflow: Effect of Hole Aspect Ratio", Second AFSOR Conference on DNS/LES, Rutgers Univ., NJ, June 1999.

Vogel, G., A. B. A. Graf, J. V. Wolfersdorf, B. Weigand, "A Novel Transient Heater-Foil Technique for Liquid Crystal Experiments on Film-Cooled Surfaces", Journal of Turbomachinery, Vol. 125, pp. 529-537, 2003.

Walters, D. K., McGovern, K. T., Butkiewicz, J. J., and Leylek, J. H., "A Systematic Computational Methodology Applied to a Jet-in-crossflow Part 2: Unstructured/Adaptive Grid Approach," ASME Paper 95-WA/HT-2, 1995.

Walters, D. K., J. H. Leylek, "A Systematic Computational Methodology Applied to a Three-Dimensional Film-Cooling Flowfield," ASME Paper No. 96-GT-351, 1996.

Walters, D. K., J. H. Leylek, "A Detailed Analysis of Film Cooling Physics: Part I: Streamwise Injection With Cylindrical Holes", Journal of Turbomachinery, Vol. 122, pp. 102-112, 2000.

Wilcox, D. C., "Turbulence Modeling for CFD", DCW Industries, Inc., La Canada, California, 1998.

Wilfert, G., S. Wolff, "Influence of Internal Flow on Film Cooling Effectiveness", Journal of Turbomachinery, Vol. 122, pp. 327-333, 2000.

Yakhot, V., S. A. Orszag, "Renormalization Group Analysis of Turbulence: I. Basic Theory", Journal of Scientific Computing, Vol. 1(1), pp. 1-51, 1986.

York, W. D., J. H. Leylek, "Leading-Edge Film-Cooling Physics – Part III: Diffused Hole Effectiveness", Journal of Turbomachinery, Vol. 125, pp. 252-259, 2003.

Yu., Y., C. H. Yen, T. I. P. Shih, M. K. Chyu, "Film Cooling Effectiveness and Heat Transfer Coefficient Distributions Around Diffusion Shaped Holes", Journal of Heat Transfer, Vol. 124, pp. 820-827, 2002.

Yuen, C. H. N., R. F. Martinez-Botas, "Film Cooling Characteristics of a Single Round Hole at Various Streamwise Angles in a Crossflow: Part I effectiveness", International Journal of Heat and Mass Transfer, Vol. 46, pp. 221-235, 2003.

Yuen, C. H. N., R. F. Martinez-Botas, "Film cooling characteristics of a single round hole at various streamwise angles in a crossflow: Part II: heat transfer coefficients", International Journal of Heat and Mass Transfer, Vol. 46, pp. 237-249, 2003.

Zhou, J.-M., M. Salcudean, I. S. Gartshore, "Prediction of Film Cooling by Discrete-Hole Injection", ASME Paper 93-GT-75, 1993.